A STUDY OF COUPLING TWO THERMOACOUSTIC LASERS

by

Rohit Surathu

A thesis submitted to the faculty of
The University of Utah
in partial fulfillment of the requirements for the degree of

Master of Science

Department of Mechanical Engineering

The University of Utah

May 2013

The University of Utah Graduate School

STATEMENT OF THESIS APPROVAL

The thesis of **Rohit Surathu** has been approved by the following supervisory committee members:

Kuan Chen	, Chair	1/5/2012 Date of Approval
K. L. DeVries	, Member	1/5/2012 Date of Approval
Geoffrey Silcox	, Member	1/5/2012 Date of Approval

and by **Timothy Ameel**,

Chair of the Department of **Mechanical Engineering** and

by Donna M. White, Interim Dean of the Graduate School

ABSTRACT

Thermoacoustics is a field studying the effects of applying heat to particular resonator geometries, resulting in the oscillations of gas and thereby producing sound waves. This field is a rich blend of many other scientific fields: acoustics, thermodynamics, and fluid mechanics. Thermoacoustic engines work on a similar principle as traditional heat engines. The main difference between a traditional heat engine and a thermoacoustic engine is that an acoustic wave drives the thermodynamic process in the latter. These engines are easy to construct, and there are no moving parts, which reduces the mechanical wear and tear. In our case, we fabricated the simpler thermoacoustic lasers to conduct the analysis. In most previous work within this field, different designs were tested and studied for a single laser operation from which extensive experimental data sets were collected and analyzed. Design and operation of a thermoacoustic laser pair is more complicated. Even though there have been a few coupling studies, detailed information about the acoustic field of multiple thermoacoustic lasers is lacking. Hence, an effort was made to study the interaction between the sound waves by acoustically coupling two thermoacoustic lasers. The acoustic coupling was varied using 4 different configurations. First, the lasers were placed parallel to each other, with their open ends separated by a 1 m distance (0^{o} crossing angle). Next, the sound waves of the two lasers were focused at a particular point, with their openings in proximity at a fixed crossing angle (30 or 90^{o}). Finally, the spatial distance between the

openings of the 30 and 90^{o} crossing lasers was increased in their own respective angles. The signals were read using three different measuring devices: a sound pressure level meter, a unidirectional microphone or an omnidirectional miniature microphone. The signals read using both microphones were collected, measured, and analyzed. The results proved that coupling between two thermoacoustic lasers was strong enough to allow synchronization (mode-locking) of the sound waves in a particular frequency and phase. The output amplitude of the synchronized signal produced from coupling two thermoacoustic lasers was always less compared to the acoustic amplitude of a single laser, suggesting out-of-phase synchronization. In a few experiments, the signals from the two coupled lasers did not synchronize because of the mistuning of the natural frequencies between them. When this happened, the uncoupled signals beat with the difference in the natural frequency. The amplitude output of the beating signal was greater than that of the single laser only when the two lasers were in-phase.

TABLE OF CONTENTS

ABSTRACT iii

LIST OF TABLES vii

ACKNOWLEDGEMENTS viii

1 INTRODUCTION 1

2 LITERATURE SURVEY 13

3 EXPERIMENTAL SETUP AND TESTING OF THE THERMOACOUSTIC LASER PAIR 19

3.1 Thermoacoustic Laser Fabrication 19
3.2 Procedure for Testing Single Thermoacoustic Laser 22
3.3 Experimental Setup and Procedure for Coupling the Laser Pair 23
3.3.1 Zero Crossing Angle (Lasers parallel to each other) 24
3.3.2 30 and 90^{o} Crossing Angles (Openings of the lasers oriented in a particular angle) 25
3.3.3 30 and 90^{o} Crossing angles, Laser openings separated at Various Distances 27
3.4 Data Acquisition using Lab-View 27
3.5 Experimental Considerations 28
3.6 Acoustic Theories and Models 29
3.7 Synchronization and Mode-Locking Phenomena 30
3.8 Error and Uncertainty Analysis 31

4 RESULTS AND DISCUSSION 42

4.1 Testing Single Thermoacoustic Laser Results 42
4.2 Acoustic Coupling Results 44
4.2.1 Zero Crossing Angle 44
4.2.2 Small Crossing Angle (30^{o}) 46
4.2.3 Large Crossing Angle (90^{o}) 53
4.2.4 Laser Pair separated at Various Distances 57

5 SUMMARY OF TEST RESULTS AND DISCOVERIES 110

5.1 Summary of Test Results 110

5.2 Discoveries 113

APPENDIX 114

REFERENCES 118

LIST OF TABLES

Table

3.1 Uncertainty factors and their tolerances.....41

4.1 Fundamental frequencies recorded using Lab-View Signal Express (30^{o} crossing angle).....109

4.2 Fundamental frequencies recorded using Lab-View Signal Express (90^{0} Crossing angle).....109

A.1 Specifications of CEN-TECH 98025 multimeter.....114

A.2 Specifications of Tenma 72-942 sound level meter.....115

A.3 Specifications of NI USB 6009.....116

A.4 Analog terminal assignments for NI USB 6009.....117

ACKNOWLEDGEMENTS

First of all, I would like to thank my advisor, Dr. Kuan Chen, for his constant guidance, encouragement, and support throughout my research. I am grateful to my committee members, Dr. K. Larry DeVries and Dr. Geoffrey Silcox.

I would like to express my admiration towards my coworkers and my friends at the University of Utah for their help. I am in debt to everyone at the U who has in one or the other way contributed towards my success.

I would like to convey my deepest gratitude towards my parents and my family members for supporting me morally through tough times.

Lastly, I would like to thank the National Research Foundation of Korea under Grant number 2009-0092786 for partially funding the study.

CHAPTER 1

INTRODUCTION

Thermoacoustics is a field that involves the study of both acoustics and thermodynamics. In other words, it is known as the study that involves sound waves and the conversion between heat and other forms of energy. When a sound wave travels through a medium, it creates pressure and velocity oscillations within the medium it travels. These oscillations will produce a "thermoacoustic" effect. The engines which produce "thermoacoustic" effects are known as thermoacoustic engines. These engines have been looked at with increased interest in recent years due to useful applications like converting thermal energy into acoustic energy (thermoacoustic heat engines) and acoustic energy into refrigeration (thermoacoustic refrigerator). Using thermoacoustic engines to recover thermal energy and first convert it into acoustic energy and then to electric energy has several advantages over traditional piston engines. The phenomenal growth in the usage of these engines was mainly due to their simplicity compared to the traditional heat engines. The mechanism responsible for the thermoacoustic effect is similar to that of the traditional heat engines. The process variable that sets it apart from the traditional heat engine is that acoustic waves drive the thermodynamic process, as opposed to a piston. Since there are no moving parts, the energy losses are significantly reduced. In addition, these engines are simple to design and manufacture, and if they can

be properly scaled and constructed, they can recover a large portion of heat lost in many traditional piston engines.

Acoustic waves find their use in various fields, like medicine, thermodynamics, fluid mechanics, and material sciences, etc. For example, ultrasound is used to shatter kidney stones. Shock waves are used in mining and material processing. They are also used in cleaning and sterilizing surfaces and medical instruments by sanitizing liquids. Recent developments in thermoacoustic engines like using solar energy or waste heat to run them makes it promising and economically sound for generating large quantities of acoustic energy. Its various applications make it an interesting topic of study among the ongoing research.

Early work in thermoacoustics dates back several centuries. Byron Higgins, in the later 1700s, was the first person to observe that when an organ pipe was heated with an external frame, it would sing, producing acoustic waves. Later, in the 19th century, glassblowers observed similar phenomena. Glass blowing was achieved by heating one end of a long glass tube to its melting point, while the other end was left cool. Glass blowers observed that when the hot end of the tube was closed, sound was emitted out of the open end. Sondhauss (1) was inspired by this glass tube phenomenon of producing sound by heating the tube. He conducted many experiments in order to determine the appropriate dimensions (length and diameter) for particular frequencies of sound. He concluded that frequency was dependent on the dimensions of the tube, which may include volume, cross-sectional areas of the opening, and the length of the neck. He named the tube after himself. Figure 1.1 shows a typical Sondhauss tube (1). Acoustic vibrations were produced by creating a steep temperature gradient over the length of the

tube. In other words, if a large temperature gradient is established within a tube containing air, sound waves will be produced. The frequency of sound is primarily dependent on the length of the tube. Later, in the 1850s Pieter Rijke developed a device similar to the Sondhauss tube. The main difference between the Sondhauss and the Rijke tube is that the Sondhauss tube has one end open and the other end closed, while the Rijke tube has both ends of the tube open with a metal mesh inside. The Rijke tube was held vertically and sound vibrations were observed by heating the metal mesh.

Lord Rayleigh (2) was the first to provide an explanation of the Sondhauss tube. In 1898, Rayleigh explained the essential timing of the device as follows: "If heat be given to the air at the moment of greatest condensation or be taken from it at the moment of greatest rare fraction, the vibrations are observed." He postulated that standing waves were being set up. He also noted that the phase difference between the pressure and velocity components in the standing wave was necessary to establish and maintain acoustic waves in the tubes. In the 1960s, Nikolas Rott (3) performed quantitative analysis in order to describe the oscillations within the tube. He concluded that the work produced by thermoacoustic engines is dependent on the thermal interaction between the walls of the tube (resonator) and the gas inside. He also defined the length in which these interactions occur as the thermal penetration depth. Later, Yazaki et al. (4) applied Rott's findings to experimental results of Taconis oscillations and found substantial agreement between theory and experimental observations.

Carter et al. (5) explained the importance of a stack inside the Sondhauss tube. He placed materials (the stack) inside the neck of the original Sondhauss tube and observed its performance. This resulted in the enhancement of the conversion of heat into acoustic

power. Feldman (6) extended Carters's work by writing a dissertation. Next, Rott continued his work explaining the thermal interactions between the stack and the gas inside the resonator. He defined that these interactions will occur within one thermal penetration depth, which was expressed in terms of thermal diffusivity of the gas (K), and the rate of angular acoustic wave frequency (ω), $\delta_k = \sqrt{\frac{2K}{\omega}}$. It is within this characteristic depth that heat is transferred to the gas from the solid boundary within one cycle of an oscillating frequency. The use of a stack will increase the laser's performance, because it provides a large surface area of solid boundary to thermally interact with the air. Without the stack, the interaction of the volume of air was limited to the area of the resonator walls, resulting in a lesser amount of work produced. So, the stack provides more area for heat exchange, and therefore more volume of air, increasing the performance of the laser. Later, Wheatley et al. (7) built thermoacoustic devices from the theoretical foundations laid by Rott and also concluded that the thermoacoustic process can be reversed, where sound is used to pump heat. This device is known as a thermoacoustic refrigerator. Wheatley et al. (8) successfully built a working thermoacoustic refrigerator and these devices are used to date in several applications.

The devices that we have mentioned so far use the properties of the standing waves within the tube or resonator. In the 1970s, P. Ceperley (9) proposed and built the first traveling wave thermoacoustic engine. This device converted heat into traveling acoustic waves rather than standing waves. It operated on the same principle as the Stirling cycle engine. Swift, Backhaus, and Gardener (10) continued research on traveling wave thermoacoustic engines.

Recent research mainly focuses on using thermoacoustic engine arrays, including "Coupling of mid-audio frequency thermoacoustic engines" and "A study of coupled thermoacoustic engines" by Symko et al. (11, 12). These studies focus on coupling an array of engines using both mass coupling and acoustic coupling techniques. The engines in these studies were coupled through a common cavity acting between them. Spoor and Swift (13, 14) also worked on coupling two thermoacoustic engines, but their goal was to cancel the vibrations present during operation. Their work of "Mode-locking of acoustic resonators and its application to vibration cancellation" included two acoustic resonators which were coupled using an interconnecting channel or an acoustic coupler in an effort to achieve antiphase oscillations. These antiphase oscillations within the geometry of the coupled resonators reduced the vibrations within.

The thermoacoustic laser used in this thesis is a quarter wave resonator which is open at one end and closed at the other. The essential components that make up the thermoacoustic laser that we studied include a Pyrex tube, a stack, and a working gas (air in this case). The acoustic pressure fluctuation of a quarter wave resonator is maximum at the closed end and minimum at the open end. The velocity fluctuation is opposite, with maximum fluctuation at the open end and minimum fluctuation at the closed end. Figure 1.2 shows the pressure and velocity fluctuations in the quarter wave resonator.

In a basic thermoacoustic laser, the stack is placed inside the resonator in order to maintain a sufficient temperature gradient. The temperature gradient developed across the stack is maintained large enough to generate acoustic waves within the tube. Many types of thermoacoustic lasers will work without a stack, but their performance could be greatly enhanced with the use of one. The geometry of the stack has great significance on its

efficiency. Figure 1.3 shows different common designs for the stack geometry. The stacks used in our experiments have a square tube geometry, as shown in Figure 1.4. Figure 1.5 illustrates the quarter wavelength thermoacoustic laser where heat is applied to the stack at the hot end and the cold end is cooled by radiation and the natural convection of the atmospheric air. This creates a temperature difference across the stack and establishes a temperature gradient.

For the laser to produce acoustic waves, the gas inside the tube is heated near the closed hot end and it diffuses towards the open cold end. "This diffusion of hot gas towards the cold end will result in sharp pressure pulses due to change in the pressure from hot to cold" (12). Due to the constant pressure of the air at the open end of the resonator, a wave is reflected and fed back into the resonator at its resonant frequency. This reflected wave provides "positive feedback" and thus generates the standing acoustic waves. The acoustic wave's setup in the resonator tube will force the gas in the resonator to undergo a cycle of compression, heating, expansion, and cooling. The process to get the thermoacoustic devices to produce acoustic waves is similar to the way a flute works (15). The pressure pulses created by blowing air through the mouth of a flute will produce sound. This leads to the change in impedance at the open end of the tube. This change in impedance encourages reflections of waves, thereby prompting the flute to resonate at a resonant frequency.

The oscillations in a thermoacoustic laser are nonlinear. These oscillations are maintained only when the heat is supplied continuously. Therefore, thermoacoustic lasers are known as examples of "nonlinear oscillators" (16). Also, thermoacoustic lasers are examples of "self-sustaining oscillators" (13, 14). "Self-sustaining oscillators are devices

where the force creating the oscillations is acted upon by the oscillation" (12). The classic example for self-sustaining oscillators is the Van der Pol oscillator (17). Since these thermoacoustic lasers are examples of self-sustaining oscillators, they are "neither driven, nor damped oscillators." The phase of the self-sustaining oscillator is "random at onset and it does not depend on the initial state of the system."

This thesis mainly focuses on coupling two thermoacoustic lasers. Before starting the coupling studies, we initiated our work by studying the nature of the acoustical wave produced from a single laser. Later, attention was focused on developing and testing a thermoacoustic laser pair. The main goal of this project was to acoustically couple the two thermoacoustic lasers and study the interaction between the acoustic waves generated by the coupling. Another goal is to determine if the acoustically coupled lasers will synchronize (mode-lock) in frequency and phase. Along the way, we compare the acoustic amplitude of the coupling lasers to the output from a single laser. We also study and observe different coupling setups which achieve synchronization. Various designs were tested and studied for a single laser operation from which extensive experimental data sets were collected and analyzed. Design and operation of a thermoacoustic laser pair is more complicated and difficult. The amount of thermal energy distributed among each laser for the laser pair should be approximately equal. The coordination of the two lasers will have a great impact in maximizing the total conversion efficiency. "Mode locking of two acoustic resonators" was studied by Swift and Spoor (13), and vibration cancellation by acoustic coupling was achieved by connecting the two resonators using a half wavelength tube (acoustic coupler). The "Huygens entrainment phenomenon and thermoacoustic engines" was another study by Swift and Spoor (14), and once again,

vibration cancellation was achieved using strong structural and mass coupling by welding the cases of the two engines. "Coupling mid-audio frequencies thermoacoustic engines" and "Study of coupled thermoacoustic engines" by Symko et al. (11) focus on achieving an intensified acoustic amplitude by coupling two thermoacoustic engines placed in a cavity sharing a common structure and the volume of gas. Despite all these studies on coupling multiple lasers, detailed information about the acoustic field of multiple thermoacoustic lasers is lacking and more test data are needed to integrate and coordinate the operations of thermoacoustic lasers in an array. This motivated the present investigation to study the effect of coupling and focusing the sound waves generated by two thermoacoustic lasers. The integration and coordination for the two lasers might result in an intensified coupled acoustic signal, which also attracted us to conduct this study. Laser kits provided by Penn State University were used to build two thermoacoustic lasers. The components of these two lasers should be nearly identical in their dimensions. Our approach starts off with coupling these two lasers using different configurations. These configurations were studied in order to vary the nature of the acoustic coupling between the two lasers. In our case, coupling was only through the volume of the air acting in between the two lasers and it was varied by orienting the lasers in different crossing angles and separating them at various distances. The coupling between the two lasers was started at 0^{o} crossing angle, where the openings of the lasers were parallel to each other and separated by a distance of 1 m. The next configuration was to focus the sound waves using two different crossing angles (30 and 90^{o}) between the two lasers, with their open ends placed very close to each other. The last approach was to increase the spatial distance between the opening of the two lasers which were

oriented at 30 and 90^{o} crossing angles. These 4 different configurations would give us enough data to understand the effect of coupling between the sound waves of the thermoacoustic laser pair.

We found that coupling between two thermoacoustic lasers was strong enough to allow them to synchronize (mode-lock) in particular frequency and phase. The output amplitude of the synchronized signal produced from coupling two thermoacoustic lasers was always less compared to the acoustic amplitude of a single thermoacoustic laser, suggesting out-of-phase synchronization. In a few experiments, the signals from the two acoustically coupled lasers did not synchronize because of the mistuning of the natural frequencies between them. When this happened, the uncoupled signals beat with the difference in the natural frequency. The amplitude output of the beat signal, when the two lasers were in-phase, was always greater than that of the single laser.

These findings build upon previous research by providing insight into the behavior of the signals produced by multiple thermoacoustic lasers. We were able to prove that the signals from the two thermoacoustic lasers can be synchronized (mode-locked) in a particular frequency or phase just through the volume of atmospheric air acting between them, without using any kind of a coupling mass or an acoustic coupler to physically connect the two lasers. Another important contribution is that, we observed that the beating signal amplitude is approximately twice that of the single laser, when the two thermoacoustic lasers were in-phase with each other.

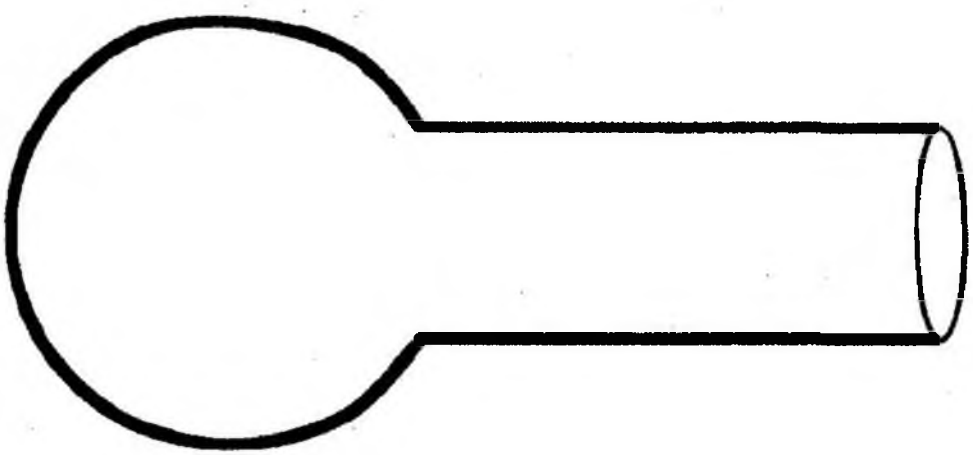

Figure 1.1: The Sondhauss tube. When heat is applied to the closed bulb end, the tube will emit sound waves at the frequency determined by the tube's dimensions.

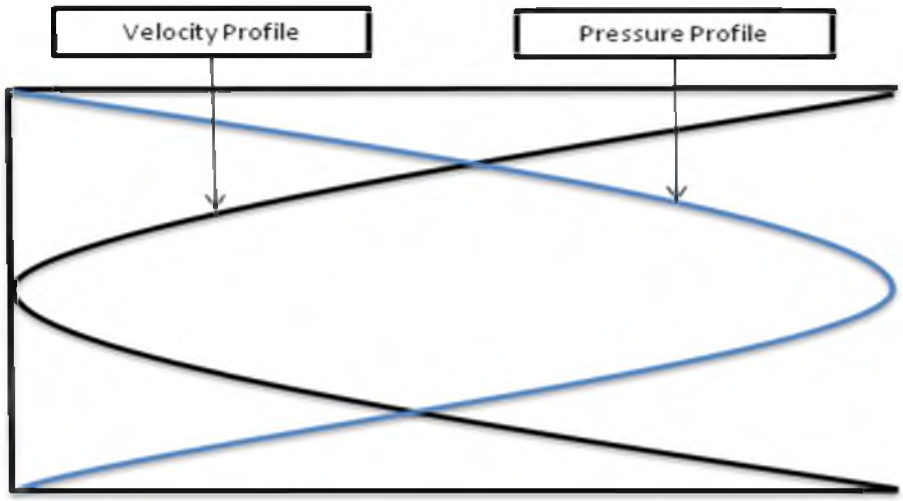

Figure 1.2: Pressure velocity diagram for a standing wave in a quarter wave resonator.

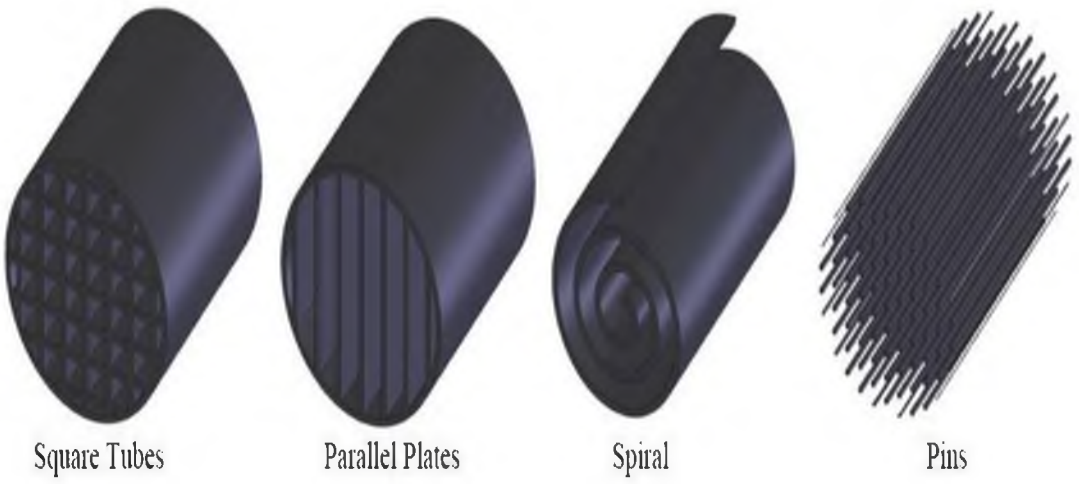

Figure 1.3: Different common designs for the stack geometry.

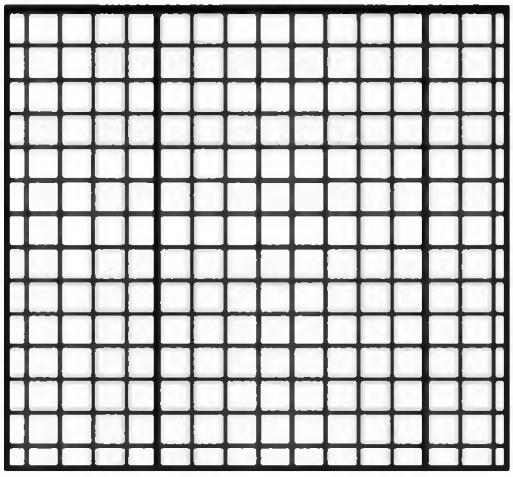

Figure 1.4: Square tube geometry of the stack.

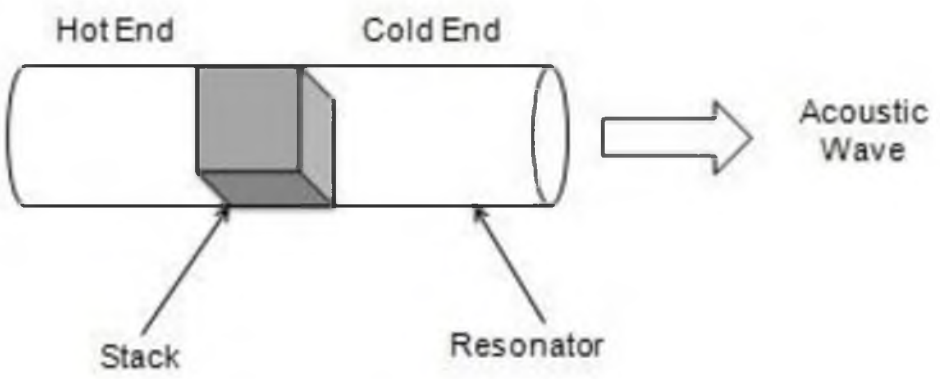

Figure 1.5: A simple quarter wave resonator with stack located in the middle of the resonator. The closed end acts as a Hot-Heat Exchanger and the open end acts as a Cold-Heat Exchanger.

CHAPTER 2

LITERATURE SURVEY

Huygens principle of coupled oscillators and synchronization was important in view of the different coupling configurations. Like other phenomena discovered accidentally, Christian Huygens did not set out to study coupled oscillators. However, he broke open a new field in physics called synchronization. In 1665, Huygens was hired by the Dutch to solve a problem at sea, keeping time to determine proper longitude of ships. In 1657, Huygens invented a steady and reliable pendulum clock using cycloid-shaped plates to confine the pendulum's suspension. He used two clocks mounted on board to ensure accurate time measurement just in case one of the clocks was to break down or need cleaning. By chance, Huygens mounted the clocks side by side on the same board in a way that they shared a common mounting (18).

Huygens noticed that there was an odd interaction between the two pendulums when hanging side by side mounted on the same board. The result was that the clocks would swing with exactly the same frequency, but 180 degrees out of phase with one another. He also noticed that, when he disturbed one of the clocks and then started it at a different phase from the other, the two clocks would return to this antiphase synchronization within approximately half an hour and remained there. Huygens investigated this strange phenomenon and wrote letters to his father explaining his

observation. Huygens (19) wrote,

> It is quite worth nothing that when we suspended two clocks so constructed from two hooks imbedded into the same wooden beam, the motions of each pendulum in opposite swings were so much in agreement that they never receded the least bit from each other and the sound of each was always heard simultaneously. Further if this agreement was disturbed by some interference, it reestablished itself in a short time.

Hugyens noticed that there was some communication between the clocks through the volume of air between the clocks. However, Hugyens observed that the clocks, when placed very close to each other but not mounted on the same board, did not synchronize. He concluded that the clocks were synchronizing only by communicating through small, undetectable forces through the board in which the clocks were mounted. Figure 1.7 illustrates the resulting behavior of Huygens' observations, where two clocks synchronize after some time, when mounted on the same board. In this case, the coupling is dependent on the mass of each pendulum and the mass of the board each was mounted to, as well as the interaction between the pendulums as a result of the conservation of angular momentum. The strength of coupling ratio is defined as a ratio of the mass of one pendulum to the mass of the entire system, including the common mounting (i.e., the board in this case).

In the last decade, many experiments and measurements have been conducted to study the coupling between two organ pipes. The coupling between two organ pipes is acoustic in nature and is through the common oscillating gas acting between them. Lord Rayleigh (2) was the first to study the coupling between two organ pipes. Later, the effects of acoustically coupling two organ pipes were also observed in detail by Bouasse (20). In both their observations, when the two organ pipes with different frequencies were brought near each other, the natural frequency of each pipe was altered. They also

observed that for strong acoustic coupling, "the two oscillators could 'kill' one or more organ pipes, a property of synchronization known as oscillation death." Many researchers used this principle of acoustic coupling from Lord Rayleigh's work and experimentally found that two organ pipes of similar frequency would entrain and behave in such a way as predicted by synchronization. One such set of experiments was conducted by Abel et al. (21) which included observations of antiphase synchronization for the first harmonic mode and in-phase synchronization for the second harmonic mode. Abel et al. (21) was able to successfully describe all the experimental observations of coupled organs in terms of synchronization. They clarified the discussion about the nature of the strong amplitude decrease for two coupled pipes, which was already observed by Lord Rayleigh. They ruled out the scenario of oscillation death and observed an "antiphase oscillation" that yields destructive interference of the acoustic waves. There are many more examples of coupled synchronization which are not of primary importance. Fireflies, cardiac rhythms, and chemical oscillations are but a few examples of natural systems that exhibit synchronous behavior and will entrain a common frequency at a stable and measurable phase difference.

Marrison (22) in 1958 was first to describe coupling between two heat-driven acoustic devices, which were joined end-to-end using a channel as an interconnection. Later "Mode-locking of acoustic resonators" and "Huygens entrainment phenomena and thermoacoustic engines" were two different coupling studies by Spoor and Swift (13, 14). Their main goal in coupling two resonators or engines was to cancel the effects of the vibrations caused during operation. They accomplished this by using an acoustic coupler developed by two different methods. One method involved a half wavelength $\frac{\lambda}{2}$ tube used

as an acoustic coupler to couple two thermoacoustic resonators. The other method was to weld two thermoacoustic cases together which resulted in coupling through the structure and mass of the system. The function of the half wavelength tube in their work is to invert the pressure between the two resonators and achieve antiphase acoustic oscillations. These antiphase acoustic oscillations would result in vibration cancellation. In order to achieve vibration cancellation (or antiphase acoustic oscillations), the coupled resonators and the acoustic coupler must favor "normal mode." An interconnecting channel (e.g. the half wavelength ($\frac{\lambda}{2}$) coupler used in Spoor and Swifts (13, 14)) is an important component required to attain strong coupling between thermoacoustic engines. The thermoacoustic engines are self-maintained oscillators; therefore, the engine pair will not naturally start and run at the same frequency, or in a particular phase, unless they are coupled strongly using some kind of coupler or interconnection.

Recently, Symko et al. (11, 12, 23) has been doing research regarding thermoacoustic engines. One of the theses, titled "Study of coupled thermoacoustic engines" (12), was a study of synchronization by coupling an array of engines using both mass and acoustic coupling. Their goal was to observe the effect of synchronization for coupled engines. Another study was "Coupling of mid-audio frequency Thermoacoustic prime movers" (11) in which the two engines were acoustically coupled through a common shared gas when attached to a common cavity. Symko's theory was to synchronize an array of thermoacoustic engines using both mass and acoustic coupling. To do so, they used two thermoacoustic engines placed in a cavity of a specific mass and volume in order to vary the effects of mass and acoustic coupling. They found that the resulting amplitude of the synchronized arrays was the sum of the amplitudes of the

individual, uncoupled engines. In Symko's work, coupling was observed only at a single orientation, when the two engines were parallel to each other and separated by a certain distance.

In this thesis, both our approach and our goals are quite different from those of the previous studies. In some of the experiments, we focused the sound waves of two thermoacoustic lasers, in order to understand the effects of coupling and determine the acoustic amplitude of the coupled sound waves. The approaches in our thesis which differentiate our work from the other coupling studies are: (1) mass coupling was not considered in our case, and the coupling was always acoustic in nature, which was through the atmospheric air acting in between the two lasers, (2) synchronization between the two coupled acoustic waves was achievable without using an interconnecting channel or an acoustic coupler, which was used in Swift and Spoors' study of "Mode-locking of acoustic resonators" (13), and (3) different configurations were used, such as focusing the sound waves of the two lasers by crossing each other at different angles. These different crossing angles between the openings of the two lasers will vary the effect of acoustic coupling between them. In the following chapters, we describe the experiments conducted to study and vary acoustic coupling, and we discuss in detail the significance of the results and findings of the various experiments.

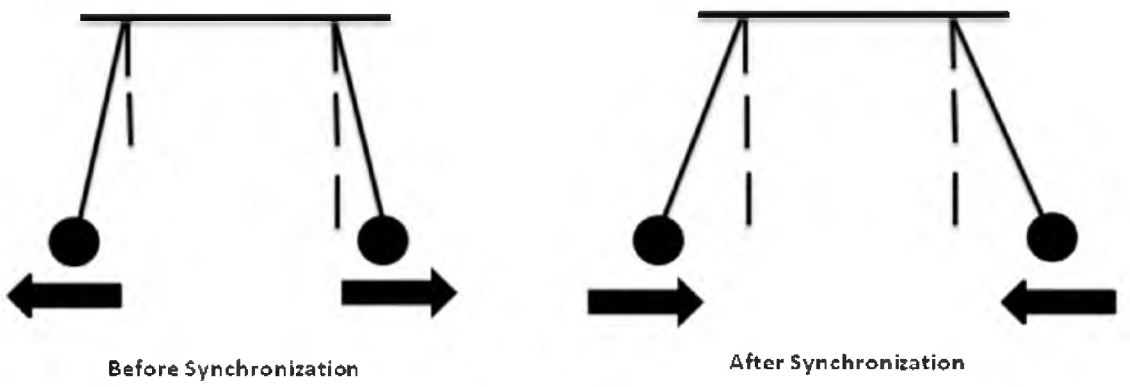

Figure 2.1: Huygens' clocks before and after synchronization.

CHAPTER 3

EXPERIMENTAL SETUP AND TESTING OF THERMOACOUSTIC LASER PAIR

3.1 Thermoacoustic Laser Fabrication

The attention of this thesis is focused on the operation and behavior of a thermoacoustic laser pair. To achieve the goal of this thesis, we break down our task into a series of investigations. We start by studying the properties of the proposed system and then describe in detail the components and fabrication of a single thermoacoustic laser. This is followed by a description of the coupling case. A typical laser used for this work is essentially a quarter wave resonator, closed at one end and open at the other end, as described in Chapter 1. Heat is applied at the closed end and the open end is cooled by natural convection in order to maintain a temperature difference across the length of the stack. In this case, air outside the open end of the tube is at constant pressure and it will provide a positive acoustic feedback and enhances the performance (16). At the open end of the laser, one of the three different devices, a sound pressure level meter, a uni-directional microphone, or an omnidirectional miniature microphone is mounted. These measuring devices were used to record sound pressure level, amplitude, frequency, and phase difference in all the experiments conducted. The microphones act as an acoustic transducer.

The thermoacoustic lasers were constructed using the laser kits provided by the Penn State University (24). These kits consisted of a 25mmx200mm Pyrex tube, a ceramic stack material, a 26-gauge nichrome (NiCr) resistance heater wire with 2.56 ohms resistance per foot, and a 24-gauge copper magnet wire with enamel insulation. To begin with, the rectangular celcor ceramic stack was reshaped into an octagonal shaped stack, using a hack saw blade. Next, 6 evenly spaced horizontal grooves of 3mm depth were made on the front face of the stack, as shown in Figure 3.1. The NiCr heater wire was adhered inside these groves. The ends of the Cu connecting wires were stripped by burning the enamel insulation. Two Cu wires were inserted through the channels of the stack and their stripped ends were twisted with NiCr wire to make good electrical contact, as shown in Figure 3.2. To ensure good electrical and mechanical connection, cylindrical crimp connectors were slipped through the twisted NiCr and Cu wires and tightly crushed. The stack adhered with NiCr wire was placed inside the Pyrex glass tube, half way between the closed and open ends. The surface of the stack with the NiCr wire winding was faced towards the closed end and was heated using an external 12-volt DC power supply. Figure 3.3 shows the layout of the thermoacoustic laser constructed using the above-mentioned procedure.

Thermoacoustic lasers similar to the one described above have been extensively studied by many researchers. Three stack designs (ceramic cube, wire mesh, and rolled metal foils) and two different heating methods (electrically heated wire and parabolic solar concentrator) were tested in Ngygen's (25) experiments. He found that the optimal position of the stack was near the middle of the Pyrex tube. This configuration alone was used in the experiments conducted in this thesis. The onset time for the standing waves

produced by the thermoacoustic laser depends on the temperature difference across the length of the stack. In experiments of Bass et al. (26), it was found that the required temperature difference for the onset of the standing waves was slightly less when the glass tube was held in a vertical position, with its open end pointing upward. This leads to better natural convection cooling of the cold end of the stack and results in a larger temperature difference across the stack, whereas in the experiments conducted in this thesis, the thermoacoustic lasers were held horizontally for the purpose of convenience. As described by Sondhauss (1), the frequency of the acoustic signal produced depends on the length of the tube. This was the same case in the thermoacoustic laser that we constructed. Once assembled and heated, each laser corresponded to a frequency of about 450-460 Hz.

A variable resistor was connected in series to a 12-volt DC power supply. This variable resistor was used to adjust the voltage difference across the NiCr wire. Since the NiCr wire used to build the thermoacoustic lasers has very low electric resistance (less than 3 Ohm per foot), the resistances of cables connecting different components in the circuit were carefully measured and taken into account in the power consumption calculation. The power consumption (P) of the NiCr wire is equal to the square of voltage drop (V) across the wire divided by the resistance (R) of the wire, as shown in the following equation. The power consumption (P) of the NiCr wire can also be calculated as the voltage (V) times the current (I) flowing in the circuit, as shown in the following equation.

$$P = \frac{V^2}{R} = V * I$$

Before each test, the resistances of the NiCr wire and the two copper wires connected directly to the NiCr wire were measured. During the experiments, the voltage difference between the two copper wires was also measured and monitored by connecting a CEN-TECH 98025 multimeter parallel to the circuit. A second multimeter was connected in series to the circuit in order to measure the flow of current. The voltage (V) and current (I), measured using the multimeters connected to each laser separately, defined the power consumed by each laser which was calculated by equation (1). The power was either increased or decreased by changing the resistance of the variable resistor which was connected in series to the thermoacoustic laser. The voltage drop across the NiCr wire was deducted from the resistance values of the NiCr and copper wires. The voltage difference between the two copper wires increased slightly when the laser was heated up, indicating that the NiCr wire resistance changes with temperature. Therefore, voltage, current, and resistance values were monitored within the circuits of both lasers to observe any change in the power consumption.

For every power input, each laser was powered with different voltages due to a difference in resistance values between the two lasers. The resistance is proportional to the length of the NiCr heater wire. We note that the variation in resistance, and hence the power supply voltage, for each laser is due to the usage of a different length NiCr resistance heater wire. We stick to the same design to construct and power the thermoacoustic laser, irrespective of the type of study done in the thesis.

3.2 Procedure for Testing Single Thermoacoustic Laser

Experiments were conducted to study the nature of the acoustic signal generated from a single thermoacoustic laser. The nature of the acoustic wave generated from a

single thermoacoustic laser was determined by measuring the sound pressure level at different distances and orientations from the opening of the laser tube. As discussed in Chapter 1, if the sound waves generated by a thermoacoustic laser are discharged into a large volume of quiescent air, the opening of the quarter wavelength tube is the node of air displacement and the antinode of pressure oscillations. Figure 3.5 shows a conceptual plot of the sound waves generated by a standing-wave thermoacoustic laser and the time variations of the air displacement and pressure inside the tube. Acoustic waves inside the tube are expected to be plane waves, with their wave fronts perpendicular to the tube axis. After exiting the tube, the waves gradually convert into spherical waves that are centered at the tube opening.

To study the nature of the spherical waves that exit the opening of the laser tube, the sound intensity was measured at various distances from the open end of the laser. Sound intensity was measured in decibels by using a sound pressure level meter oriented in three different styles: parallel, perpendicular, and at a 45^{o} angle to the axis of the laser. Figure 3.6 shows the placement of the sound pressure level meter in all three different orientations.

3.3 Experimental Setup and Procedure for Coupling the Laser Pair

Different types of systems of synchronized oscillators (Huygens clocks and Organ pipes) similar to the ones that we use in our experiments were discussed previously in Chapter 2. However, it was observed that only one type of coupling would occur: the acoustic coupling. Huygens' (18) observation of mass coupling (discussed in Chapter 1) was not observed in this case, because there was no common mass for the two thermoacoustic lasers. Since the mass (i.e., the volume of the room, measuring l*b*h.) in

which the experiments were conducted cannot be changed, mass coupling was considered negligible. Acoustic coupling was the only coupling observed in this case, which is similar to the coupling in organ pipes (21). Acoustic coupling in this study was through the common gas between the lasers and was assumed to depend on spatial distance and the angle between the two lasers.

For a system of two coupled thermoacoustic lasers, the acoustic coupling depends on different crossing configurations. To test the acoustic coupling effect, a set of experiments were designed by placing two lasers parallel to each other (0^o). The variation in acoustic coupling was also observed by focusing the waves of the two lasers, when the openings of both lasers are oriented at a particular angle (30^o and 90^o). Additional experiments were also conducted by varying the distance between the opening ends of the two lasers at a constant crossing angle (both 30^o and 90^o orientations).

3.3.1 Zero Crossing Angle (Lasers Parallel to each Other)

Two thermoacoustic lasers were positioned parallel to each other at a separation distance of approximately 1 m, as shown in Figure 3.7. The separation distance was measured from the axial center of one laser to the other. These two thermoacoustic lasers, labeled TA1 and TA2, were placed on an optical bench and heated by 20 W of electric power. Variable resistors R1 and R2 were connected in series with the lasers TA1 and TA2, respectively. As discussed previously, these variable resistors were used to adjust the voltage difference across the NiCr resistance wire in an effort to have equal power consumption for each laser. To collect the information about the system and study the interaction between the two signals, we placed the microphones near the open end of both lasers. The microphones used for reading the signals are labeled M1 and M2. They were

connected to an oscilloscope to analyze the signal, as shown in Figure 3.8. Each microphone measures the acoustic wave frequency and phase. This information was recorded over a 1-min period for both of the following cases: (1) the lasers operating alone, and (2) the arrangement of two lasers operating simultaneously.

3.3.2 30 and 90° Crossing Angles (Openings of the Lasers Oriented in a Particular Angle)

The acoustic waves of TA1 and TA2 were allowed to focus at a particular point and we note the effects of acoustic coupling in this scenario. The openings of the two lasers were placed in proximity, and directed towards each other at a particular angle. These two lasers were powered by approximately the same electrical energy inputs (P = 24.38W). The nature of the coupled signal, mainly its amplitude and frequency, was measured for the laser pair in the following situations.

a) TA1 is ON, TA2 is OFF;

b) Both TA1 and TA2 are ON;

c) TA1 is OFF, TA2 is ON.

The first setup has the two lasers TA1 and TA2 at 30° crossing angle. The acoustic intensity of the signal was measured with a sound pressure level meter placed at a distance of 4 cm from the open ends of the laser pair along the common axis, as shown in Figure 3.9. A Tenma 72-942 sound level meter was used to measure the sound pressure levels. This unit confirms to the IEC651 type 2, ANSI S1.4 type 2 for sound level meters. Specifications of the instruments used are given in the Appendix. In our experiments, we turned on TA1 first and waited until its frequency and amplitude reached a steady state. TA2 was subsequently turned on and this allowed the waves generated by TA1 to trigger

the standing waves in TA2. These effects of acoustic coupling were studied and compared to that of a single laser operating alone. Further experiments were conducted at a higher power rate of about 30 to 35 W with the sound pressure level meter placed 20 cm away from the opening of the two crossing lasers.

In order to study and observe the nature of the produced sound waves, the sound pressure level meter was replaced with microphones. The microphones were used to read the sound wave frequencies, amplitudes, and the phase angles of the two thermoacoustic lasers. Two different microphones were used. The first, labeled LM, is a unidirectional microphone having a large surface area and a diameter of 5 cm, as shown in Figure 3.10. The LM was placed at a distance of 4 cm away from the opening of the two lasers. If a large solid surface is placed close to the tube opening, the waves reflected from the solid surface may affect the standing acoustic waves inside the tube. This may extinguish the sound waves, changing the tube opening from a pressure anti-node to a pressure node. As a result, a small microphone was used in some cases. The second microphone, labeled SM, is a miniature microphone with a very small surface area and diameter of 0.5 cm, as shown in Figure 3.11. It is an omnidirectional electrot condenser microphone with a gain of -65dB. The small surface area of this microphone prevented the blocking and reflecting of the sound waves. This microphone was placed 2 cm away from the openings of the two lasers. Conclusions are made in Chapter 4 by comparing the measurements from both the LM and SM. These experiments were repeated for a large crossing angle of 90^{o} between the standing wave laser pair, as shown in Figure 3.12.

3.3.3 30 and 90° Crossing Angles, Laser Openings Separated at Various Distances

The effects of acoustic coupling of the 30° and 90° crossing lasers were studied, with varying distances between the openings of the lasers. Each time, the two lasers were moved further apart in increments of 2 cm (from 2 to 12 cm) at a particular angle (30 or 90°), as shown in Figure 3.13. The microphone (LM) was used to record the signal in this case. It was placed 4 cm away from the opening of the two lasers, at a constant position irrespective of the separation distance between them. When the lasers were further apart, the blocking and reflecting of the sound waves by the LM is minimal. This will also be the case if we choose to use the SM, since its surface area is smaller and the blocking and reflection is minimal wherever the lasers are placed.

3.4 Data Acquisition Using Lab-View

A data acquisition card was used to measure and record the amplitude, frequency, and the phase difference of the signals read by both microphones. In particular, the National Instruments DAQ card (NI 6009) was connected to the microphones. These connections and the experimental setup are illustrated in Figure 3.14. Figure 3.15 shows a picture of the DAQ card with the two channels a_1 and a_2, (positive and negative).

Lab-View signal-express was used to analyze the signals from the microphone. The sampling rate for the (NI 6009) DAQ card was set to 18k in order to maximize the number of data points used to form the sinusoidal wave form of the signals that were collected. The number of data points collected varied, and depended on the time interval for each experimental run. To evaluate some of the results, the values read by the Lab-View Signal Express were exported into Excel. Different analytical tools like Statistics,

Frequency and Time domain measurements, Amplitude and Levels in Lab-View Signal Express were used to analyze and compare the effects of coupling of the laser pair for all three crossing configurations, at different power input rates.

3.5 Experimental Considerations

The lasers used to test the acoustic coupling were identical in every aspect. There were small variations in the dimensions and mass of the stack, and in the length of the heat resistance NiCr wire and connecting copper wires. However, these were usually negligible. These lasers were replaced frequently after running a set of experiments, because they degrade over time and use. Each laser was powered up within a range of 20-35 watts of electrical power through copper wires and NiCr heater wires. Sometimes, these wires short out and break, requiring rewiring of the lasers. The lasers were also heated and cooled repeatedly, causing the ceramic stack to lose some of its mass. To counter this, the ceramic stack was replaced as and when necessary.

Correct wait time between two consecutive runs was crucial. The stack was initially heated to 150 F and it was allowed to cool down to room temperature before the next run. This was very important, as the heated stack can affect the acoustic behavior of the lasers. The wait time used was approximately 60 min.

In a few experiments, the 24-gauge copper magnet wire was replaced with a 26-gauge one. This wire had a smaller cross section. Recall that in our experiments, the copper and the NiCr resistance wires were heated with 30 W of electric power. The high power consumption degrades the 26-gauge wire quicker than the 24-gauge one, which negatively affects the experimental setup. This calls for proper care of every component used in the experiments.

Finally, an important design consideration was to replace the laser tube containing the ceramic stack, because there is a chance for the tube to deform due to rapid heating and cooling. As a result, the quality of the laser can be greatly affected and there might be a need replace the tube of the laser. Great care was taken to prevent the above-mentioned laser problems. For result reproducibility, a large number of experimental scenarios are required. This wore out the lasers and therefore, they were frequently replaced.

3.6 Acoustic Theories and Models

Acoustic theories have been used to calculate and analyze the acoustic waves both inside and outside the glass tube (27). The wavelengths and frequencies of the acoustic waves generated by standing-wave thermoacoustic lasers of identical length should be nearly the same, since they depend primarily upon the tube length. The amplitude of the acoustic waves, on the other hand, depends on the power consumption of the electric heater and the position and temperature gradient of the ceramic stack. At the focusing point of a thermoacoustic laser pair, the sound waves generated by two thermoacoustic lasers can be expressed as (25, 27), $p_1' = A_1 \cos(\omega_1 t)$, $p_2' = A_2 \cos(\omega_2 t + \phi_{21})$,where p', A, ω, and ϕ correspond to the pressure perturbation, amplitude, frequency, and phase angle of the sound wave, respectively. We can use superposition to combine the waves, $p' = p_1' + p_2'$, If $\omega_1 = \omega_2$, the root mean square value of the pressure perturbation of the combined wave is, $p_{rms}' = [\frac{A_1^2}{2} + \frac{A_2^2}{2} + A_1 A_2 \cos(\phi_{21})]^{\frac{1}{2}}$, where p_{rms}' is the root mean square of p'.

The sound pressure level and energy density can be computed from the following equations (26, 28), SPL (in decibels) = $20\ \log_{10}(p'_{rms}(\text{in Pa})/20^{-6}$, $e = 0.5\rho_0 \text{v}^2 + 0.5p'^2/(\rho_0 C^2)$.

3.7 Synchronization and Mode-Locking Phenomena

Two self-maintained oscillators, such as pendulum clocks, organ pipes, or thermoacoustic lasers, can alter each other's frequencies enough to lock in frequency and phase if they are sufficiently coupled. When the difference in natural uncoupled frequencies (also called detuning) is large, the coupling is weak and the oscillators "beat" at a different frequency like the coupled maintained acoustic oscillators (13). As detuning decreases or as the coupling increases, the beat slows down and eventually stops, at which point the lasers are locked. The change in frequency of one laser depends on its phase relative to the other, so the locked state at a particular detuning is characterized by a corresponding phase difference between the two lasers. In general, the amplitude of waves also depends on the phase difference and there can be a net flow of energy from one laser to the other if the amplitudes are not equal (14). In any state where coupling is strong enough to lock the lasers, they do not beat.

We use the following notation (14) for two lasers that are synchronized or mode-locked.

$$\Theta_1(t) = \Re\{\Psi_1(t)e^{i[\omega t+\phi_1(t)]}\ ,$$

$$\Theta_2(t) = \Re\{\Psi_2(t)e^{i[\omega t+\phi_2(t)]}\}\ ,$$

where the $\Re\{\}$ operator retrieves the real part $\Theta_{1,2}$ refer to displacements, pressures, velocities, or any other similar variables of interest that depend on time *t*. We assume that the amplitudes $\Psi_{1,2}$ and the phases $\phi_{1,2}$ are real and vary slowly compared to the angular frequency ω. The locked and synchronized state is characterized by the relative phases between the lasers and the ratio of their amplitudes, which are respectively given by, $\phi = \phi_1 - \phi_2$, $\zeta = \frac{\Psi_1}{\Psi_2}$. TA1 and TA2 have natural frequencies ω_1 and ω_2, respectively. When the lasers are uncoupled, the difference in the lasers' uncoupled natural frequencies is given by a mistuning or detuning factor; $\Delta\omega = \omega_2 - \omega_1$.

3.8 Error and Uncertainty Analysis

Uncertainty analysis of the experimental measurements was performed using the methods and procedures outlined by Kline and McClintock (25, 28). All the uncertainty estimates were based on 95% confidence levels. We made uncertainty estimates for various parameters that include the following: lengths, distances, and angles that are a part of the design; voltage, current, and resistance that are used to power the setup; sound pressure level, amplitude, and frequency that are important parameters measured during the experiment. The factors and their uncertainty intervals are given in Table 3.1. For factors such as separation distance and crossing angle, the uncertainty interval was assumed as given in Table 3.1. For other factors, Manufacturer's specifications were used to record the uncertainty intervals. These include sound pressure level and voltage.

A theorem from Kline and McClintock (28) was also used to determine the uncertainty in the calculation of power input to the thermoacoustic laser. The uncertainty values are given by, $w_P = [\left(\frac{\partial P}{\partial V}\right)^2 * w_V^2 + \left(\frac{\partial P}{\partial R}\right)^2 * w_R^2]^{\frac{1}{2}}$, where P is the power

calculated from V and *R*. Recall that V is the voltage difference across the NiCr wire and R is the resistance of the wire and w_P, w_V, w_R denote the uncertainties in power, voltage, and resistance, respectively. The uncertainty of power input varies from "11.5 to 8.2% for *P* from 18.9 to 37.4 W" (25).

The multimeter was calibrated for a 12-volt DC power supply. The sound pressure level meter and the omnidirectional miniature microphone (SM) have been calibrated recently by the manufacturer with a one year warranty of accuracy.

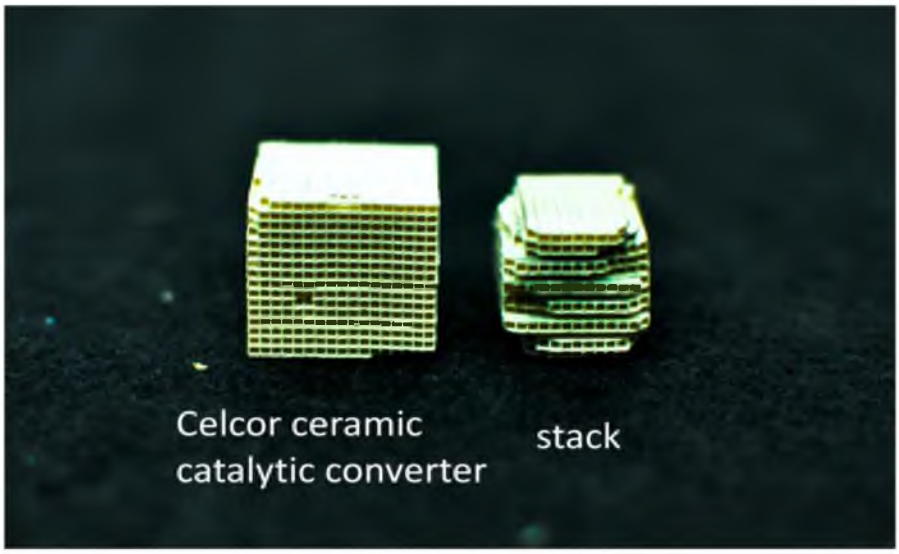

Figure 3.1: Ceramic stack was reshaped into an octagonal shaped stack.

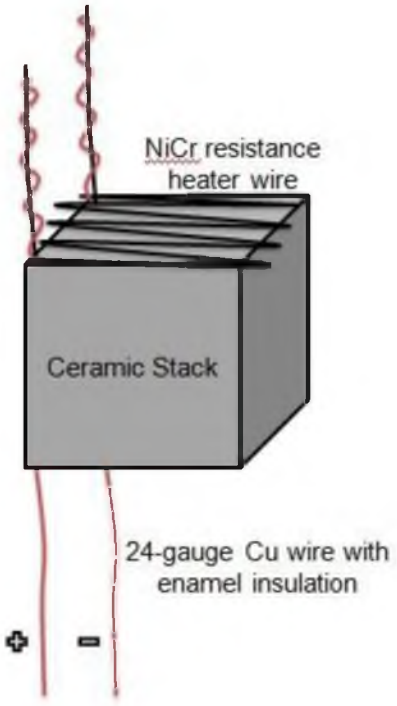

Figure 3.2: 26-gauge NiCr heater wire adhered to one end of the ceramic stack and wound around the Cu wire leads.

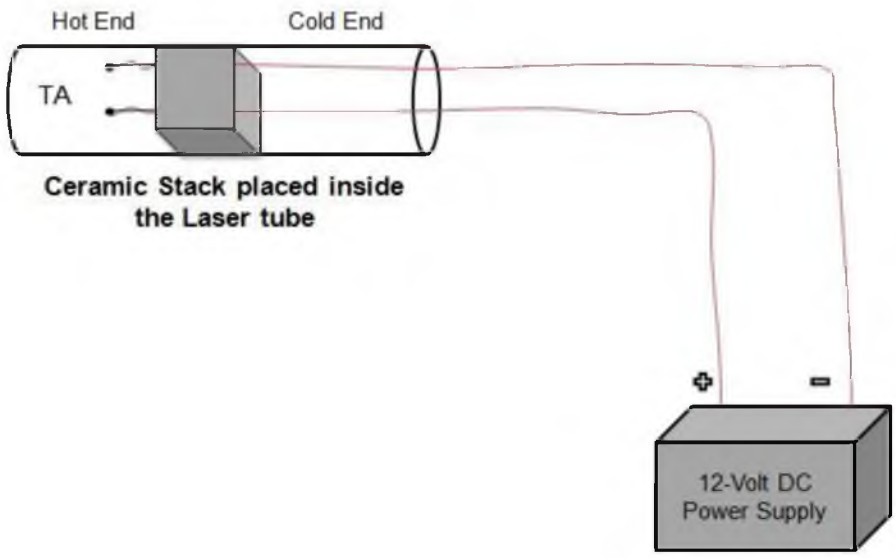

Figure 3.3: A Thermoacoustic laser powered by a 12-volt DC power supply.

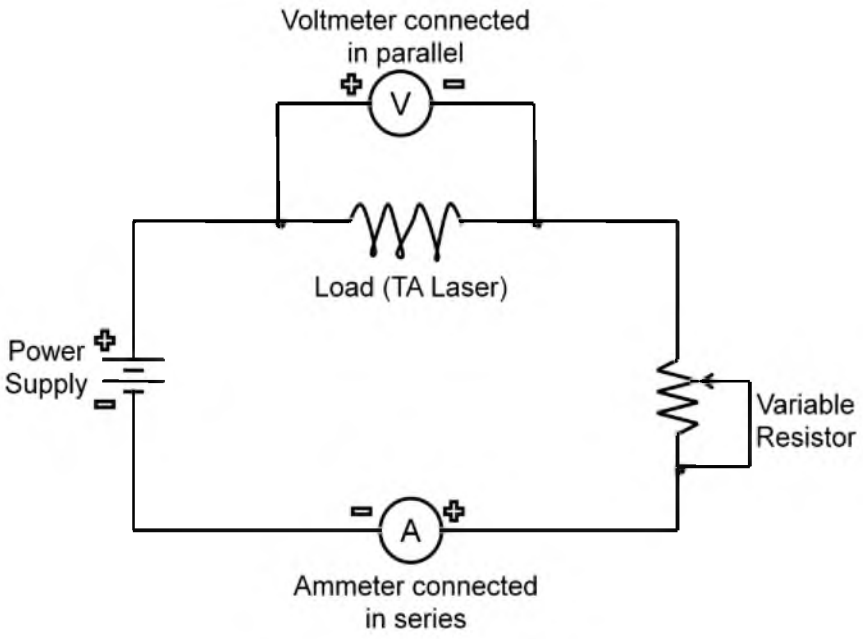

Figure 3.4: Circuit diagram showing the connections made to power up a single thermoacoustic laser. The variable resistor is connected in series to the thermoacoustic laser. Multimeters are connected to measure voltage and current within the circuit.

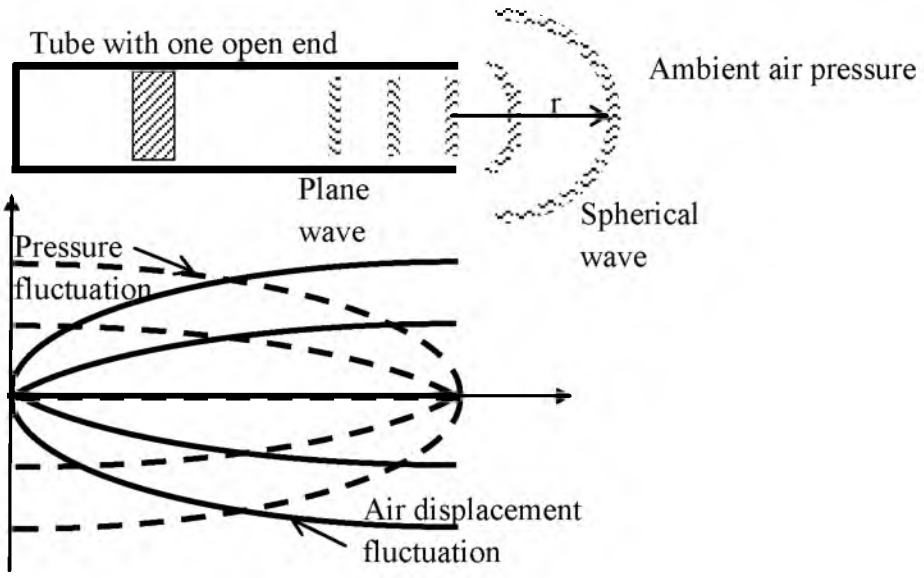

Figure 3.5: Conceptual plot describing the velocity and pressure fluctuations in a quarter wave resonator (25).

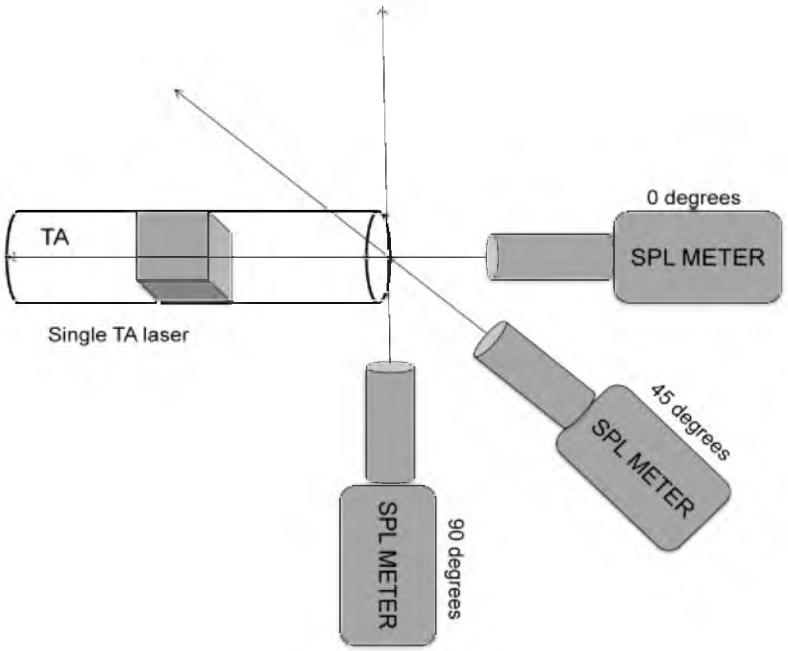

Figure 3.6: Sound pressure level meter used to measure the pressure level in all three orientations and various distances from the open end of the laser tube.

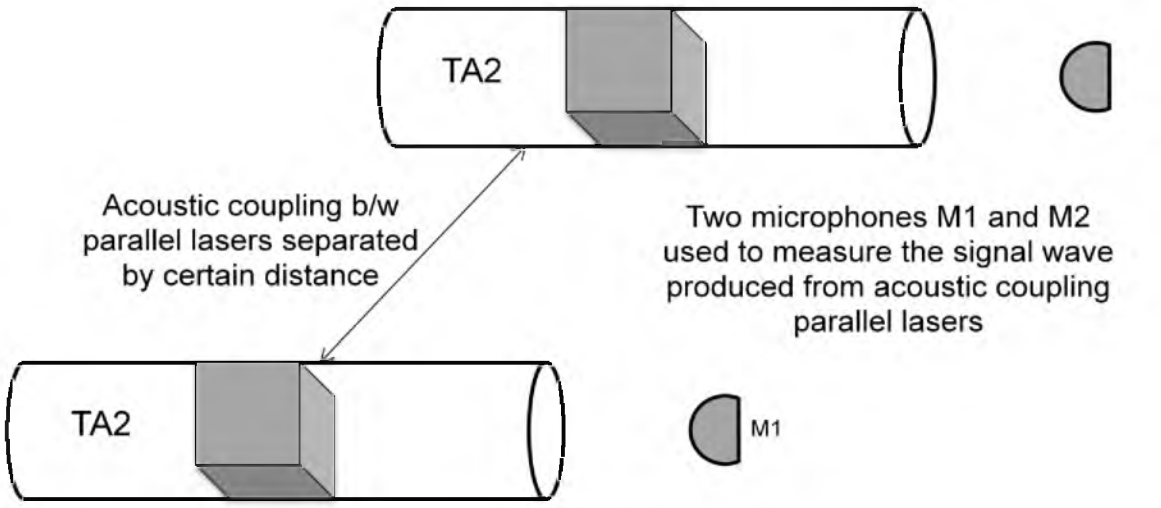

Figure 3.7: Two thermoacoustic lasers placed parallel to each other, separated by a distance of 1 m.

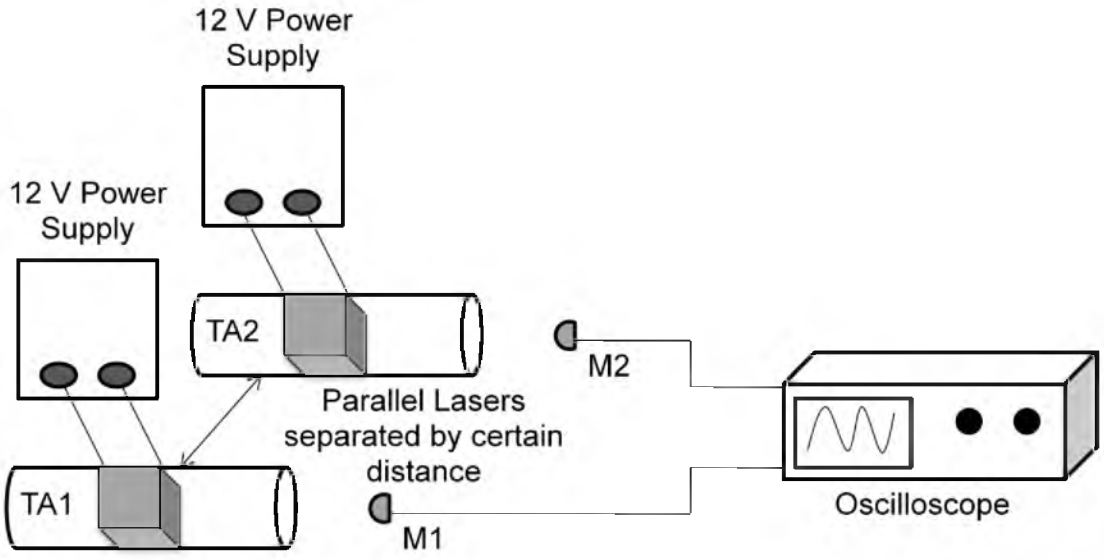

Figure 3.8: Experimental setup for studying the interaction of the sound waves from two lasers which are placed parallel to each other (0^o crossing angle).

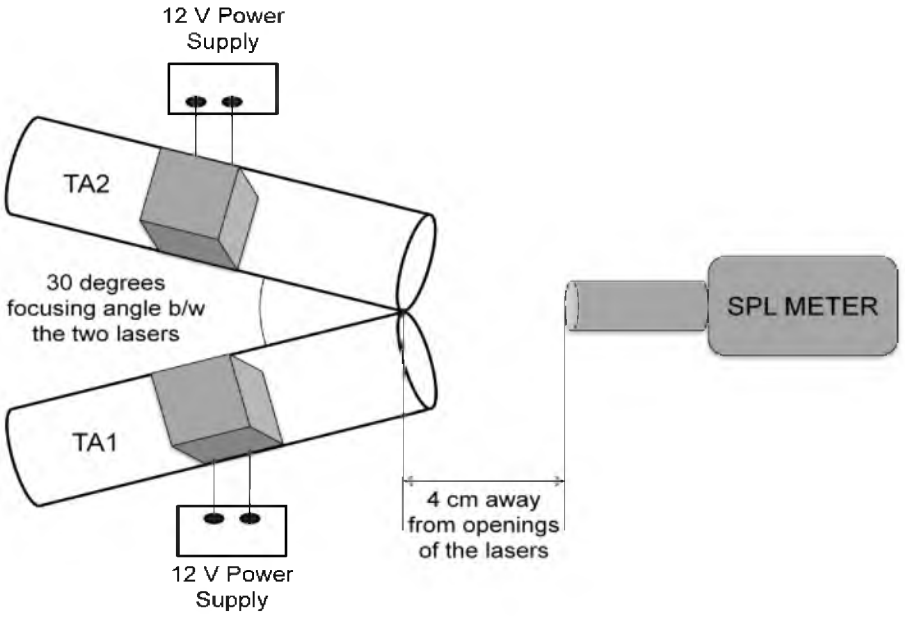

Figure 3.9: The Sound Pressure Level meter used to measure the pressure level for the 30^{o} crossing laser pair.

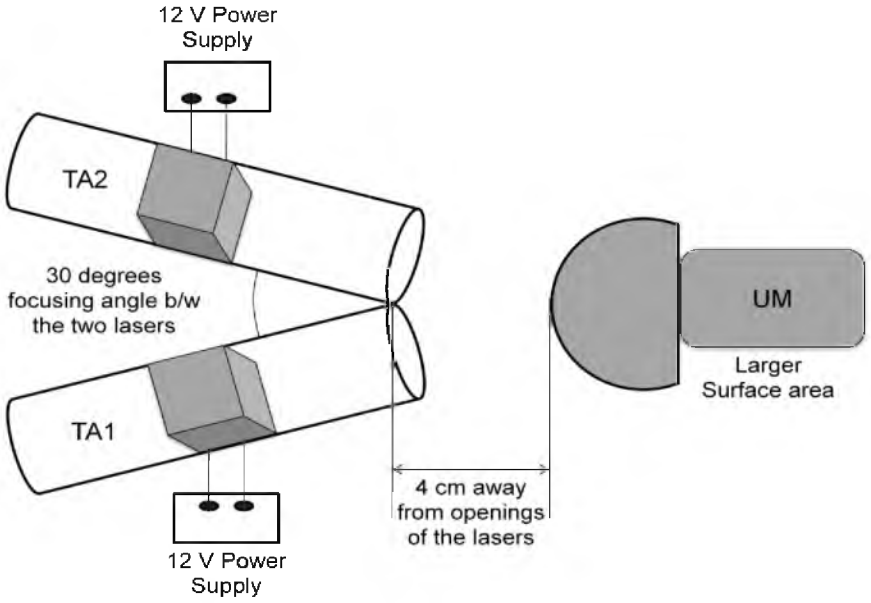

Figure 3.10: The unidirectional Larger Surface area Microphone (LM) used to measure amplitude, frequency, and phase for the 30^{o} crossing laser pair.

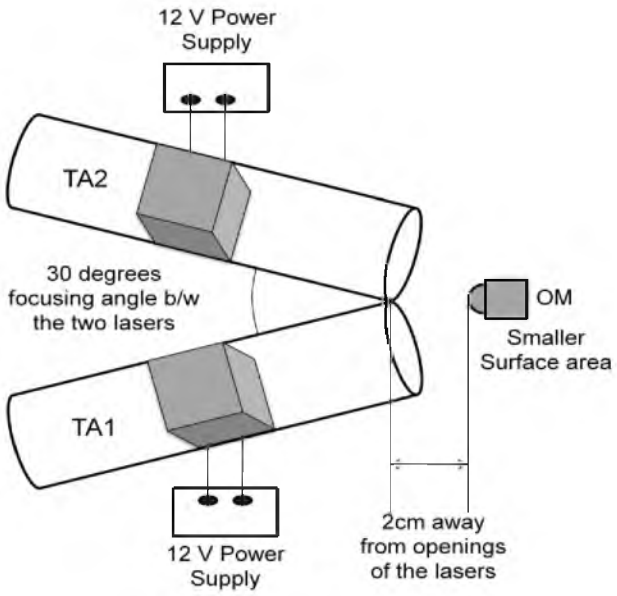

Figure 3.11: The omnidirectional Small Surface area Microphone (SM) used to measure amplitude, frequency, and phase for the 30^{o} crossing laser pair.

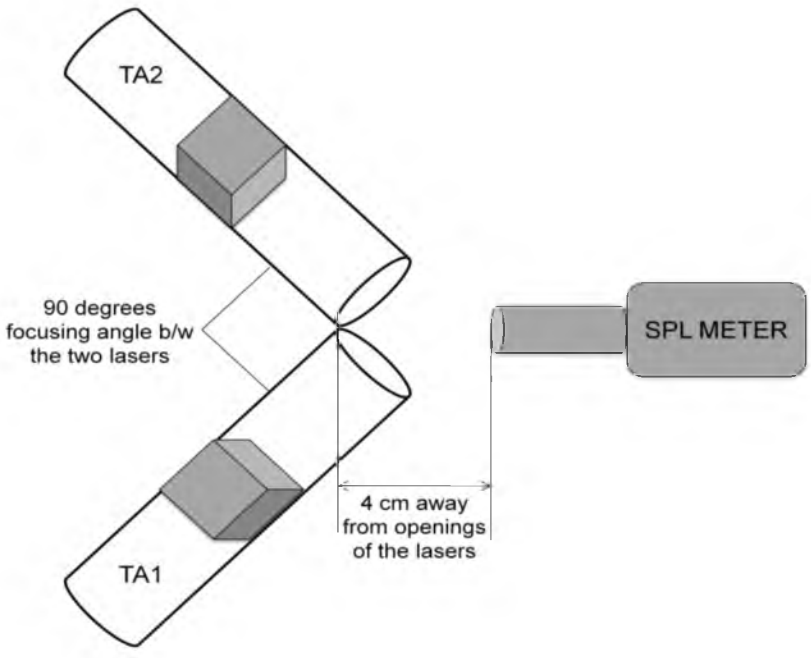

Figure 3.12: The Sound Pressure Level meter used to measure the pressure level for the 90^{o} crossing laser pair.

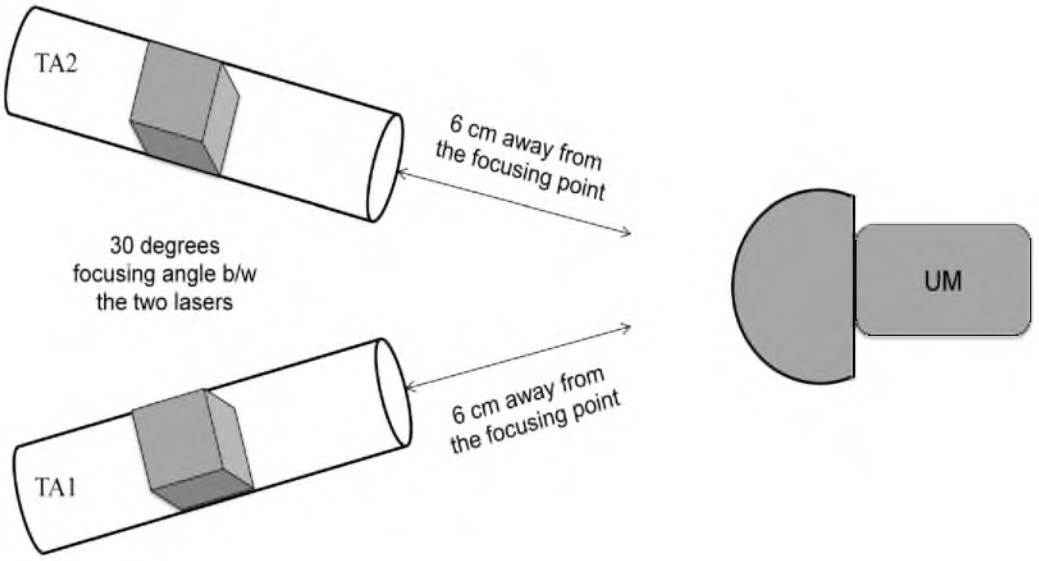

Figure 3.13: The microphone (LM) used to measure amplitude, frequency, and phase for 30^{o} crossing lasers, when the openings of the lasers were separated by varying distances. (6 cm in this case)

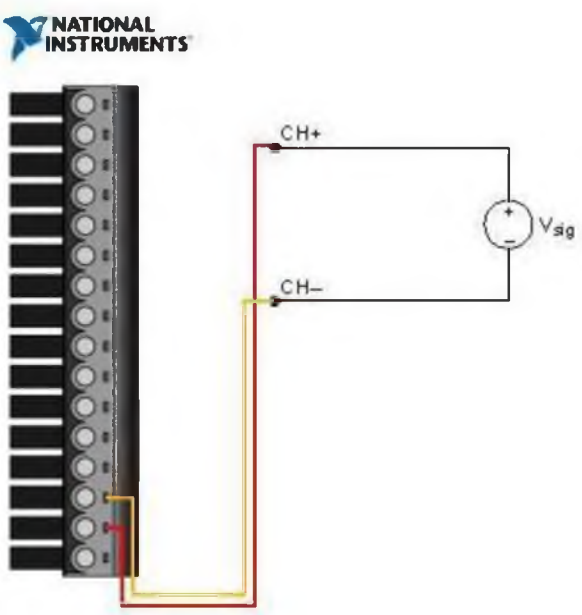

Figure 3.14: Schematic of the NI6009 DAQ card with the connections.

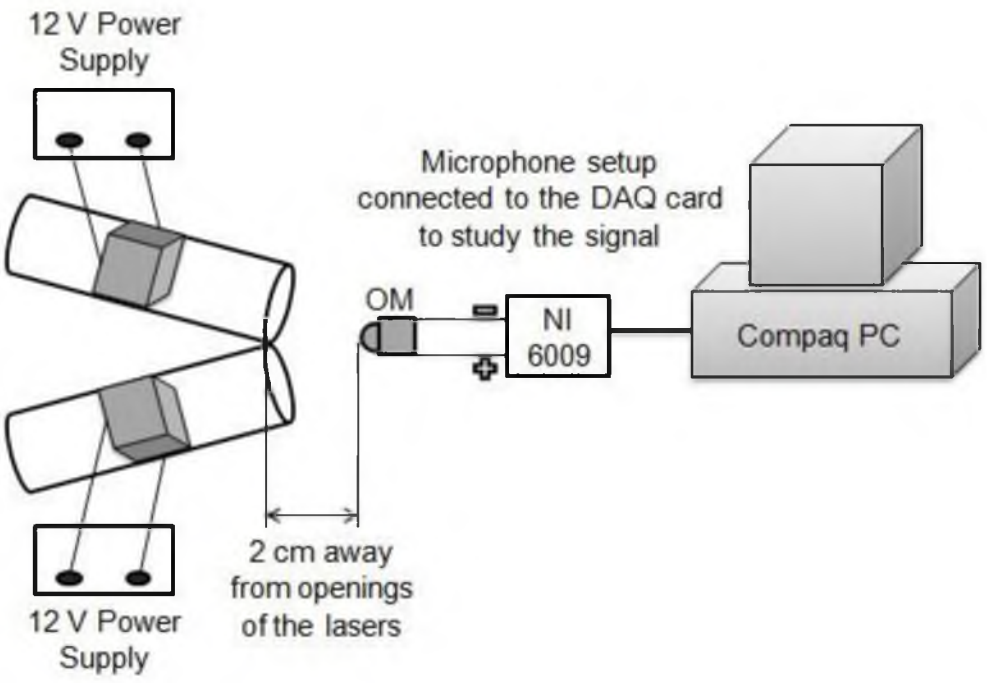

Figure 3.15: The experimental setup for studying the interaction of the sound waves from the two lasers which are crossing each other at 30 and 90^{o}.

Table 3.1: Uncertainty factors and their tolerances.

Important Uncertainty Factors and their intervals (tolerances)	
Uncertainty Factors	*Intervals*
Length of NiCr Heater Wire	0.002 m
Separation Distance	0.002 m
Crossing Angle	2^{o}
Voltage	0.25 V
Resistance of NiCr Heater Wire	0.017 Ω
Sound Pressure Level	1.5 dB

CHAPTER 4

RESULTS AND DISCUSSION

4.1 Testing Single Thermoacoustic Laser Results

The previous chapters presented a description of the thermoacoustic laser, its properties, synchronization theory, and the equipment used in the experiments. In this chapter, we present the results from the experiments and discuss them in detail. Conclusions are drawn from the collected data as pertinent to various applications of synchronized thermoacoustic lasers. As previously described in Chapter 3, sound pressure levels for an operating single laser at different orientations (0, 45, and 90 degrees) and distances were measured, in order to study the nature of the spherical waves produced at the open end of the laser tube.

Figures 4.1 and 4.2 depict the variations in sound pressure levels for the three different orientations and two input power rates. The sound pressure level at the open end of the laser tube was about 120 dB for an electric power input of 25 W. In both cases, the sound pressure level decreased by 20 dB for each increment of 2 cm, from r = 2 cm to r = 20 cm. This confirms that the pressure level of the sound waves generated outside the laser tube decreases with distance according to 1/r (given by the inverse distance law) (29). These sound waves are almost independent of the direction except in the close vicinity of the tube opening, where the plane waves turn spherical, as described in

Chapter 3 (25).

The pressure levels recorded at different orientations show that the pressure variations differ only slightly. The pressure level was the highest when the sound pressure level meter was placed in the axial direction close to the open end of the laser tube. The sound intensity varies from high to low with respect to changing the orientation from 0 to 90^{o}. Note that this happens only when the sound pressure level meter was palced close to the open end of the laser tube. However, in all three orientations, at any distance greater than 10 cm from the open end of the laser tube, the sound intensities were almost the same.

Previously, researchers have experimented with a similar thermoacoustic prime mover with a 72.7 cm long tube that had a radius of 4.32 cm. They recorded a sound level of over 140 dB with a frequency of 116 Hz. The sound intensity of their prime mover is high when compared to the thermoacoustic laser used in this thesis. This was mainly due to the larger tube they used. Chen and Garrett[30] used sunlight collected by a 1 m diameter Frensel lens to drive a simple quarter wave thermoacoustic laser. This laser measured 120 dB of acoustic pressure level at a distance of 1 m from the open end of the laser tube on a clear day. The experiments of Chen and Garret are highly relevant in today's energy considerations since they use a renewable source of energy (25).

As seen in both Figures 4.1 and 4.2, at r = 0.4 m, there was a slight increase in pressure level. We conjecture that this could be due to either the reflected sound waves or phase differences between harmonics. Arnott et al. (31) found that the sound pressure level of the fundamental mode of the laser that they used in their experiments monotonically decreases with distance, while this is not always true for higher harmonics.

For instance, at a harmonic of about 225 Hz, the sound pressure level at 0.343 m was almost 15 dB higher than that at 0.172 m (25) . From all experiments, it was observed that every measurement was the same when the laser is powered high as compared to low, except for a slight increase in the sound pressure levels.

4.2 Acoustic Coupling Results

4.2.1 Zero Crossing Angle

This experiment was designed to study the interaction between the sound waves by coupling the signals of two thermoacoustic lasers placed parallel to each other and separated by 1 m distance (zero crossing angle). The experimental setup for this test is as described in Section 3.2.1. Recall that two microphones, M1 and M2, were used to measure and record frequency and phase. The data recorded for this coupling were compared to that of a single thermoacoustic laser. A third microphone, LM, was also placed at the center of the separating distance between the two lasers. This microphone has a larger recording surface area and therefore, it was not used to read the frequency and phase difference close to the laser tube opening because it would end up blocking and reflecting the waves.

The frequency of the thermoacoustic laser is entirely dependent on the length of the tube (1). Because the tube lengths of both lasers are equal, the frequency measurements from the three microphones are almost identical. The only factor that can change is the wavelength of the sound waves due to the variation in the air temperatures within the laser tubes. However, if the power consumption rates and the resistance wire lengths are almost identical and both lasers have reached steady state operation, the

average air temperatures in the two lasers should be very close and the wavelengths of the sound waves should be about the same (25).

Figure 4.3 and 4.4 show the signals read by M1 and M2. The signal recorded by M1 was stationary on the oscilloscope screen, because the oscilloscope was triggered using signal read from M1. The arrows in both Figures 4.3 and 4.4 indicate the movement of the signal read using M2. This movement indicates the phase change of the signals periodically going from in-phase to out-of-phase. As shown in Figure 4.4, at a particular time, the two signals will couple with each other in such a way that causes constructive interference. In all the experimental runs, synchronization was not observed by acoustically coupling the signals of TA1 and TA2. This was mainly due to the spatial distance between the two lasers. When the lasers are far apart, they operate with their separate natural frequencies. This will cause the signals to "beat" at the difference frequency. The atmospheric air between the lasers also acts as resistance and it does not allow the signals to couple in a single phase, increasing the "detuning." When the separating distance between the two lasers is larger, the detuning is increased and the coupling becomes weaker. Therefore, in this particular case, synchronization or phase locking between the parallel lasers was not observed.

The change in amplitudes at the two different phase angles are opposite in nature. The amplitude increased slightly when the acoustically coupled signals of the two lasers were in-phase with each other, while it decreased when the signals were out-of-phase. The same phenomenon was observed with the third microphone. The arrows in Figure 4.5 indicate that the amplitude of the signal recorded by the LM oscillates between its

maximum and minimum values when the phase difference between the signals of the lasers TA1 and TA2 changed from 0 to 180 degree.

4.2.2 Small Crossing Angle (30^o)

This experiment was designed to study the interaction between the sound waves of two thermoacoustic lasers when their openings are very close to each other and the angle between their longitudinal axes is 30^o (see Figure 3.8). The initial results discussed in this section are collected using a sound pressure level meter. The phase difference Φ_{21} does not change with time and the sound pressure level remains constant. As shown in Figure 4.6, the sound pressure level at the focusing point when both lasers were switched on is lower than the sound pressure level when only one laser was turned on. This indicates that the phase difference between the two sound waves does not change with time and is close to 180 degrees.

When TA1 is turned on first, the large velocity fluctuation at its opening triggers the sound wave excitation of TA2. The frequency of laser TA1 is sensitive to the conditions at its open end. When the open ends of both lasers TA1 and TA2 are close to each other, they interact and alter each other's frequencies enough to phase lock. In order for this to occur, the natural frequencies of the lasers TA1 and TA2 should be approximately the same.

As shown in Figure 4.6, the sound pressure level drops when the two sound waves are synchronized, because the air expelled out of TA1 corresponds to a positive air displacement and the air displacement in TA2 is negative. The acoustic pressure oscillations at the opening ends of the two lasers are out of phase (13), thus encouraging

an opposite movement of gas in each laser. This explains why the pressure oscillations of the two waves cancel each other and the sound pressure level at the focusing point was low when both lasers TA1 and TA2 are turned on.

After the sound pressure level measurements, we replaced the sound pressure level meter with the microphone (LM) in order to study the nature of the coupled signal. Figure 4.7 illustrates the signal recorded when only a single laser TA1 is running and Figure 4.8 illustrates the signal recorded when both lasers TA1 and TA2 are running. As shown in Figure 4.8, the signals beat and they never lock in phase. This is due to large detuning caused by the reflecting wave from the solid surface of the LM. When the LM is close to the openings of the two lasers, sound waves are blocked and reflected back. This reflected wave affects the standing acoustic waves inside the tube. Thus, the natural frequencies of both lasers change, causing detuning. This detuning results in weak coupling between the lasers and as a result, these uncoupled lasers beat at the difference frequency. This is very similar to the case of coupled, maintained acoustic oscillators (13). Figure 4.8 shows the unlocked signal, where we can see that the signals beat, changing the phase from in-phase to out-of-phase at regular intervals. The amplitude increases when the two lasers couple in-phase and the amplitude decreases when they are out-of-phase. The amplitude recorded when the signals coupled in-phase was 63 mill volts, which was twice the amplitude of 31 mill volts recorded for a single laser operation. This demonstrates the effect of reflecting waves caused by the larger surface area of the LM.

The time variations of the phase angle recorded from the LM do not agree with the measurements of the sound pressure level meter. This is because of the smaller

surface area of the sound pressure level meter compared to the LM. The sound pressure meter has a lesser impact in blocking and reflecting back the waves. Therefore, the signals collected using the sound pressure level meter do not beat and they lock and synchronize in a particular phase. To support the sound pressure level measurements and eliminate the effect caused by the reflecting wave, we replaced the LM with a miniature microphone (SM). This was to minimize the reflecting wave and therefore decrease detuning between the two lasers.

Before we started using the SM, a sound pressure level meter was again used. It was placed at 20 cm away from the openings of the two lasers in order to avoid the reflections caused by its surface area. In this case, the lasers had higher power ratings, with TA1 and TA2 running at 32.4 and 34.3 W, respectively. We started by switching on TA1 and recorded a sound pressure level of 95 dB. A few seconds later, while TA1 was still running, we switched on TA2, but the signals did not immediately lock in frequency and phase. Initially, the signals were beating, with increasing and decreasing sound pressure level. When the lasers beat at the difference frequency, the highest sound pressure level recorded was approximately 100 dB. This beating of the initial unlocked signals was only observed for the first few seconds of the 2 min experimental run. After both lasers ran for a few seconds, they locked in frequency and phase. The sound pressure level for the locked signal kept decreasing until it reached a minimum steady value around 80 dB. Figure 4.9 shows this decrease in the sound pressure level when both lasers were running. This indicates that the phase difference between the two sound waves is close to 180 degrees.

In order to capture the time taken to achieve synchronization, the sound pressure level meter was replaced with an omnidirectional miniature microphone (SM). The SM also measures the frequency, phase, and amplitude of the signals. These readings were compared with those obtained from the sound pressure level meter. Figure 4.10 (a) and (b) illustrate the signal recorded when only laser TA1 is running. Maximum amplitude recorded in this case is 76.5 mill volts. Figure 4.11 (a) illustrates the signal recorded when both lasers TA1 and TA2 are running. In this experiment, we first switch on TA1 (powered with 32.4 W) and later TA2 (powered with 34.3 W). Synchronization was not observed immediately, because the signals do not lock in frequency and phase. The signals beat for the first 15 seconds (approximately) of the 2 min experiment run. In order to understand the nature of this beating signal wave form, the time interval is reduced to 0.240 seconds, as shown in Figure 4.11 (b). After running both lasers TA1 and TA2 for 15 seconds, the beat frequency slows and then abruptly stops, at which point the two lasers lock in a particular frequency and phase. Once synchronization was achieved, the signal amplitude decreased gradually, as shown in the latter half of Figure 4.11 (a). To observe the nature of the synchronized wave form, the time interval is reduced to 0.240 seconds, as shown in Figure 4.11 (c). The amplitude recorded for the synchronized signal when both lasers were operating was smaller than the amplitude recorded when only laser TA1 was operating. This implies antiphase synchronization.

We conducted an additional experiment by turning on TA2 (powered with 34.3 W) first and later TA1 (powered with 32.4 W). Figure 4.12 (a) illustrates the signal recorded when both lasers TA1 and TA2 were running. In this particular case, the signals beat during the first 40 seconds (approximately) of the 2 minute experiment run. This was

25 seconds longer compared to the previous case. In order to observe the nature of the beating signal, the time interval is reduced to 0.240 seconds, as shown Figure 4.12 (b). After running both lasers for 40 seconds, the beat frequency once again slows and then abruptly stops, at which point the two lasers lock in a particular frequency and phase. The amplitude of the synchronized signal decreased gradually, as shown in the latter half of Figure 4.12 (a). In order to observe the nature of the synchronized signal, the time interval is again reduced to 0.240 seconds, as shown in Figure 4.12 (c). Figure 4.13 illustrates in detail the time taken to achieve synchronization in both of the previously described experiments (TA1 turned on before TA2 and TA2 turned on before TA1), and also shows that the maximum amplitude recorded for a synchronized signal is less than that of the uncoupled signal, implying out-of-phase synchronization.

The difference in the time required to achieve synchronization for the above two experiments can be explained by the different power ratings of the two thermoacoustic lasers. TA2 has a slightly higher power rating and therefore, when it is turned on after TA1, its sound wave is able to produce a constant oscillation relatively quickly. At this point, it will start coupling with the already oscillated sound wave of TA1 and eventually synchronize. Conversely, the sound wave generated by TA1 required more time to reach a constant oscillation, resulting in delayed coupling and hence delayed synchronization. In order to achieve faster synchronization, the ratio of the amplitudes ($\zeta = \frac{\Psi_1}{\Psi_2}$) should be close to 1, or in other words, the amplitude outputs of the two lasers should be the same ($\Psi_1 = \Psi_2$). We observed relatively delayed synchronization in both of the previous cases. A slight variation in the temperature of the oscillating gas (air) in these two lasers caused by the different power ratings will enable the difference in natural frequencies ($\Delta\omega$).

Therefore, detuning between the two lasers becomes larger, which will result in delayed synchronization.

Another important explanation for delayed synchronization is due to the mismatch of the initial frequencies of the two lasers. Shown in Table 4.1 are the fundamental frequencies of the two lasers TA1 and TA2 (operating individually) at different time intervals during the experimental run. When we tried to couple the sound waves of TA1 and TA2, which were operating with their fundamental frequencies, it required a certain amount of time for the two lasers to match their frequencies ($\omega_2 = \omega_1$). So, in other words, when the difference between the two lasers' fundamental frequencies ($\Delta\omega = \omega_2 - \omega_1$) is approximately equal to zero, they synchronize. In the two previously described experimental runs, in which one laser was turned on before the other one, the time required to obtain synchronization was dependent on which laser was switched on first. The laser with the higher power rating ramps up its ω at a higher rate; therefore, when laser TA2 is turned on after TA1, the two lasers reach a common ω in a shorter amount of time, as compared to the opposite scenario (turning on TA2 before TA1). This point is graphically represented in Figure 4.14, in which the fundamental frequencies of the two individually operating lasers are shown on the same plot. The start time for TA2 is artificially shifted to be roughly 10 seconds later than that of TA1. As a result, the time required for the two lasers' fundamental frequencies to match (synchronize) was close to 15 seconds, which is in agreement with our previously discussed experimental observations.

Recall that we used the Frequency and Time domain measurements in Lab-View Signal Express to analyze the results. When we playback the recorded signal in both

cases described above, we observe that the frequency and period of the uncoupled beating signal tried to change and alter until it locked. Once locked, the frequency of the coupled signal is read approximately at 450 Hz, as shown in Figure 4.15. These measurements indicate that before the signals from TA1 and TA2 lock in a particular frequency and phase, they alter each other's frequencies, causing detuning between the lasers. The detuning and its period of occurrence totally depend upon two factors: (1) the time taken for the difference between the fundamental frequencies of the lasers TA1 and TA2 to equal zero ($\Delta\omega = \omega_2 - \omega_1 = 0$), and (2) the time taken for the amplitude ratio ($\zeta = \frac{\Psi_1}{\Psi_2}$) between the two lasers TA1 and TA2 to reach a value of 1±0.038.

We also computed the total harmonic distortion percentage (THD%) for the uncoupled signal from TA1 and compared it with the THD% of the synchronized signal from lasers TA1 and TA2. We made the observation that the THD% for an uncoupled sound wave was around 3% at the start and it remained approximately the same till the end of the experimental run, whereas the THD% for the antiphase synchronized sound wave increased from approximately 6% to a range between 20 and 40%, as can be seen in Figure 4.16.

Comparing measurements made using both the LM and SM microphones, we conclude that the observations made using the SM are comparable to the measurements made using the sound pressure level meter. Figure 4.6 represents the measurements of the sound pressure level at a lower power input rate and Figure 4.9 represents the measurements at a higher power input rate. We observed that the sound pressure level recorded when both lasers TA1 and TA2 are ON was always less than the sound pressure level for TA1 or TA2 operating individually. Similar observations were also made using

the SM, as shown in Figures 4.11 and 4.12. Our observation proves that continuous synchronization and phase locking can be achieved when lasers acoustically couple, with their openings very close to each other and the angle between their longitudinal axes is 30^{o}, whereas using the LM (which has a larger surface area) proved the effect of reflecting waves and its impact in increasing the detuning between the two lasers. In this case, synchronization was not observed, but an increase in the amplitude, approximately twice compared to the amplitude measurement of a single laser, was recorded when the signals from both lasers were in-phase.

4.2.3 Large Crossing Angle (90^{o})

This experiment was designed to study the interaction between the sound waves of two thermoacoustic lasers when their openings are very close to each other and the angle between their longitudinal axes is 90^{o} (see Figure 3.11). The initial results discussed in this section were collected using the sound pressure level meter. When the lasers were powered at a lower rate, in the neighborhood of 20-25 W, the signals never phase locked (note that the experimental run was only 30 seconds), whereas, when we increased power rating of the lasers, in the neighborhood of 30-35 W, the signals locked in a particular frequency and phase. In this case, the duration of the run was 2 minutes and the sound pressure level meter was placed at 20 cm away from the openings of the two lasers to avoid reflections. The decrease in sound pressure level of the synchronized signal was recorded and is shown in Figure 4.17. Therefore, we can conclude that when the lasers were powered at the higher rate, the sound wave frequencies alter each other to lock in frequency and phase. Another important conclusion from this observation is that the experimental run in the lower power rating case was only 30 seconds.

Synchronization might have been observed if the experimental run had been increased to 1 or 2 minutes.

In order to observe the nature of the coupled signal, the sound pressure level meter was replaced with the LM. Figure 4.18 illustrates the signal recorded when only laser TA1 is running and Figure 4.19 illustrates the signal recorded when both lasers TA1 and TA2 are running. As shown in Figure 4.19, the signals beat and they never lock in phase. This was similar to the previous case when the LM was used for the small crossing angle 30^{o}. When the large surface area of the LM is close to the openings of the two lasers, sound waves are blocked and reflected back. This reflected wave altered the frequencies of both lasers and caused detuning. The amplitude increases when the two lasers couple in-phase and the amplitude decreases when they are out-of-phase. The amplitude recorded when the signals coupled in-phase was 57 mill volts, which is 1.6 times the amplitude of 37 mill volts that was recorded for a single laser operation. In this particular case of using the LM, we always observed detuning, irrespective of the angle at which the two lasers were oriented. Detuning was common for both angles (small and large), because the large solid surface of the microphone had a great impact in blocking and reflecting the sound waves. These reflected sound waves affected the pressure fields at the opening of the two lasers and therefore, synchronization was not achieved while using the LM.

As similarly done in the previous case of small crossing angle (30^{o}), the sound pressure level meter was replaced with an omnidirectional miniature microphone (SM). The SM also measures the frequency, phase, and amplitude of the signals. These readings were compared with those obtained from the sound pressure level meter. Figure 4.20 (a)

and (b) illustrate the signal recorded when only laser TA1 is running. Maximum amplitude recorded in this case was 80.2 mill volts. Figure 4.21 (a) illustrates the signal recorded when both lasers TA1 and TA2 are running. In this experiment, we first switch on TA1 (powered with 32.4 W) and later TA2 (powered with 33.8 W). Synchronization was observed immediately, and the signals lock in frequency and phase. To observe the nature of the synchronized wave form, the time interval is reduced to 0.240 seconds, as shown in Figure 4.21 (b). The amplitude recorded for the synchronized signal when both lasers were operating was smaller than the amplitude recorded when only laser TA1 was operating. This implies antiphase synchronization.

We conducted an additional experiment by turning on TA2 (powered with 33.8 W) first and later TA1 (powered with 32.4 W). Figure 4.22 (a) illustrates the signal recorded when both lasers TA1 and TA2 were running. In this particular case, the signals beat during the first 12 seconds (approximately) of the 2 minute experiment run. This was 12 seconds longer compared to the previous case. In order to observe the nature of the beating signal, the time interval is reduced to 0.240 seconds, as shown Figure 4.22 (b). After running both lasers for 13 seconds, the beat frequency once again slows and then abruptly stops, at which point both lasers lock in a particular frequency and phase. The amplitude of the synchronized signal decreased gradually, as shown in the latter half of Figure 4.22 (a). In order to observe the nature of the synchronized signal, the time interval is again reduced to 0.240 seconds, as shown Figure 4.22 (c). Once again, the instance in time at which synchronization occurs for each experimental run is labeled in Figure 4.23.

The immediate synchronization in the first case (turning TA1 before TA2) is due to the close match in the initial frequencies of the two lasers. Shown in Table 4.2 are the fundamental frequencies of the two lasers TA1 and TA2 (operating individually) at different time intervals during the experimental run. When we tried to couple the sound waves of TA1 and TA2, which were operating with their fundamental frequencies as listed in Table 4.2, the time it took for the two lasers to match their frequencies ($\omega_2 = \omega_1$) was negligible. So, essentially, immediate synchronization was achieved, whereas in the second case (turning TA1 after TA2), there was the 13-second delay until the lasers synchronized. This indicates that the timing associated with turning on the second laser plays a critical role in determining how fast synchronization is achieved.

We conclude from all the measurements made for both the 30 and 90^o crossing experiments that synchronization between two lasers is possible when their open ends were placed close to each other. The synchronized locked signal was always out-of-phase, which resulted in decreased amplitude compared to that of a single laser. This decrease in amplitude for the locked signal is on an average comparatively 75% less than the amplitude of the single laser. The fundamental frequencies (as shown in Table 4.1 and 4.2) of the two lasers are much more influential than the crossing angle (30 and 90^o) in achieving synchronization. Sound pressure level recorded in this section is the logarithmic measure of the effective pressure of the sound relative to its reference value. It is given by the following equation, as described previously in Chapter 2,

SPL (in decibels) = 20 $\log_{10}(p'_{rms}$(in Pa)/20^{-6}),

where p'_{rms} is the rms of the sound pressure being measured and the relative reference value is 20 μPa. For a single thermoacoustic laser, the sound pressure level recorded was 122 dB. Using the above equation, we obtain a p'_{rms} value of 25.178 Pa. $v'_{rms}(LM)$ generated by the microphone (LM) from Lab View Signal Express is approximately 31 mill volts. $v'_{rms}(SM)$ generated by microphone (SM) from Lab View Signal Express is approximately 76 mill volts. Thus, the gain can be calculated using the following relation Gain of Microphone $=\frac{v'_{rms}}{p'_{rms}}$. Therefore, Gain of microphone (LM) is 1.23 mV/Pa and Gain of microphone (SM) is 3.01 mV/Pa.

4.2.4 Laser Pair Separated at Various Distances

We studied the effect of acoustic coupling, when the openings of two lasers were moved away from each other in their respective crossing angles (30 and 90°). Recall from Chapter 3 that we moved the two lasers farther apart in increments of two centimeters (from 2 to 12 cm) at a particular angle (30 or 90°), as shown in Figure 3.13. In this particular case study, we only used a microphone to measure frequency, amplitude, and phase difference between the two separated lasers.

Figures 4.24, 4.25, and 4.26 illustrate and compare the signal generated from a single laser with the coupled signal from two lasers oriented at 30°, at separating distances of 2, 6, and 12 cm, respectively. These figures illustrate that the signals never locked in frequency or phase. These unlocked signals beat changing their phase from one phase to another. We also observed an increase in amplitude when the lasers were in-phase and decrease in amplitude when they were out-of-phase. The increased amplitude when the two signals were in phase was high compared to the amplitude of the signal

from a single laser. This beating of the signal was same irrespective of the distance by which the lasers were separated. Maximum and minimum values of the amplitude, when the signals coupled in-phase, were measured from all the data points collected for each experiment in this case study. We analyzed these values in MATLAB and compared them with the measurements from a single laser.

The main reason for not achieving synchronization in this case of coupling, as compared to the previously observed 30^{o} crossing angle in Section 4.2.2, is the increase in the spatial distance between the openings of the two lasers. As the lasers were moved apart from one another, the probability of the lasers to lock in frequency or phase was decreased. The atmospheric air in the room where we conducted the experiments acts as a reflection to the signals produced by either of the lasers. This air acting in between the two lasers increases in volume as we increase the separating distance from 2 to 12 cm. The "detuning" between the lasers becomes greater as the separation distance was increased. We conclude that coupling is weak in this case and it will not allow the signals from the two lasers to lock in frequency and phase. We also observed that the coupled signal is smooth and noise-free at 2 cm separating distance. When the separation distance increased to 6 cm, there was some noise added into the system, as shown in Figure 4.25. This is due to the increase in volume of atmospheric air acting in between the lasers and the LM. Similarly, an effective increase in noise was observed at 12 cm separating distance, as shown in Figure 4.26.

Figures 4.27 (a) and (b) compare the effect of 30^{o} crossing lasers with each of the single lasers. These figures give detailed information about how the acoustic signal of a single laser (either TA1 or TA2) and the acoustically coupled signal from 30^{o} crossing

lasers (TA1 and TA2) behave at different separating distances. As seen in Figure 4.27 (a), the highest amplitude recorded in this study was 39.52 mill volts. The amplitude decreased significantly from 39 to 22 mill volts as the separation distance between the lasers increased 2 to 4 cm, respectively. This drop was approximately 41.8%, as shown in Figure 4.28. The decrease in amplitude was minimized when we increased the separation distance from 4 to 6 and to 8 cm. As we increased the separation distance above 8 cm, the amplitude read remained the same at 15.3 mill volts, which was still greater than the value obtained from a single laser.

We observed from all the measurements that the amplitude is inversely proportional to the separating distance. This inverse proportionality is only observed until the separation distance between the two lasers reaches 8 cm and after this point, there is no further drop in amplitude.

Figures 4.29, 4.30, and 4.31 illustrate and compare the signal generated from a single laser with the coupled signal from two lasers oriented at 90^{o}, at separating distances of 2, 6, and 12 cm, respectively. These figures illustrate that the signals never locked in frequency or phase. These unlocked signals beat, changing their phase from one phase to another. We also observed an increase in amplitude when the lasers were in-phase and decrease in amplitude when they were out-of-phase. This beating of the signal was the same irrespective of the distance by which the lasers were separated. All the observations and the conclusions in this particular section for crossing lasers at different separated distances are the same irrespective of the oriented angle (30 or 90^{o}).

Figures 4.32 (a) and (b) compare the effect of 90^{o} crossing lasers with each of the single lasers. These figures give detailed information about how the acoustic signal of a

single laser (either TA1 or TA2) and the acoustically coupled signal from 90^{o} crossing lasers (TA1 and TA2) behave at different separating distances. As seen in Figure 4.32 (a), the highest amplitude recorded in this study was 39.52 mill volts. The amplitude decreased significantly from 39.5 to 22.9 mill volts as the separation distance between the lasers increased from 2 to 4 cm, respectively. This drop was approximately 41.8% on average, as shown in Figure 4.33. The decrease in amplitude was minimized when we increased the separation distance from 6 to 8 to 10 and to 12 cm. This decrease is only around 7 to 8% on average, as shown in Figure 4.33.

Shown in Figure 4.27 (b) and 4.32 (b) are the minimum recorded values, which were in direct proportion to the maximum values collected for both 30^{o} and 90^{o} crossing lasers. Similar to the function of the sine waves, the peaks of the collected signal wave above and below the origin recorded the maximum amplitude as 39.52 mill volts and minimum amplitude as -39.33 mill volts, respectively.

From all the measurements and observations made from Figures 4.24 to 4.33, we observed that the amplitude measured for the in-phase coupled signal by crossing at various separating distances is greater than the amplitude of an individually acting laser. This behavior is similar irrespective of the angles and distances considered.

We also note that the amplitude recorded is inversely proportional to the separation distance in both 30^{o} and 90^{o} orientations, according to the inverse law (1/r) (29). Figure 4.34 illustrates the ratio of the amplitude output when both lasers TA1 and TA2 were in-phase to the amplitude output of laser TA1. This ratio is approximately 1.82 for 30^{o} and 1.49 for 90^{o} when the lasers were in-phase. For separating distances of 2 and 4 cm, the variation in the amplitude ratio for both 30 and 90^{o} crossing angles is highly

significant, whereas, when the separating distance increased to 6 cm and above, the amplitude ratio was approximately the same at both 30 and 90^{o} crossing configurations. All the measurements that were described will conclude Chapter 4. Results for all the coupling configurations are summarized and the discoveries made will be detailed in Chapter 5.

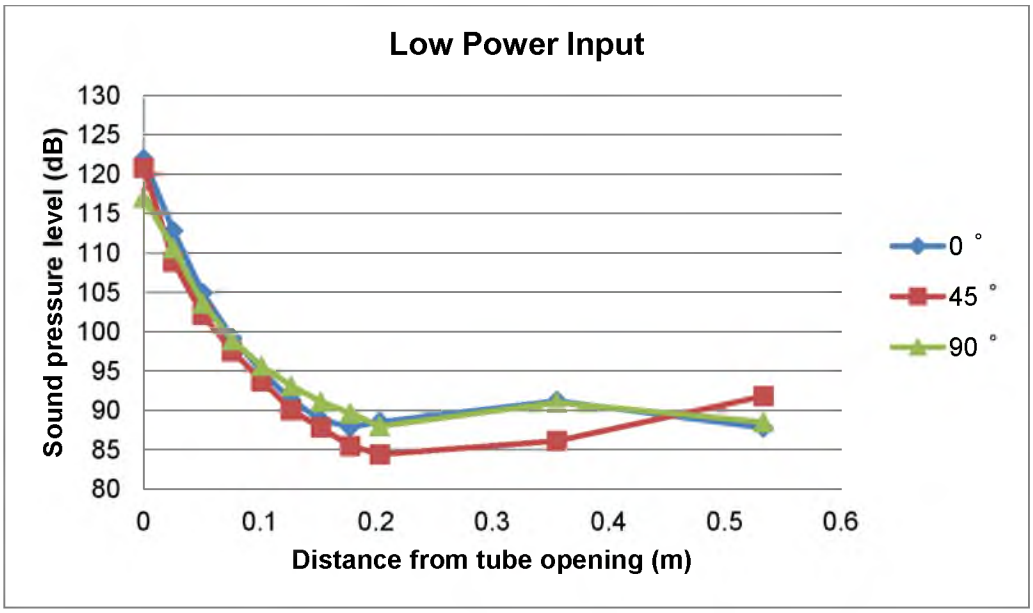

Figure 4.1: Sound pressure levels measured in all three orientations (0, 45, and 90 °) for low powered lasers.

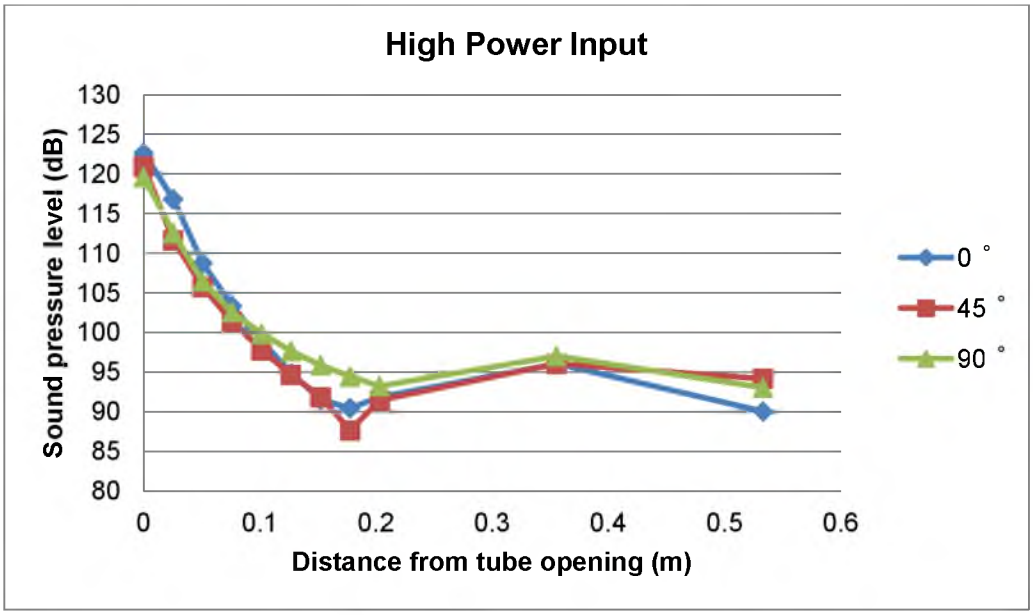

Figure 4.2: Sound pressure levels measured in all three orientations (0, 45, and 90 °) for high powered lasers.

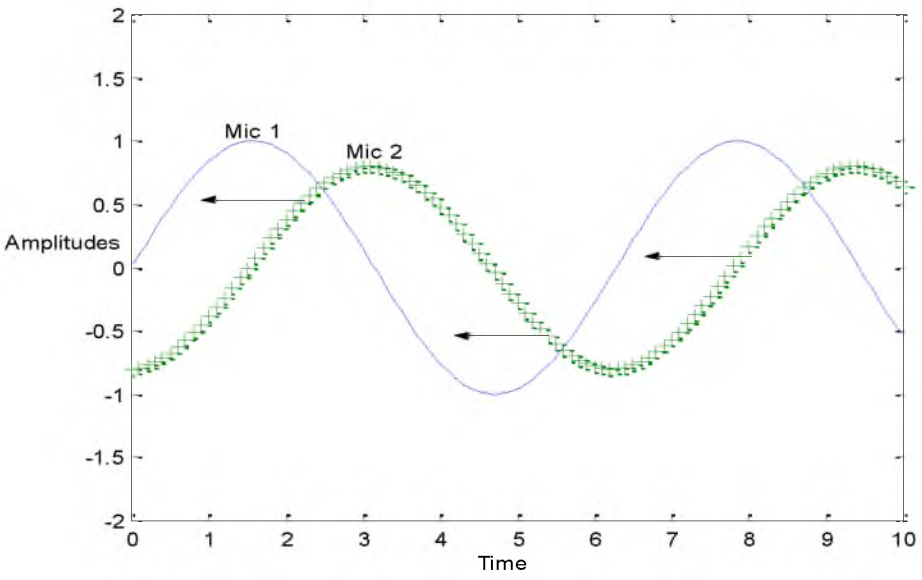

Figure 4.3: Out-of-phase sound waves measured by M1 and M2 when two TA lasers were seperated by 1 m.

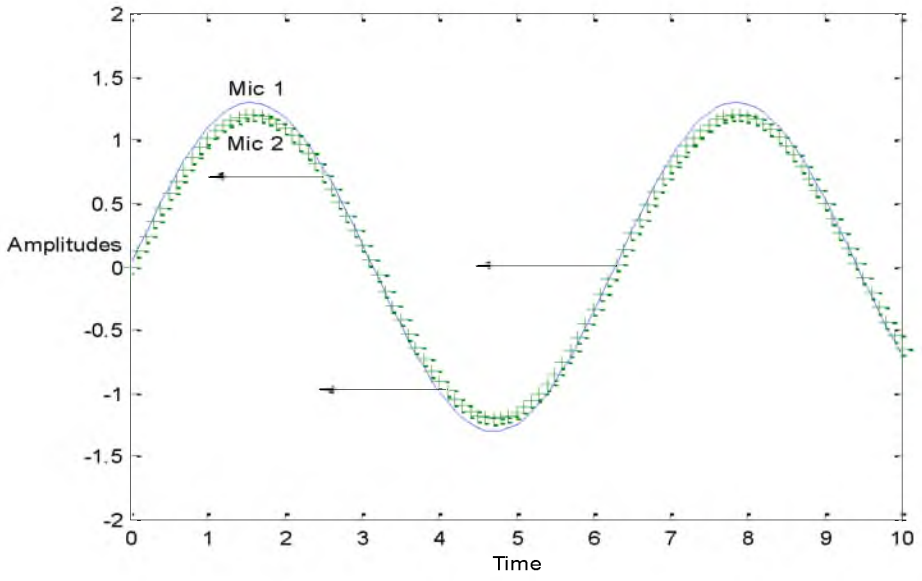

Figure 4.4: In-phase sound waves measured by M1 and M2 when two TA lasers were seperated by 1 m.

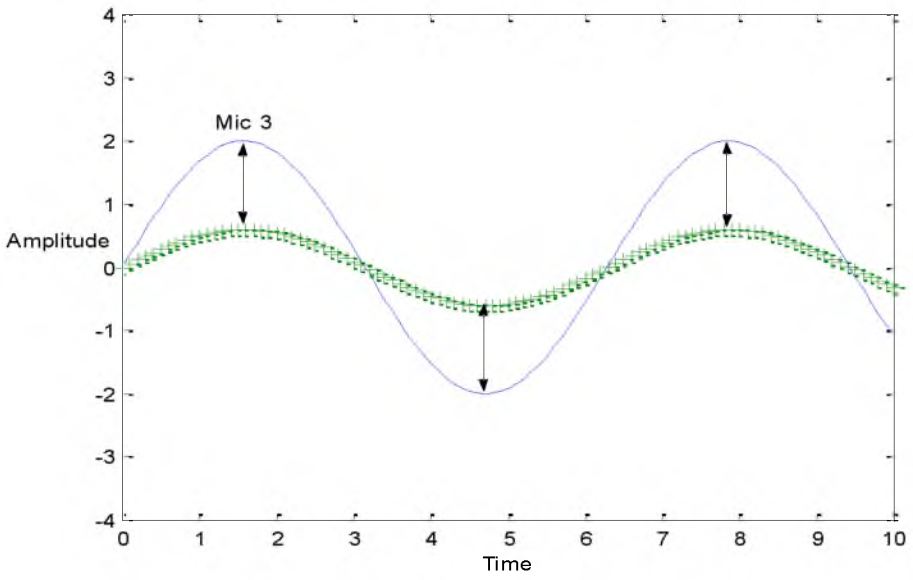

Figure 4.5: The beat signal changing from in-phase to out-of-phase, measured by the LM (microphone 3) (25).

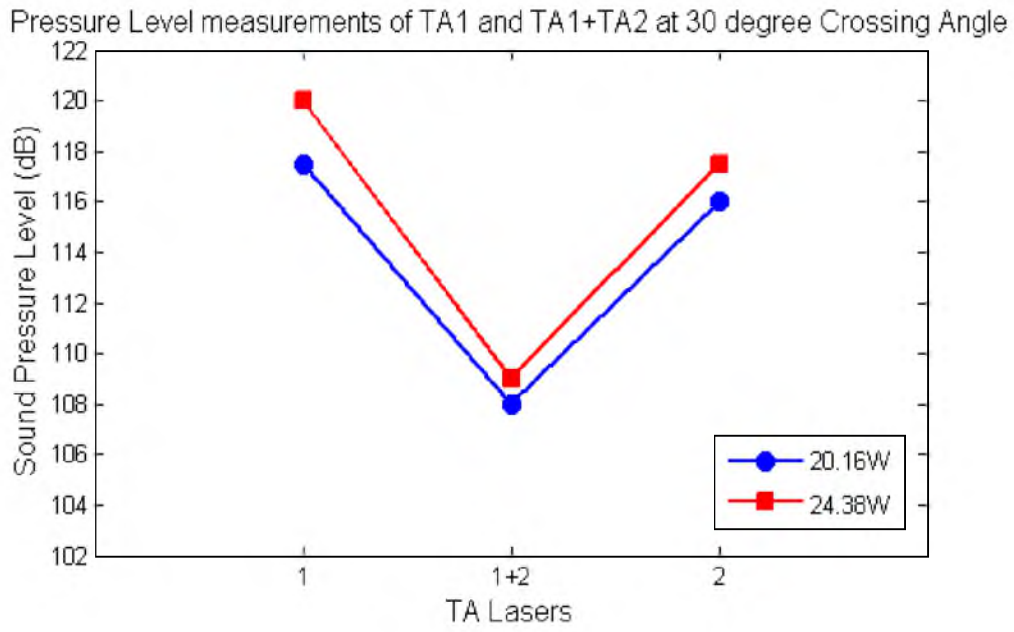

Figure 4.6: Sound pressure levels recorded at 30 ^{o} crossing angle (low powered lasers).

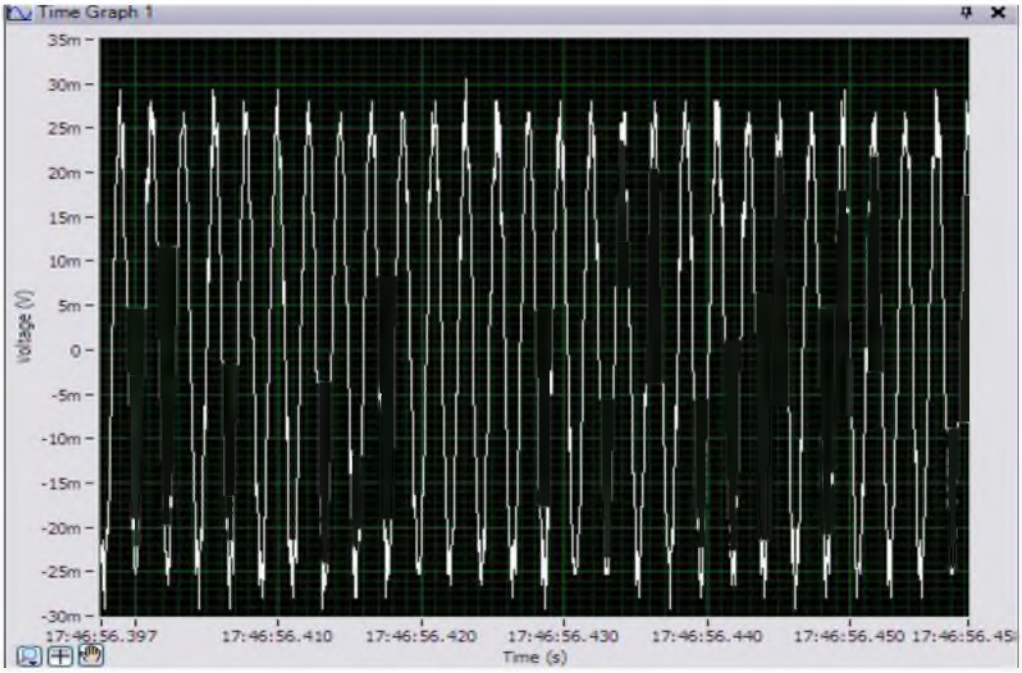

Figure 4.7: A typical pressure waveform recorded when a single laser TA1 is operating. The time interval is 0.06 seconds.

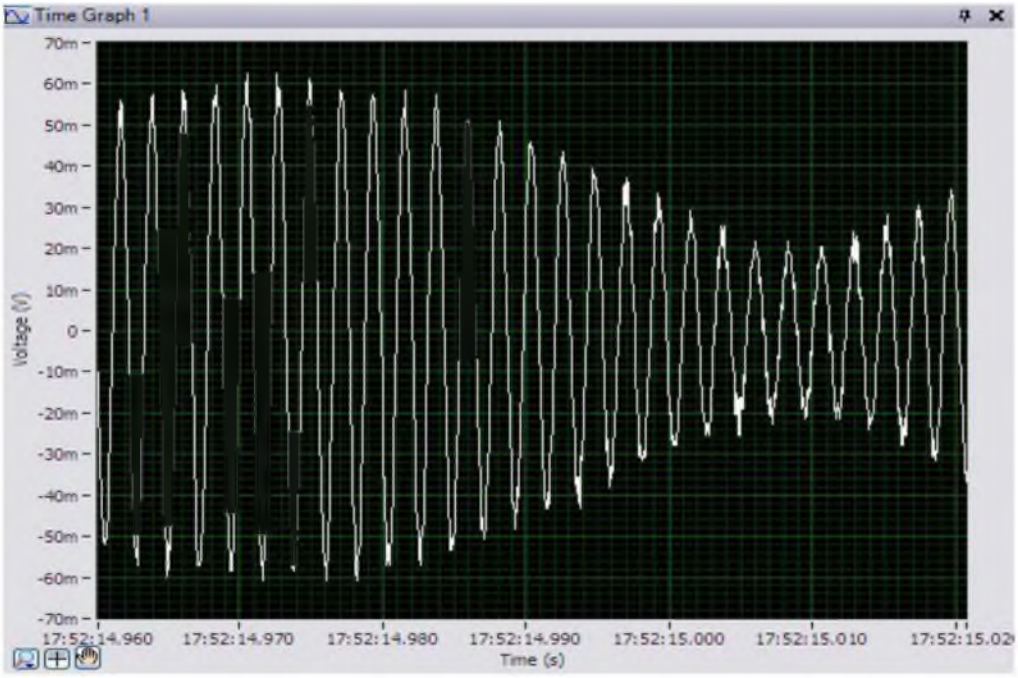

Figure 4.8: A typical pressure waveform of the beat signal recorded when the two lasers TA1 and TA2 are crossing to each other at 30^{o}. The time interval is 0.06 seconds.

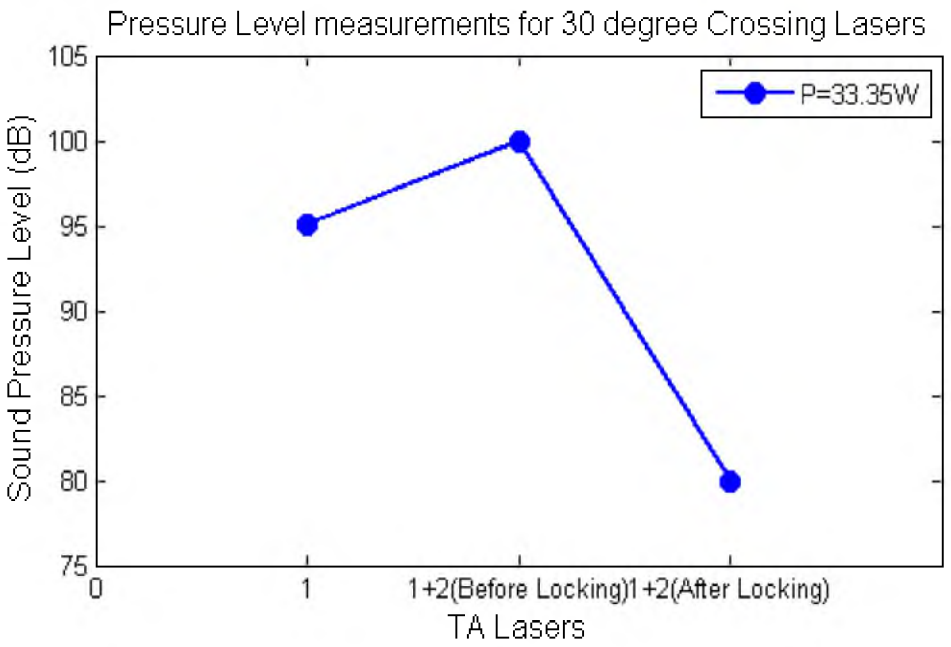

Figure 4.9: Sound pressure levels recorded at 30^{o} crossing angle (High powered lasers).

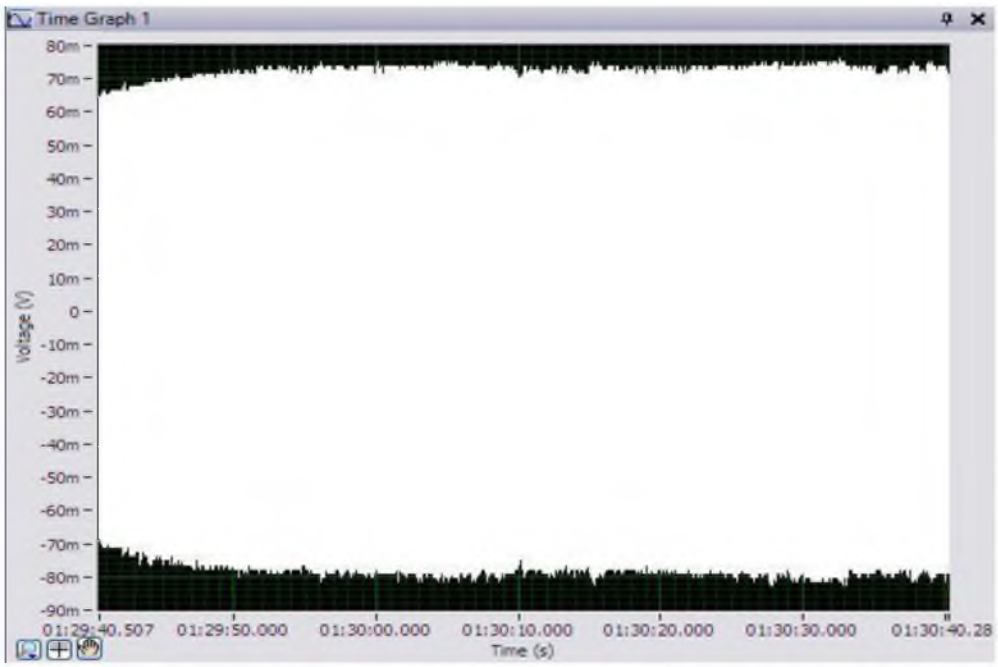

(a)

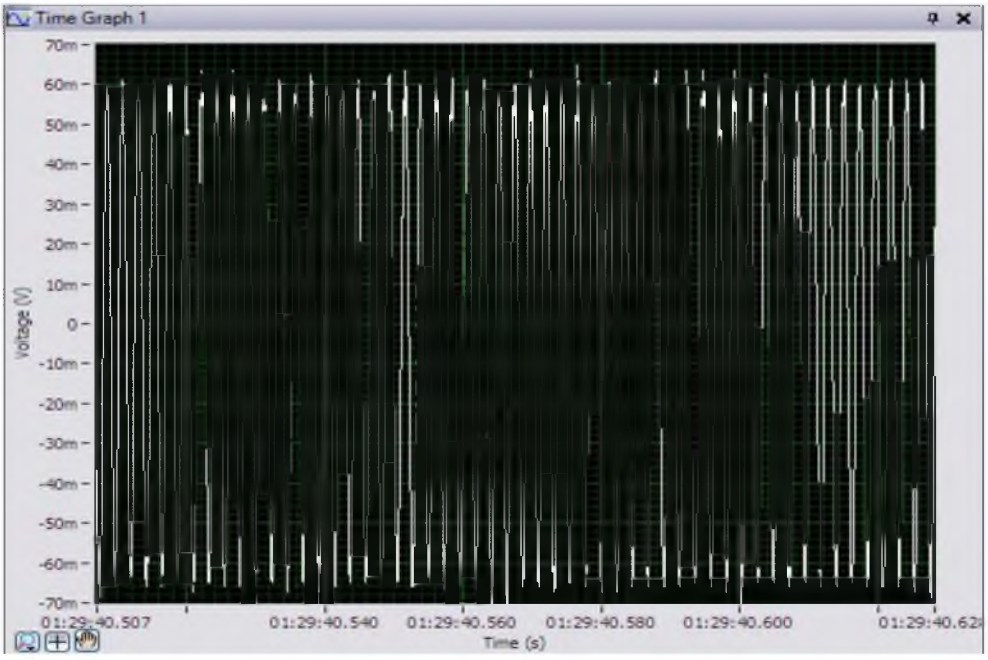

(b)

Figure 4.10: A typical pressure waveform recorded when only TA1 is operating. The time interval in (a) is 60 seconds and the time interval in (b) is 0.120 seconds.

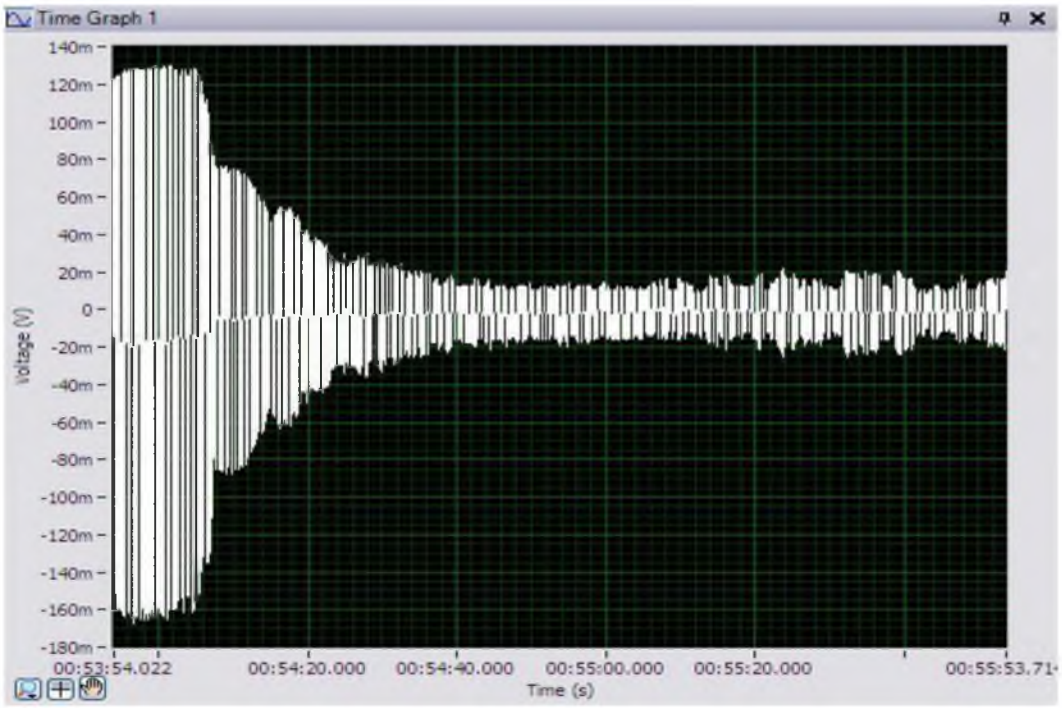

(a)

Figure 4.11: A typical pressure waveform recorded when the two lasers TA1 and TA2 are crossing each other at 30^{o} (TA1 is switched on before TA2). (a) represents this pressure wave form recorded over a time interval of 120 seconds, (b) represents a pressure waveform of the unlocked beat signal recorded with a time interval of 0.240 seconds, and (c) represents a pressure waveform of the locked (synchronized) signal recorded with a time interval of 0.240 seconds.

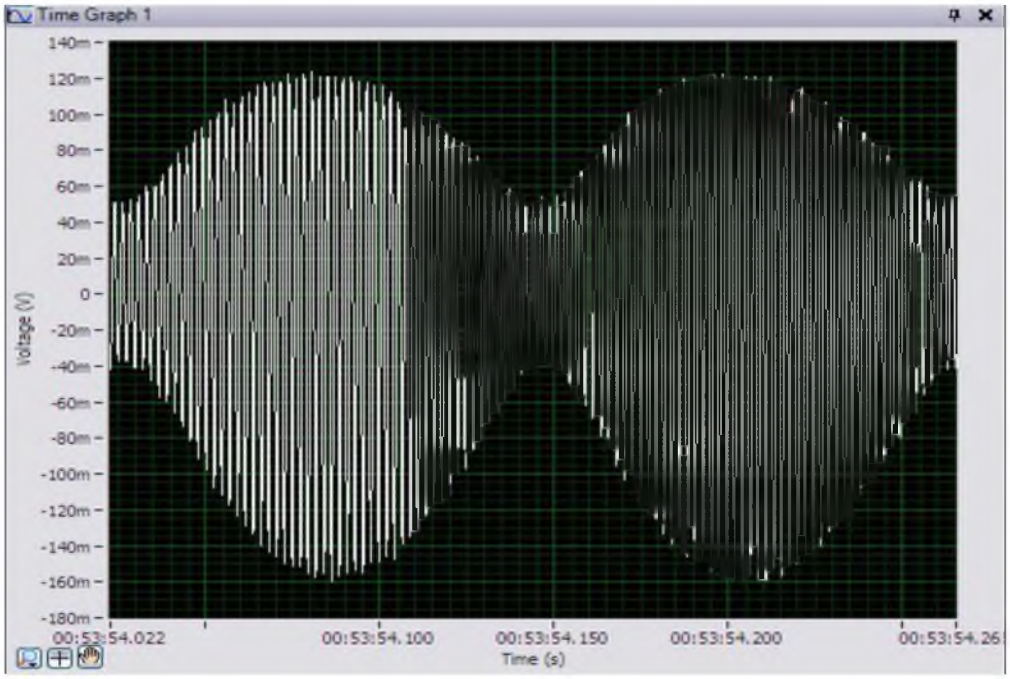

(b)

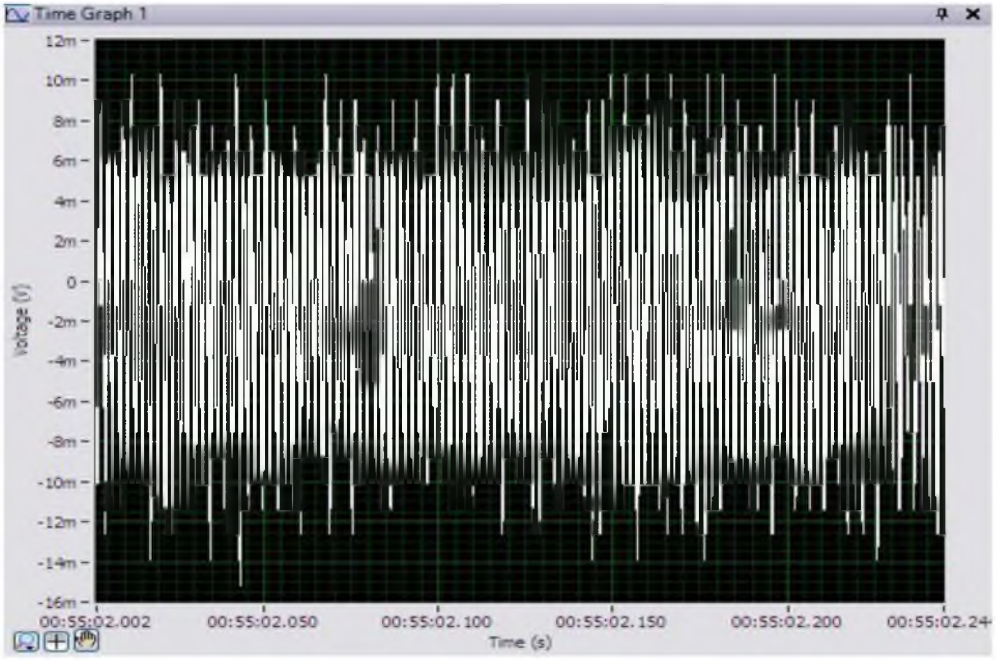

(c)

Figure 4.11: Continued

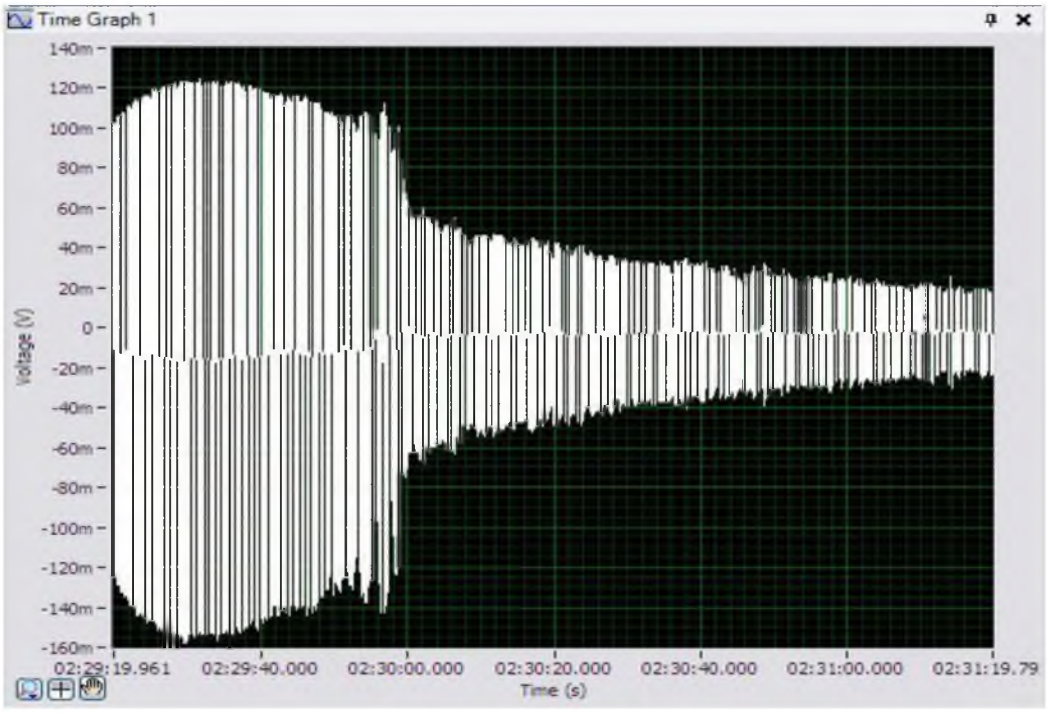

(a)

Figure 4.12: A typical pressure waveform recorded when the two lasers TA1 and TA2 are crossing each other at 30^{o} (TA2 is switched on before TA1). (a) represents this pressure wave form recorded over a time interval of 120 seconds, (b) represents a pressure waveform of the unlocked beat signal recorded with a time interval of 0.240 seconds, and (c) represents a pressure waveform of the locked (synchronized) signal recorded with a time interval of 0.240 seconds.

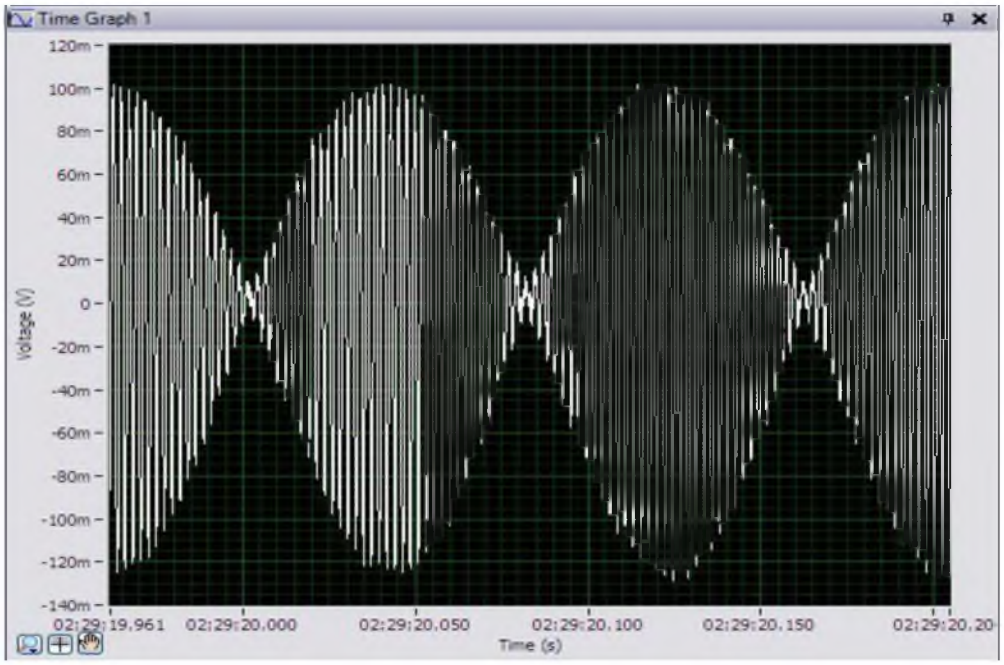

(b)

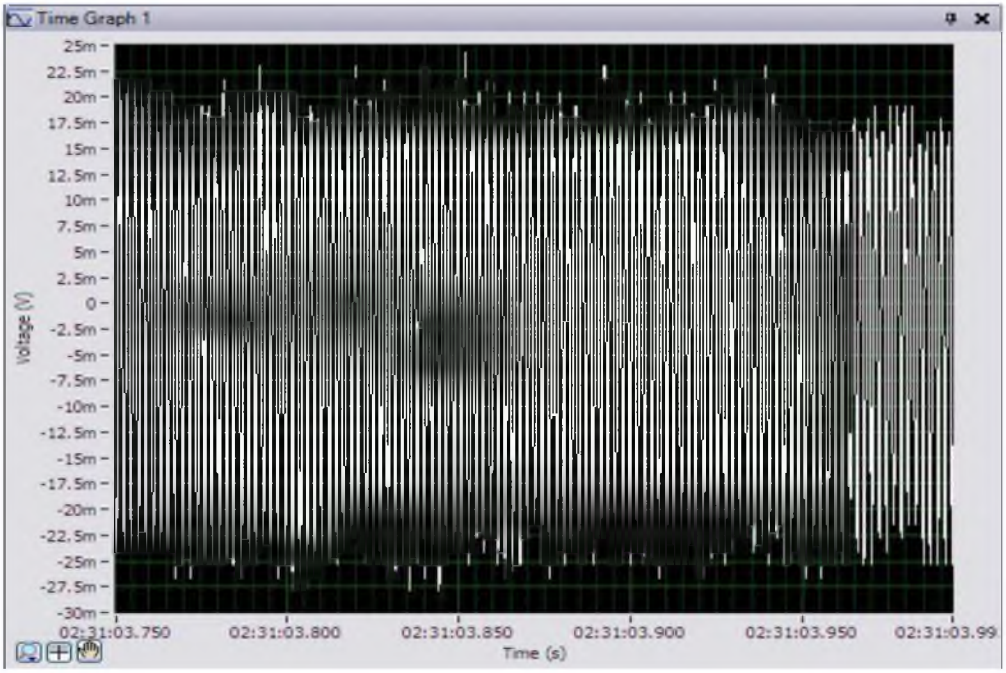

(c)

Figure 4.12: Continued

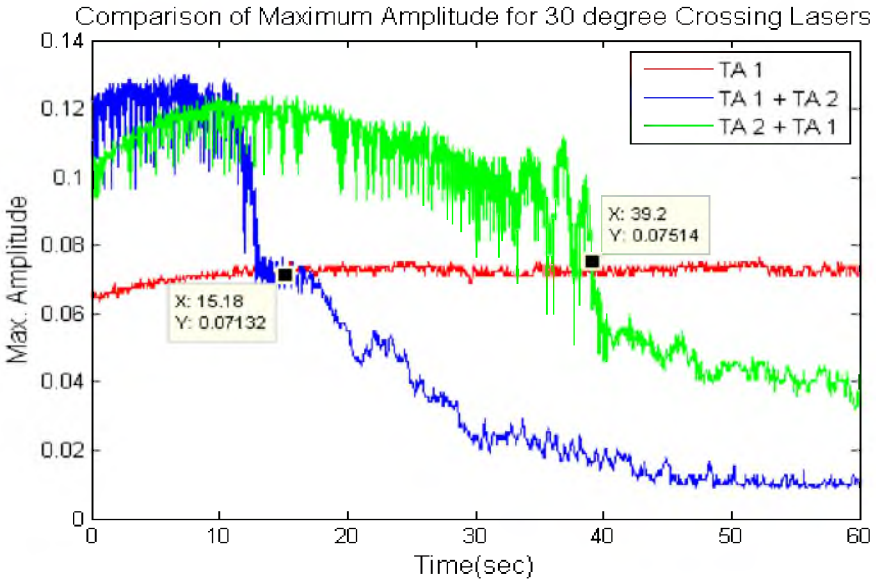

Figure 4.13: Comparison of max amplitudes for 30° crossing lasers to determine the occurrence of synchronization for different experimental runs. The two labeled points represent the approximate time when synchronization was achieved for each experiment.

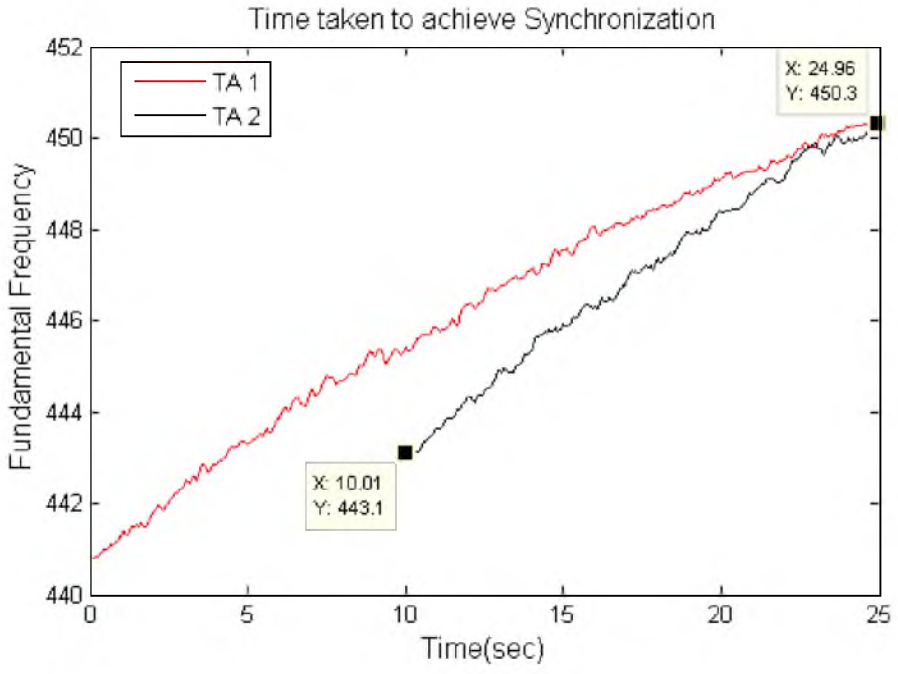

Figure 4.14: Approximate plot to determine the time taken to achieve synchronization for 30° crossing lasers.

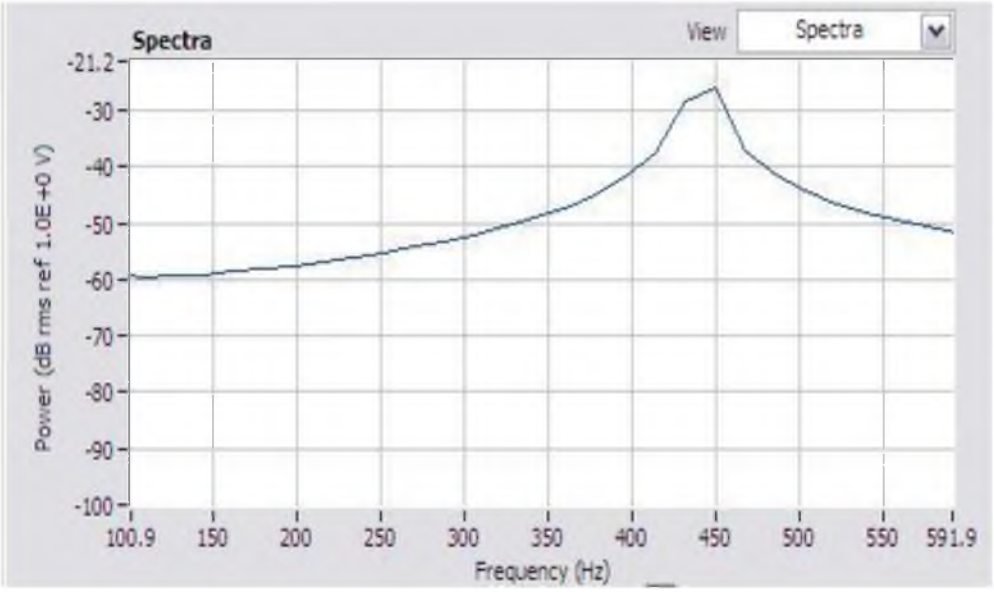

Figure 4.15: Frequency chart analyzed using Lab-View Signal Express, describing the natural frequency of the sound wave after the signals from the two lasers TA1 and TA2 were synchronized.

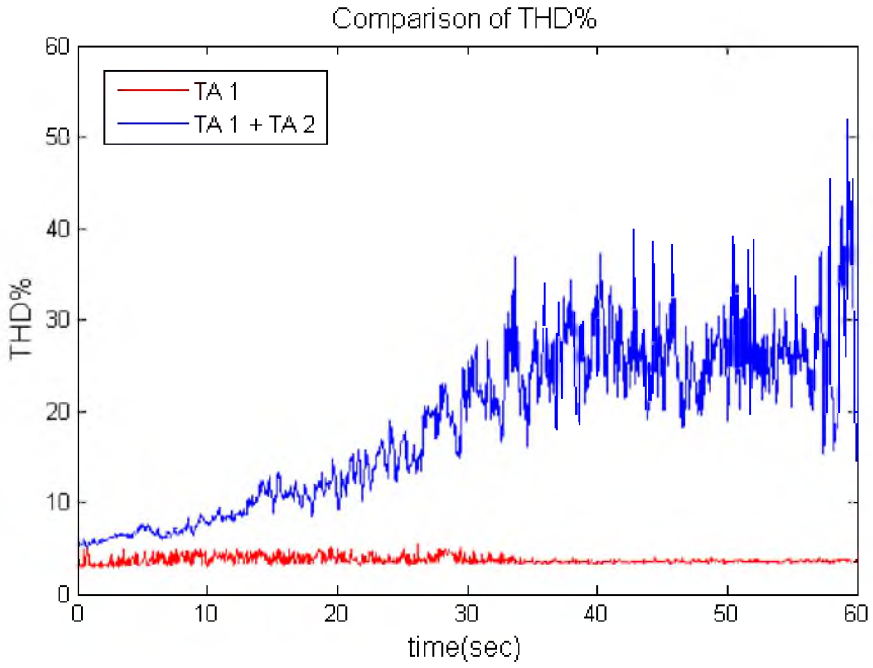

Figure 4.16: Comparison of total harmonic distortion percentages for the lasers crossing to each other at 30^{o} with that of a single laser.

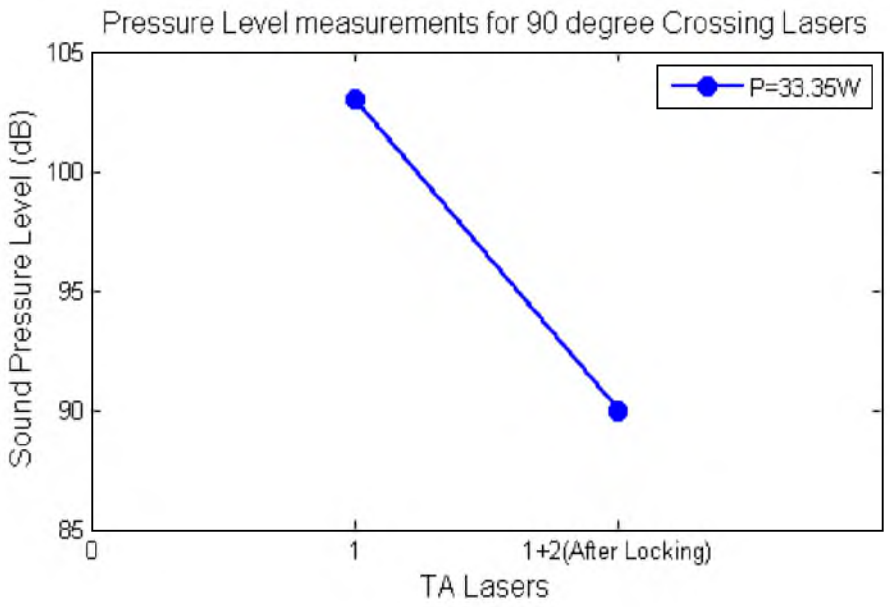

Figure 4.17: Sound pressure levels recorded at 90^{o} crossing angle.

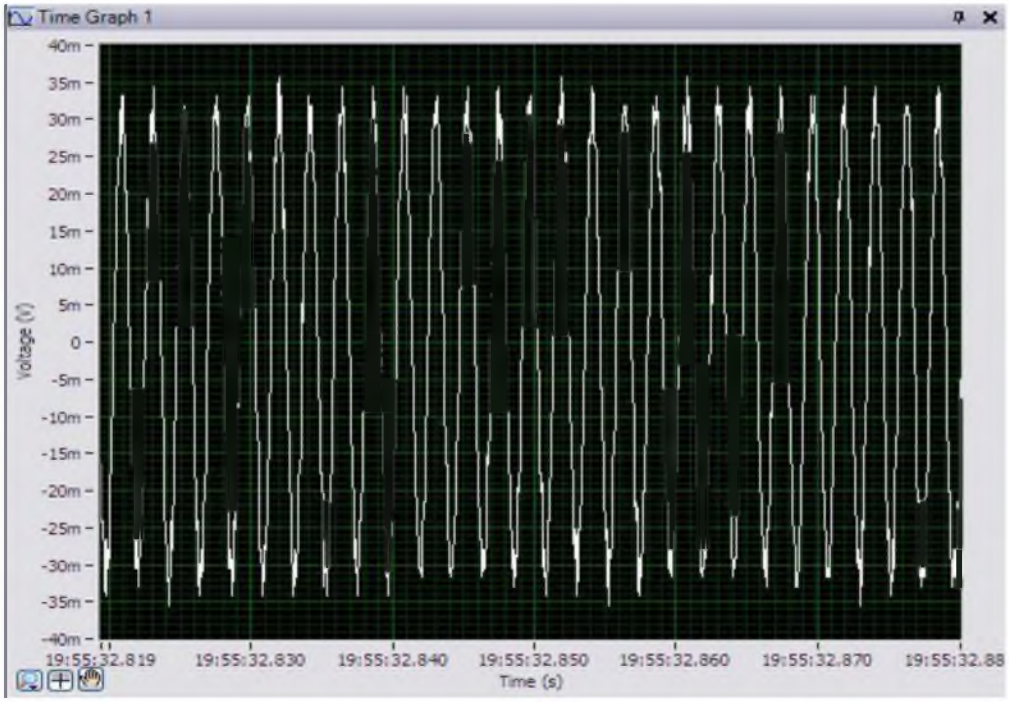

Figure 4.18: A typical pressure waveform recorded when only TA1 is operating. The time interval is 0.06 seconds.

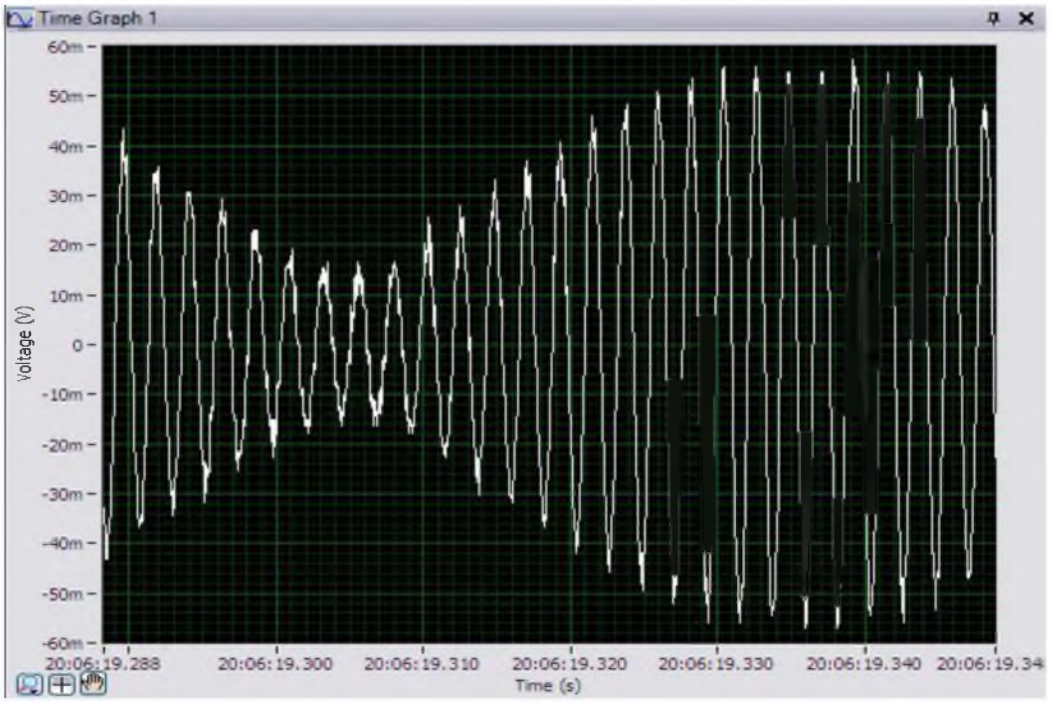

Figure 4.19: A typical pressure waveform of the beat signal recorded when two lasers TA1 and TA2 are crossing each other at 90^{o}. The time interval is 0.06 seconds.

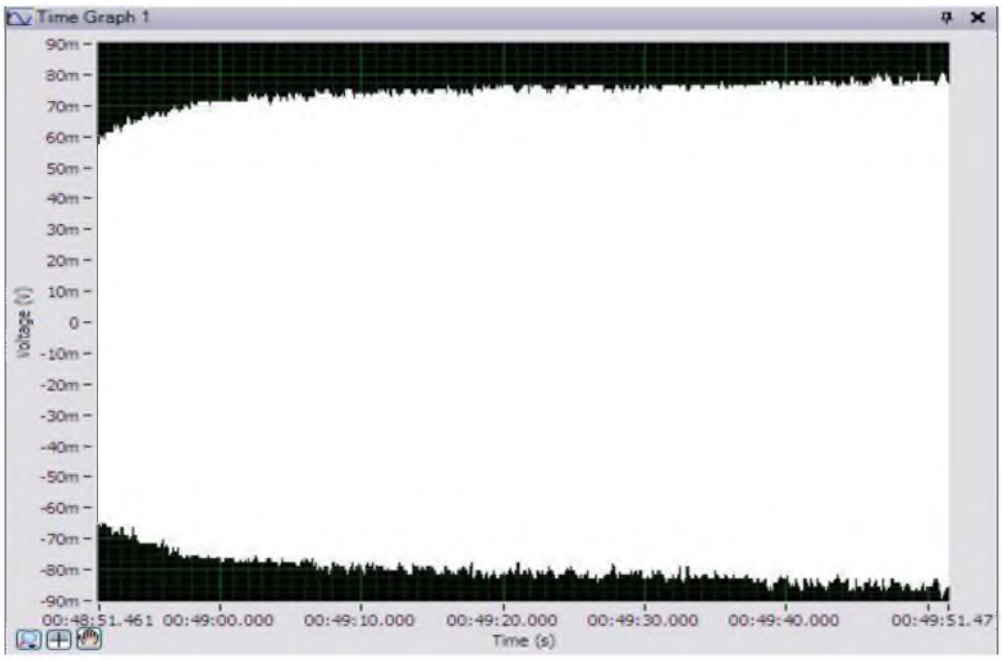

(a)

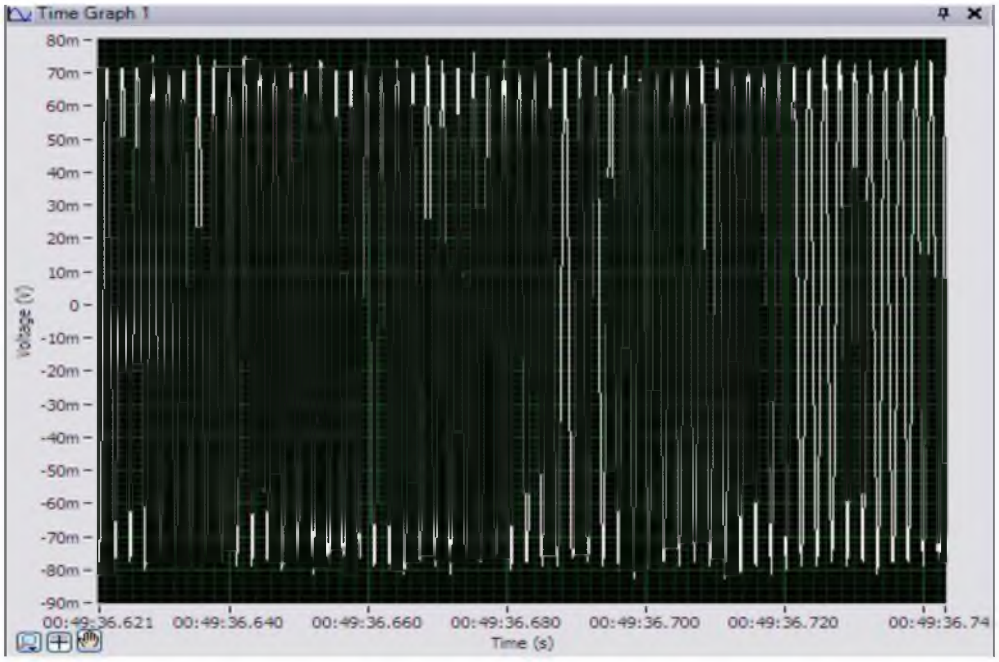

(b)

Figure 4.20: A typical pressure waveform recorded when only TA1 is operating. The time interval in (a) is 60 seconds and in (b) is 0.120 seconds.

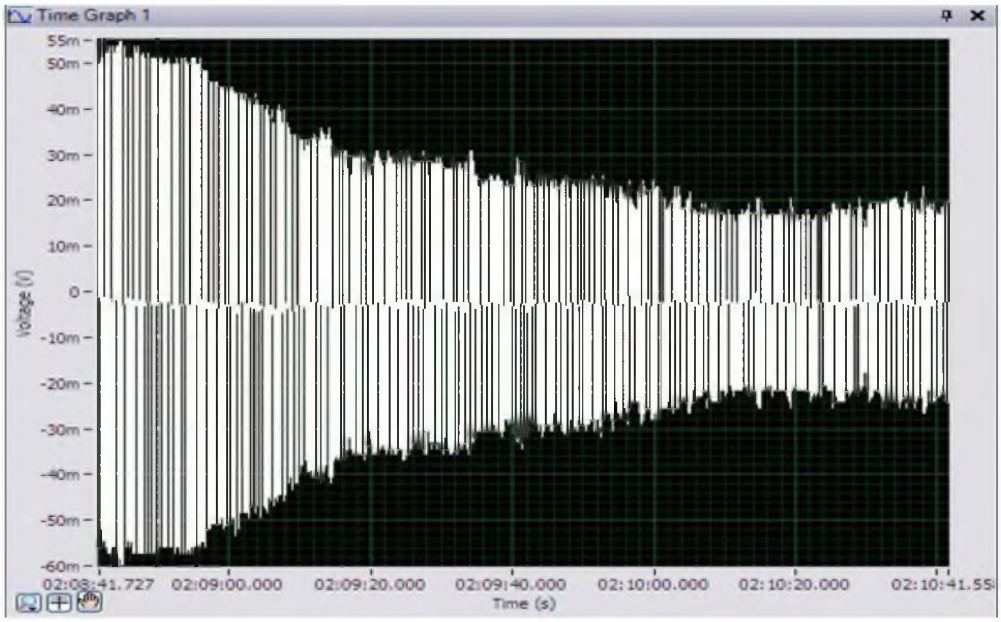

(a)

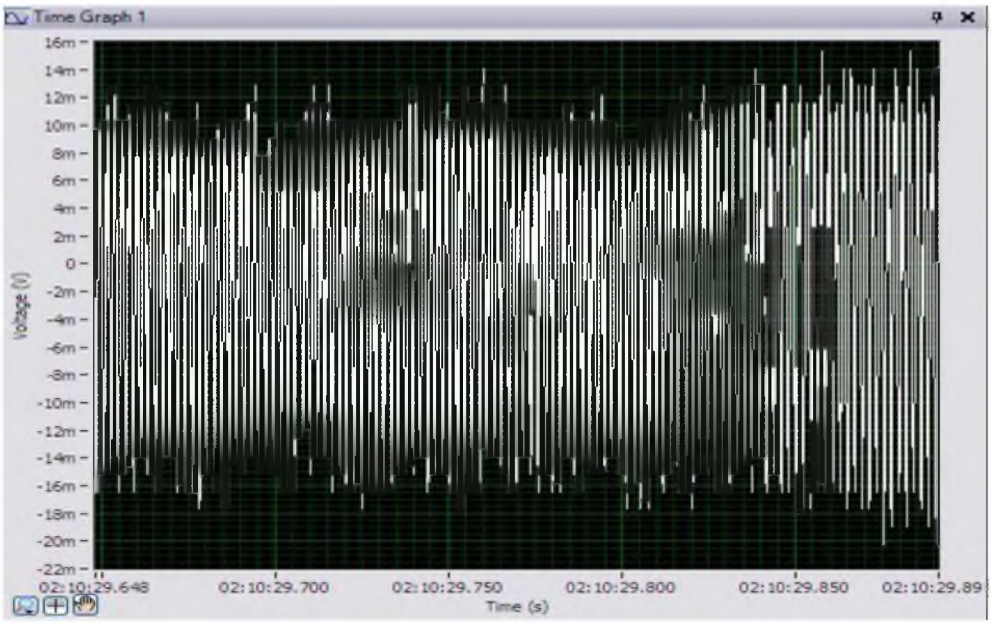

(b)

Figure 4.21: A typical pressure waveform recorded when the two lasers TA1 and TA2 are crossing each other at 90^{o} (TA1 is switched on before TA2). (a) is a pressure wave form recorded over a time interval of 120 seconds, and (b) is a pressure waveform of the locked (synchronized) signal recorded with a time interval of 0.240 seconds.

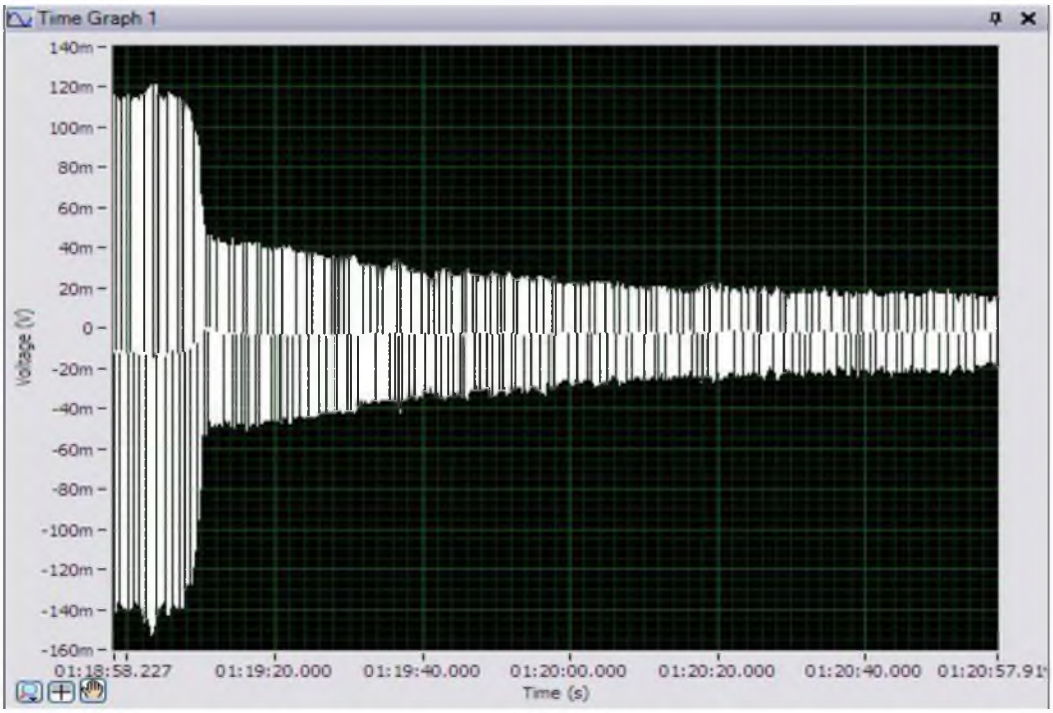

(a)

Figure 4.22: A typical pressure waveform recorded when the two lasers TA1 and TA2 are crossing each other at 90^{o} (TA2 is switched on before TA1). (a) represents this pressure wave form recorded over a time interval of 120 seconds, (b) represents a pressure waveform of the unlocked beat signal recorded with a time interval of 0.240 seconds, and (c) represents a pressure waveform of the locked (synchronized) signal recorded with a time interval of 0.240 seconds.

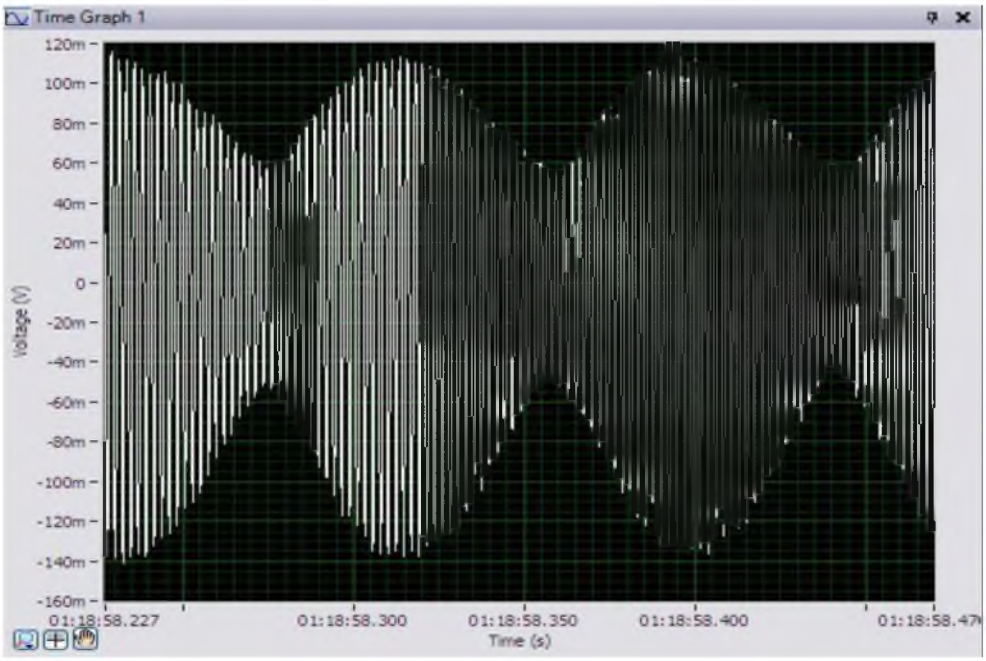

(b)

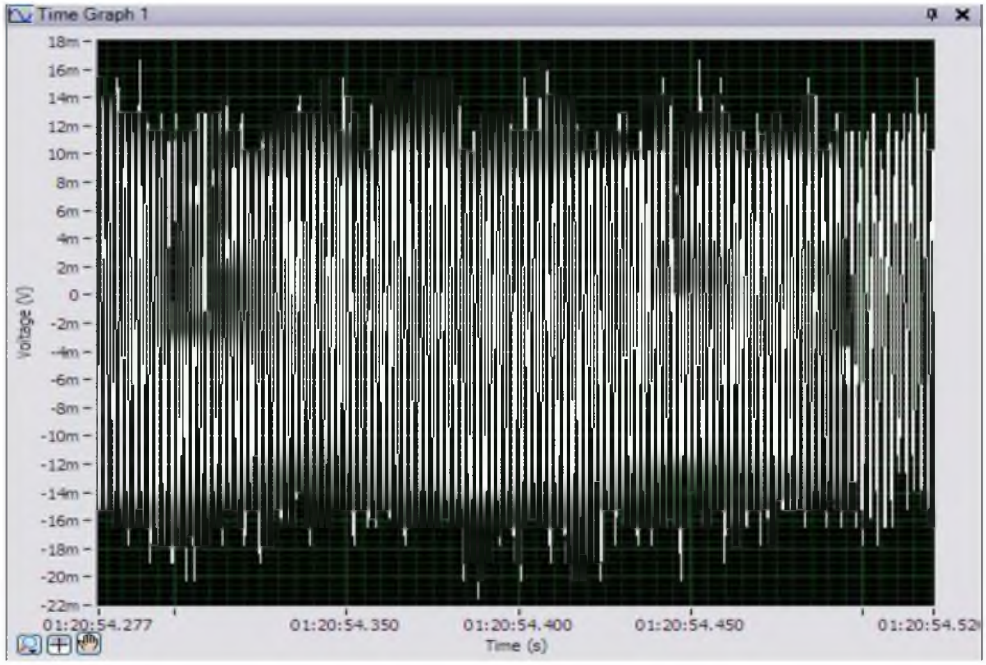

(c)

Figure 4.22: Continued

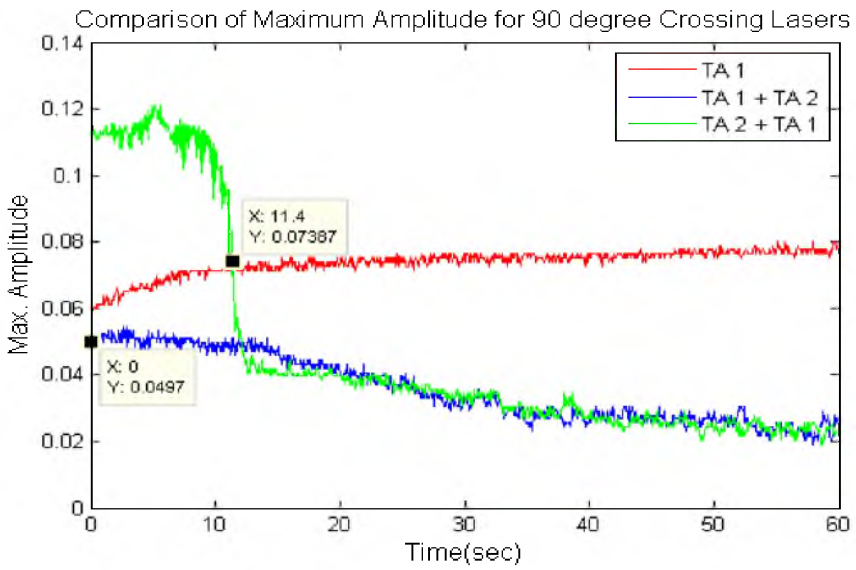

Figure 4.23: Comparison of max amplitudes for 90° crossing lasers to determine the occurrence of synchronization for different experimental runs. The two labeled points represent the approximate time when synchronization was achieved for each experiment.

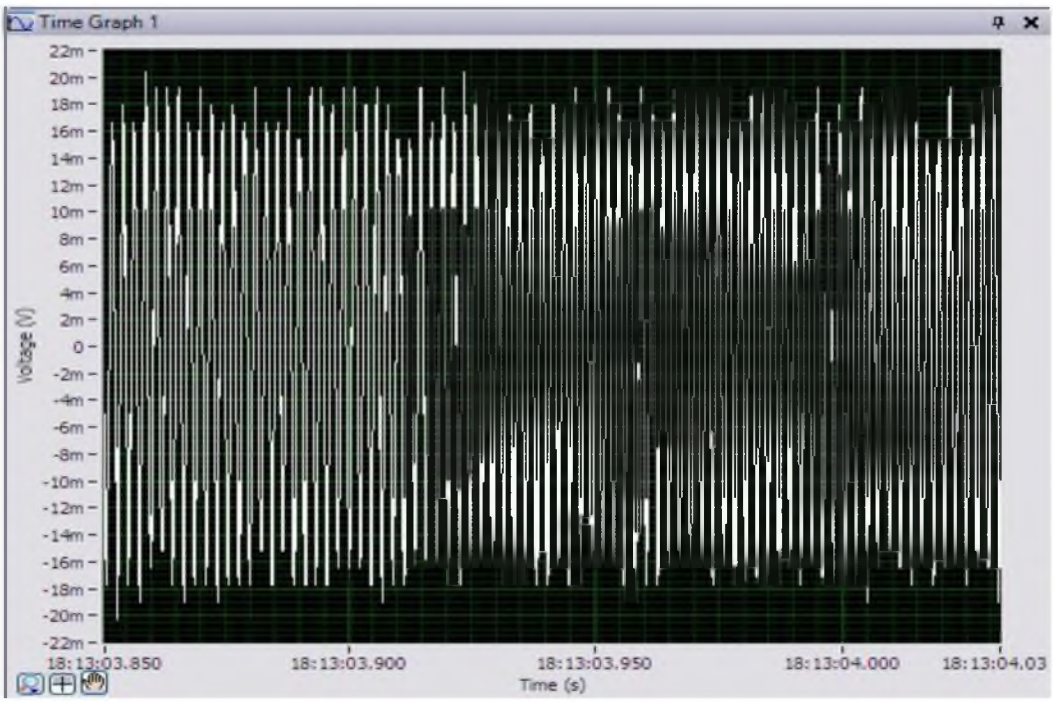

(a)

Figure 4.24: A comparison of signals for 30° crossing lasers with that of a single laser (2 cm spatial distance), where (a) represents the signal from a single laser in a time interval of 0.18 seconds, (b) represents the signal from a single laser in a time interval of 0.06 seconds, (c) represents the "beat" signal from 30° crossing lasers in a time interval of 0.18 seconds, and (d) represents the "beat" signal from 30° crossing lasers in a time interval of 0.06 seconds.

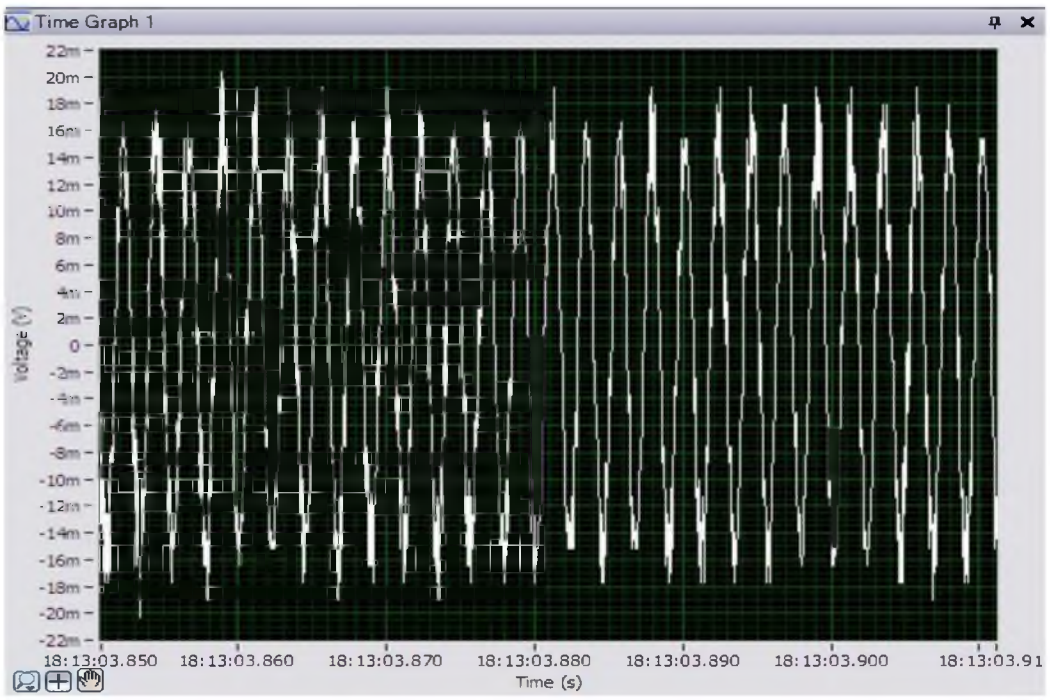

(b)

Figure 4.24: Continued

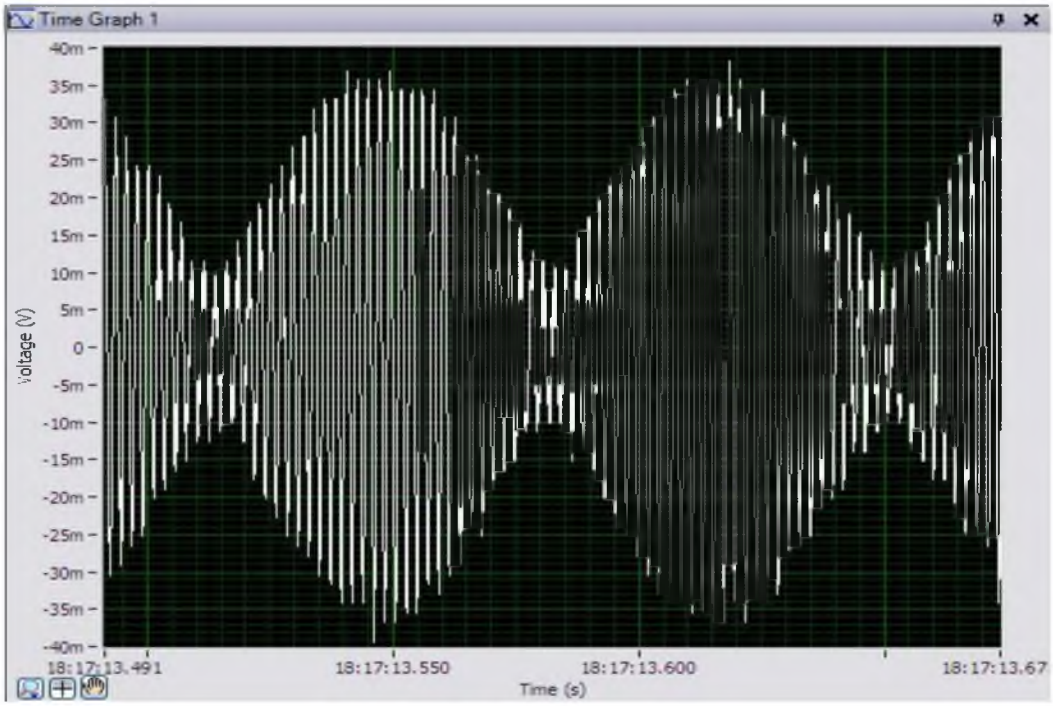

(c)

Figure 4.24: Continued

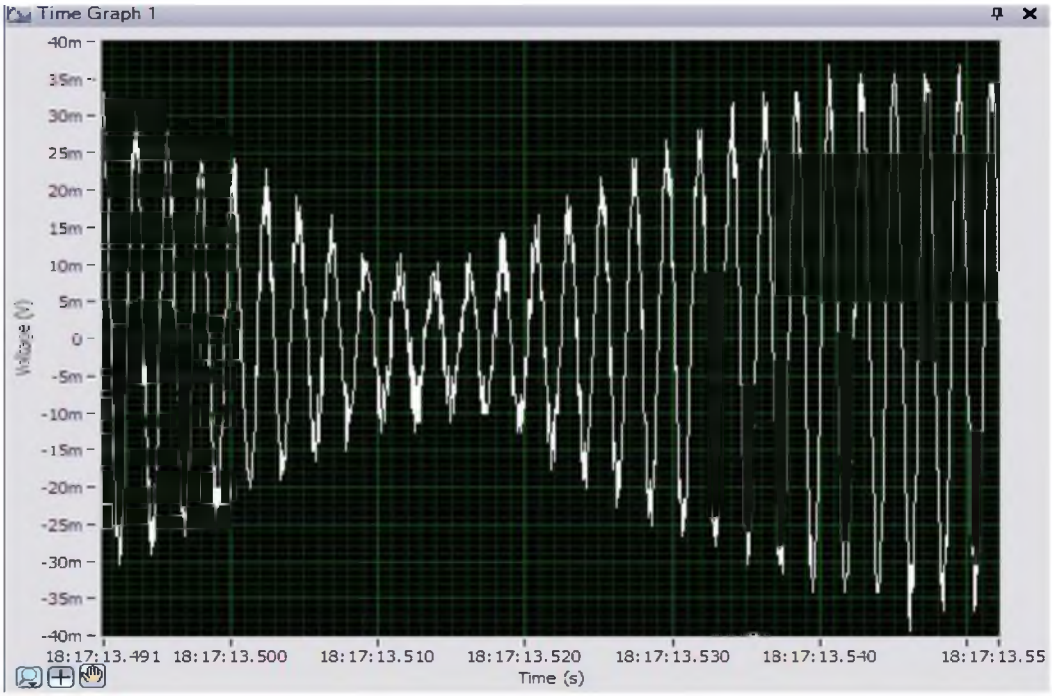

(d)

Figure 4.24: Continued

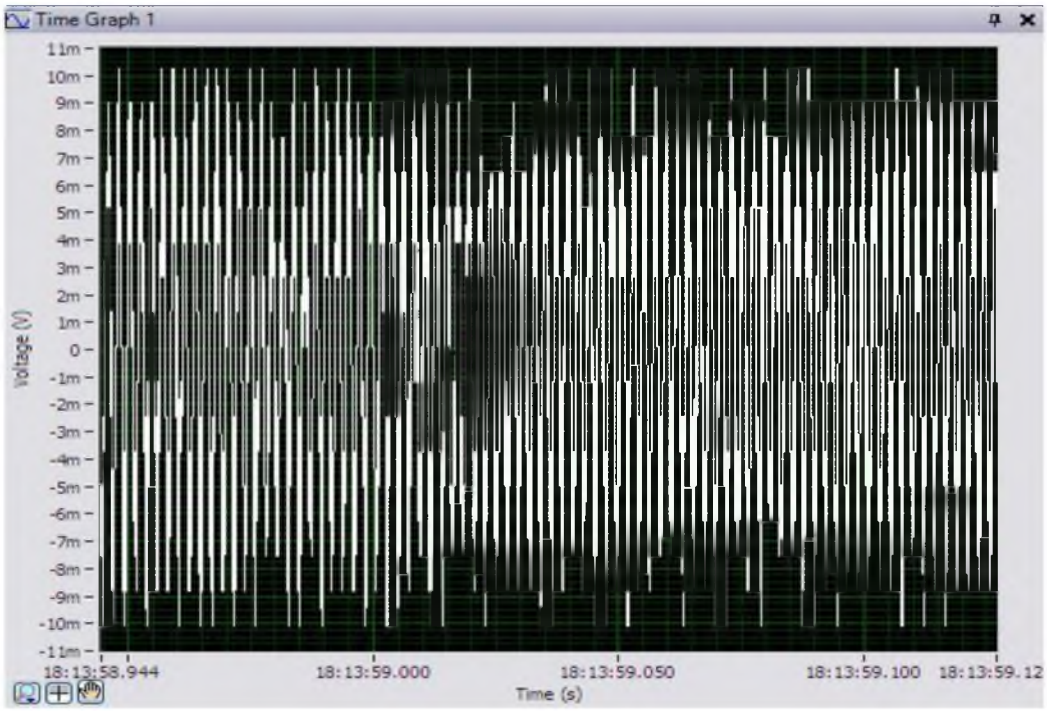

(a)

Figure 4.25: A comparison of signals for 30^{o} crossing lasers with that of a single laser (6 cm spatial distance), where (a) represents the signal from a single laser in a time interval of 0.18 seconds, (b) represents the signal from a single laser in a time interval of 0.06 seconds, (c) represents the "beat" signal from 30^{o} crossing lasers in a time interval of 0.18 seconds, and (d) represents the "beat" signal from 30^{o} crossing lasers in a time interval of 0.06 seconds.

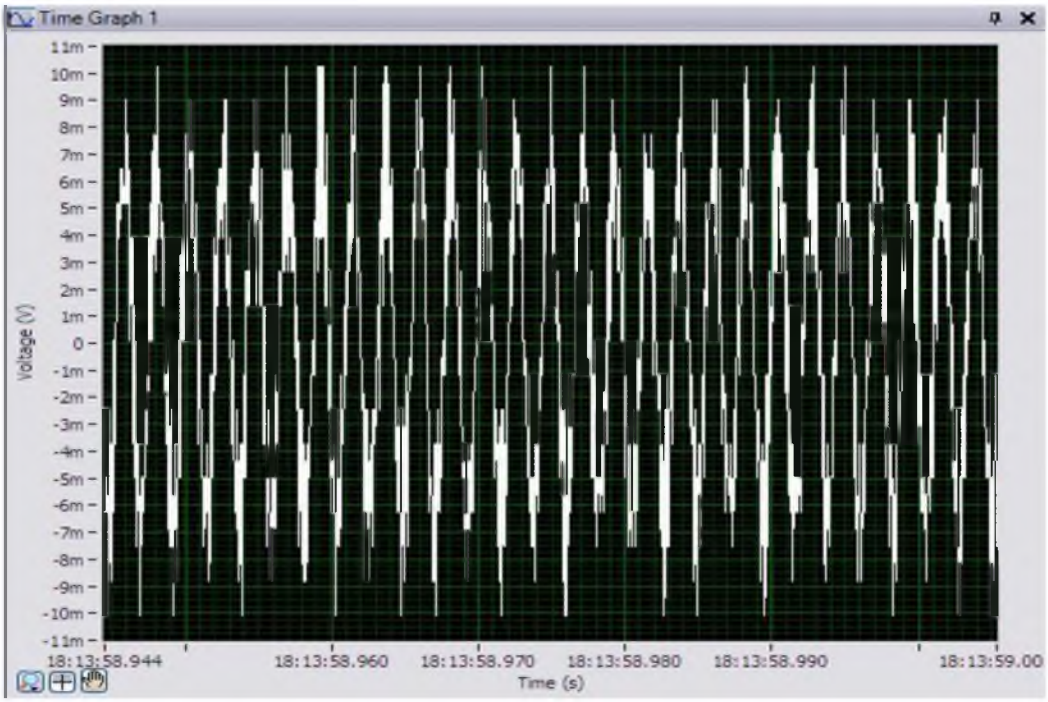

(b)

Figure 4.25: Continued

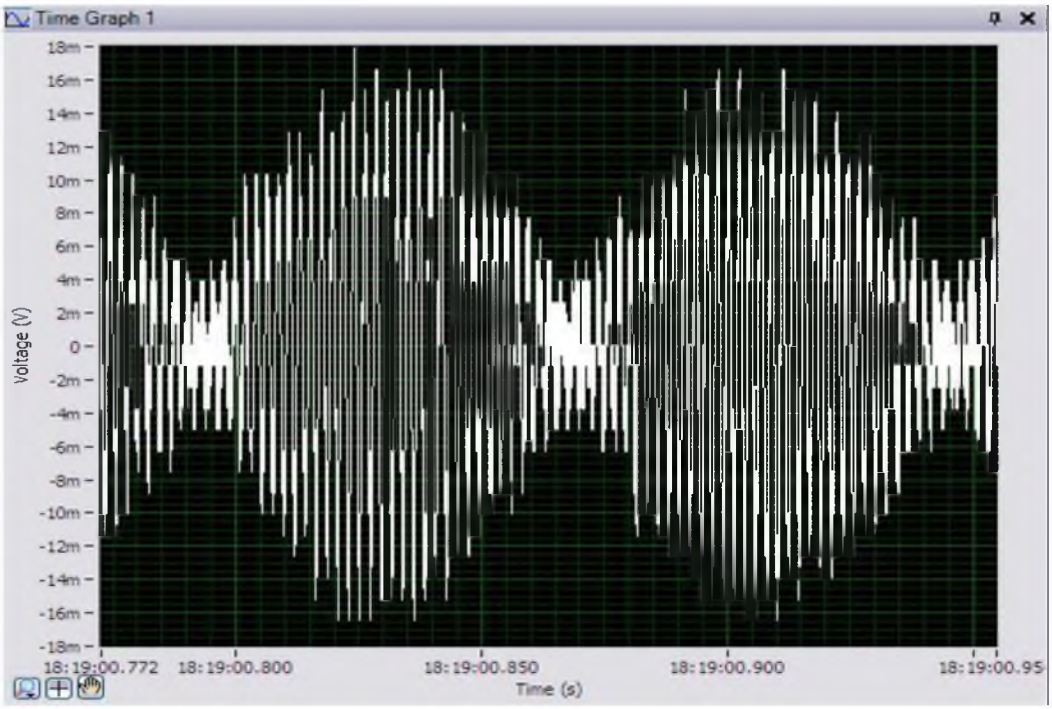

(c)

Figure 4.25: Continued

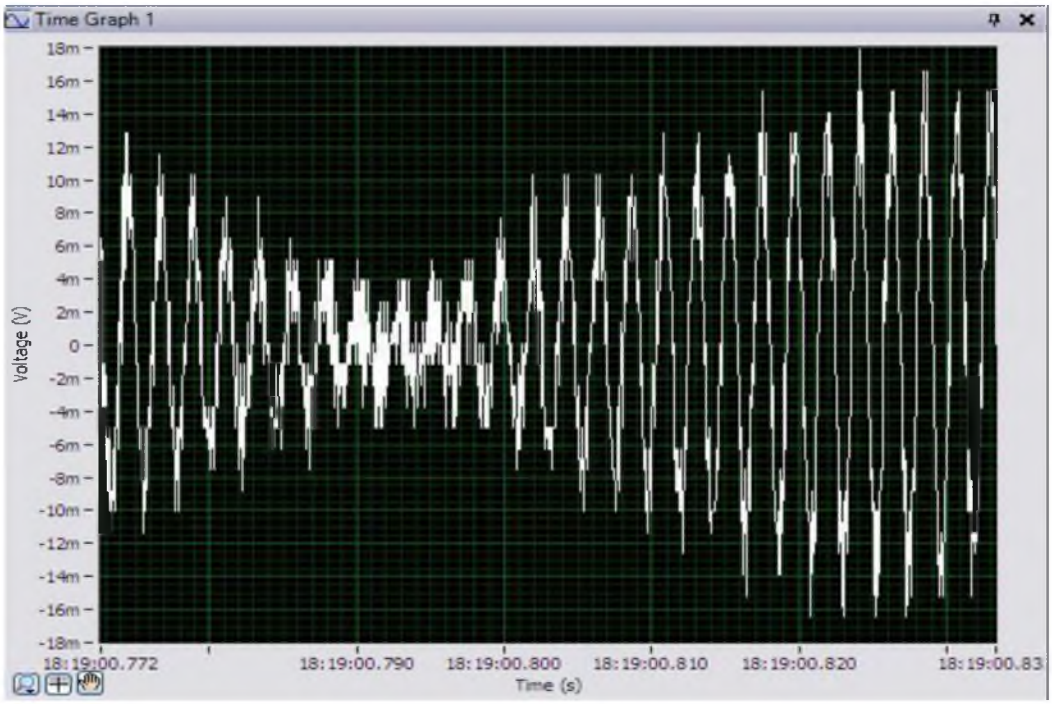

(d)

Figure 4.25: Continued

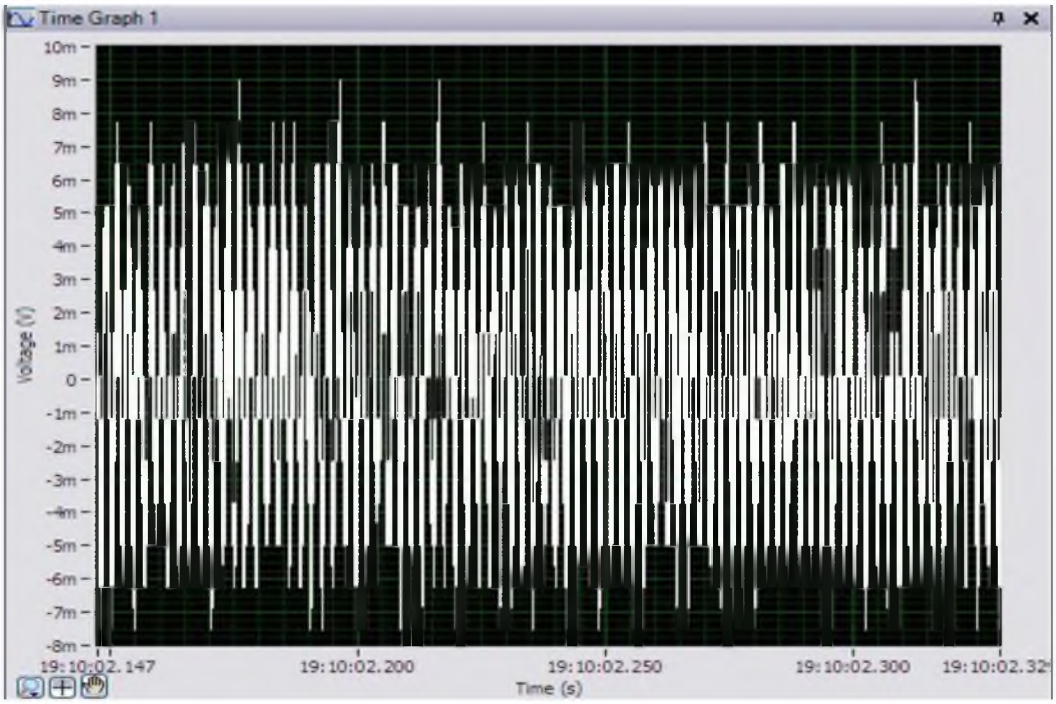

(a)

Figure 4.26: A comparison of signals for 30° crossing lasers with that of a single laser (12 cm spatial distance), where (a) represents the signal from a single laser in a time interval of 0.18 seconds, (b) represents the signal from a single laser in a time interval of 0.06 seconds, (c) represents the "beat" signal from 30° crossing lasers in a time interval of 0.18 seconds, and (d) represents the "beat" signal from 30° crossing lasers in a time interval of 0.06 seconds.

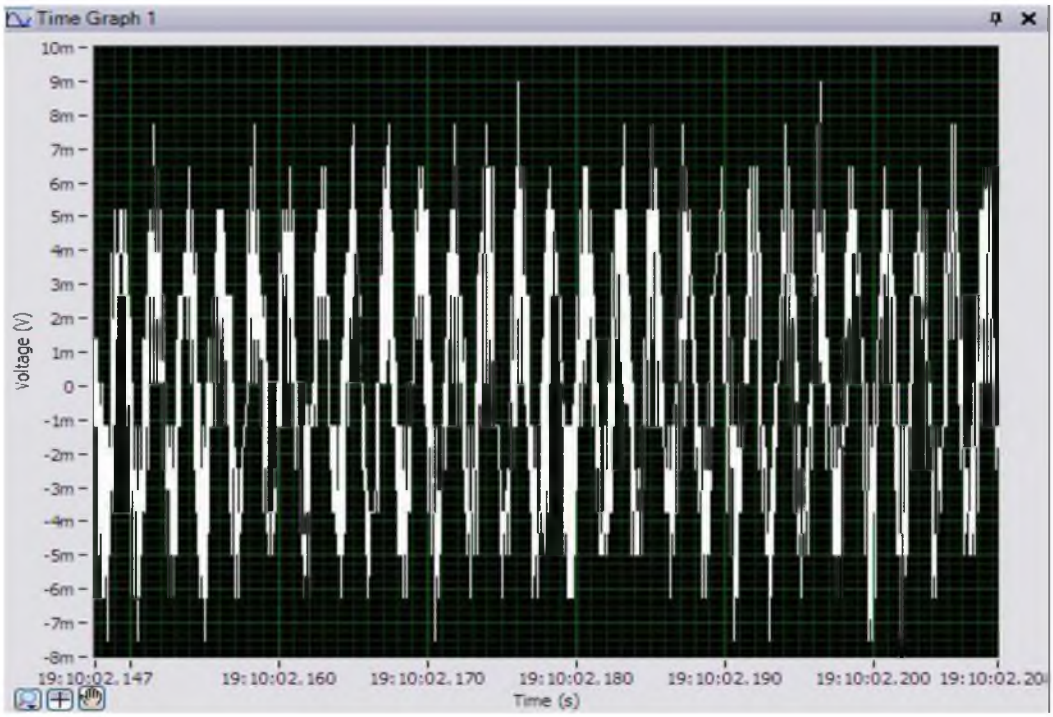

(b)

Figure 4.26: Continued

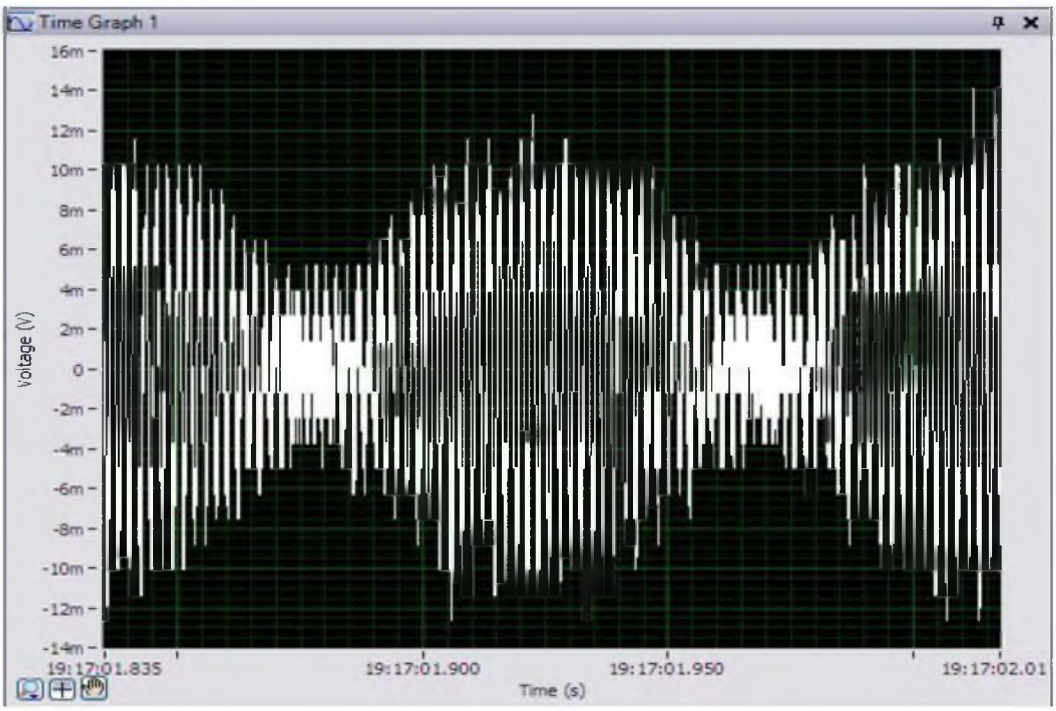

(c)

Figure 4.26: Continued

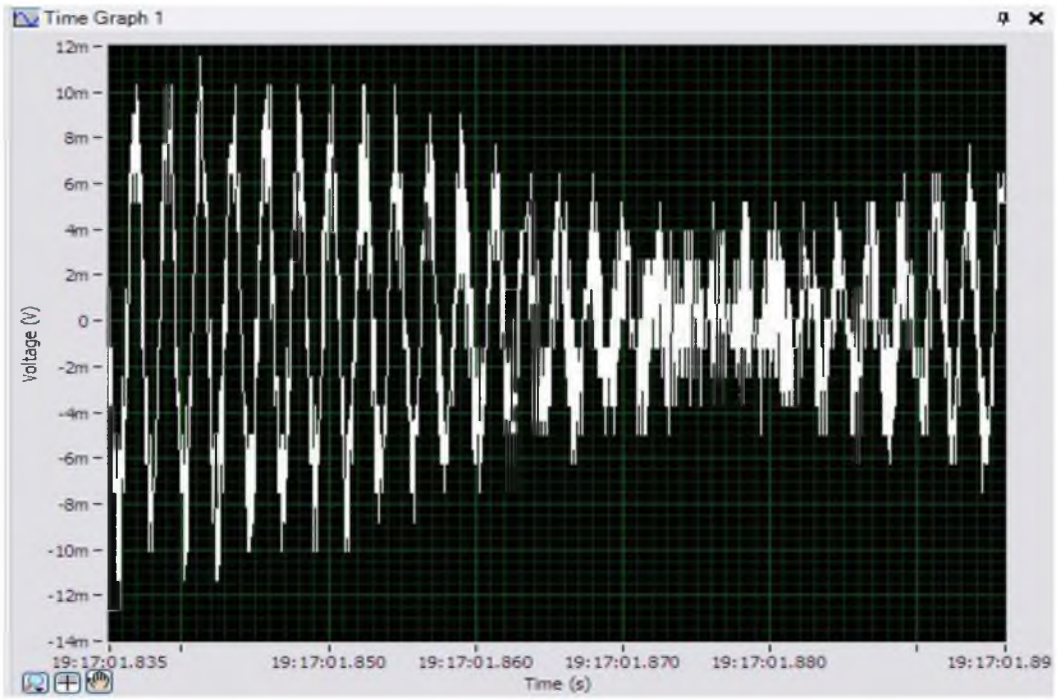

(d)

Figure 4.26: Continued

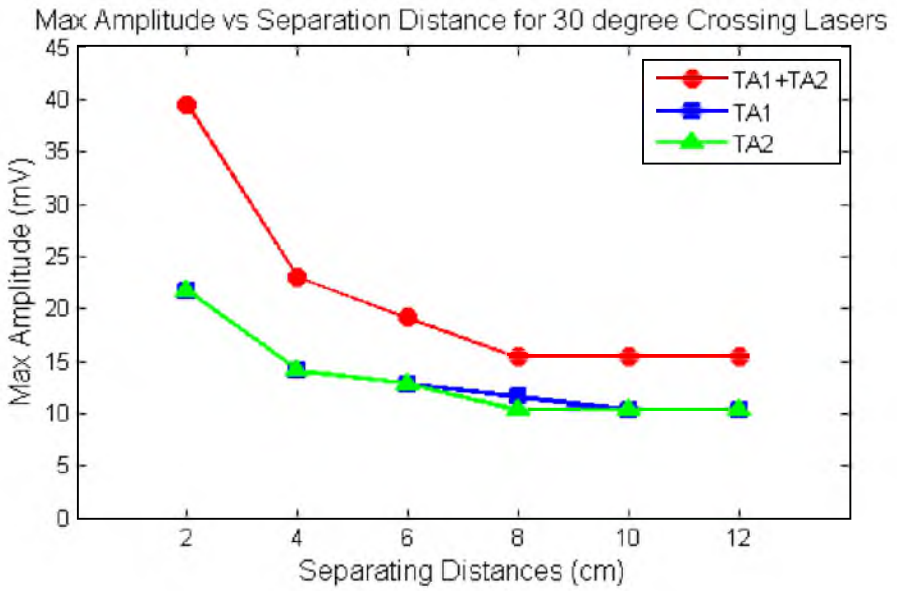

(a)

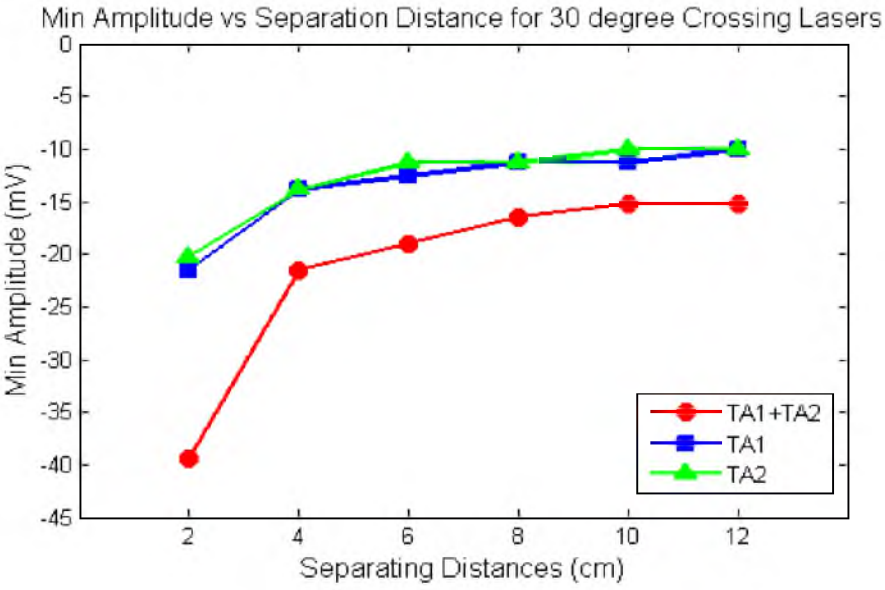

(b)

Figure 4.27: Amplitude recorded for the beating signal when both 30^{o} crossing lasers TA1 and TA2 were in-phase in comparison to that of a single laser (TA1 or TA2) at various separating distances, where (a) represents the Maximum Amplitude, and (b) represents the Minimum Amplitude.

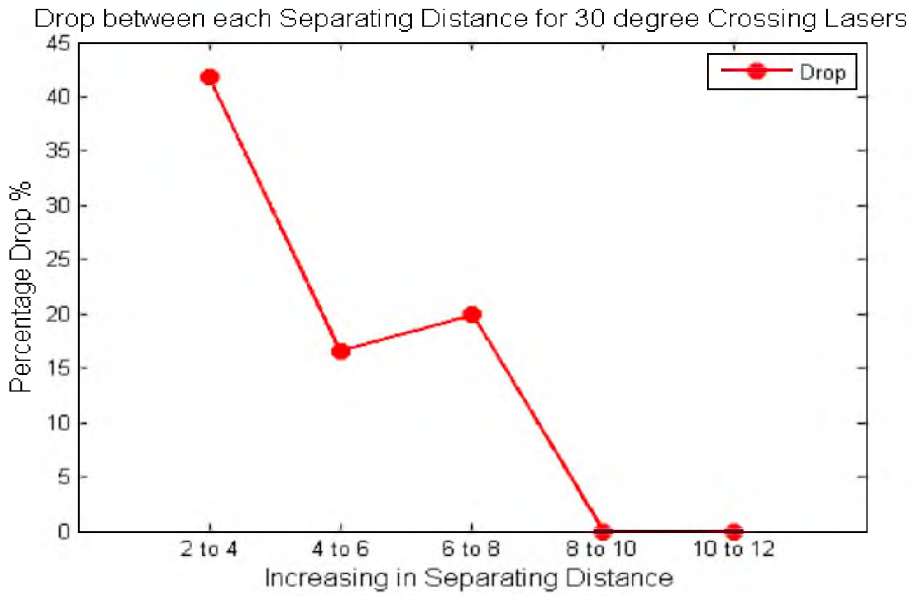

Figure 4.28: Percentage drop in maximum amplitude as the separating distance between the two acoustically coupled 30^{o} crossing lasers is increased from 0 to 12 cm.

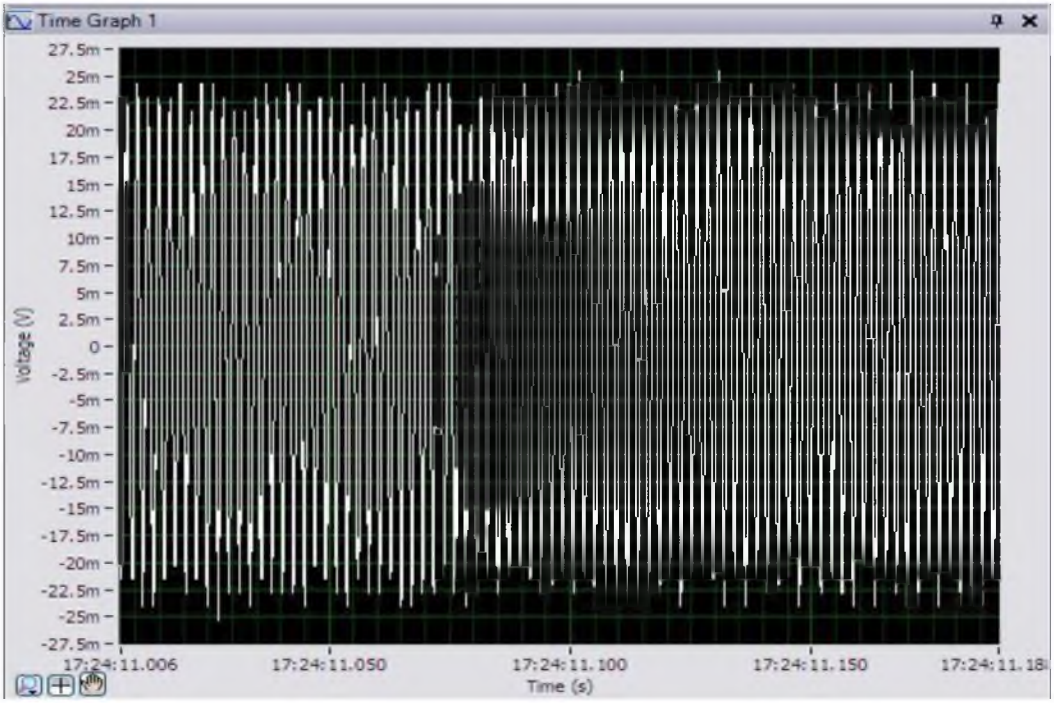

(a)

Figure 4.29: A comparison of signals for 90° crossing lasers with that of a single laser (2 cm spatial distance), where (a) represents the signal from a single laser in a time interval of 0.18 seconds, (b) represents the signal from a single laser in a time interval of 0.06 seconds, (c) represents the "beat" signal from 90° crossing lasers in a time interval of 0.18 seconds, and (d) represents the "beat" signal from 90° crossing lasers in a time interval of 0.06 seconds.

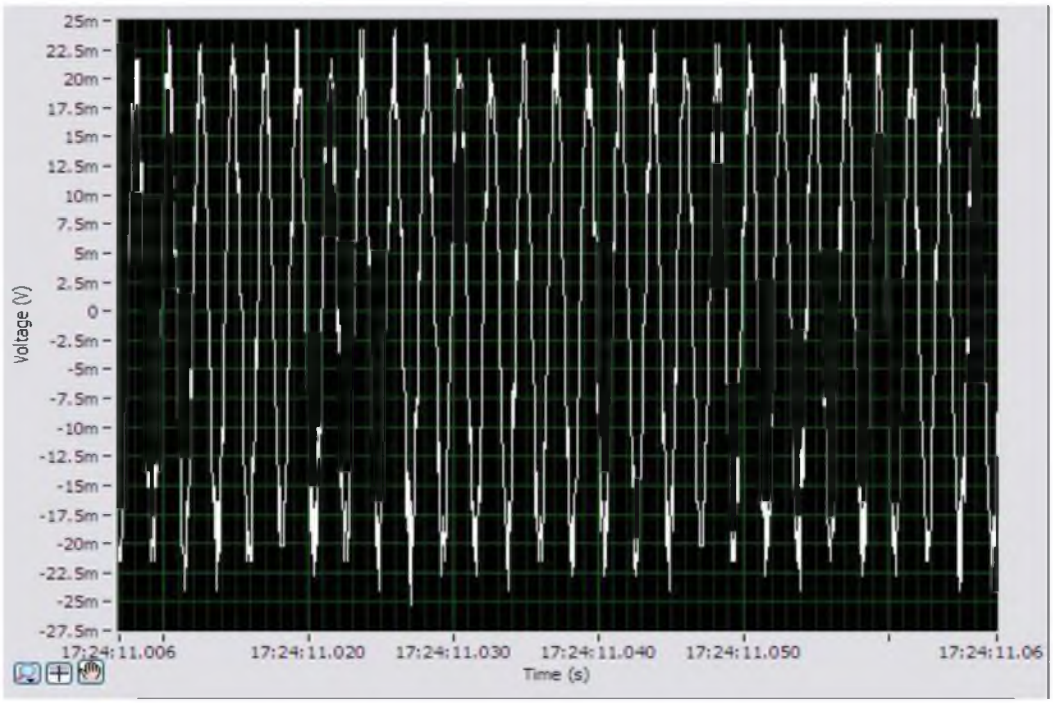

(b)

Figure 4.29: Continued

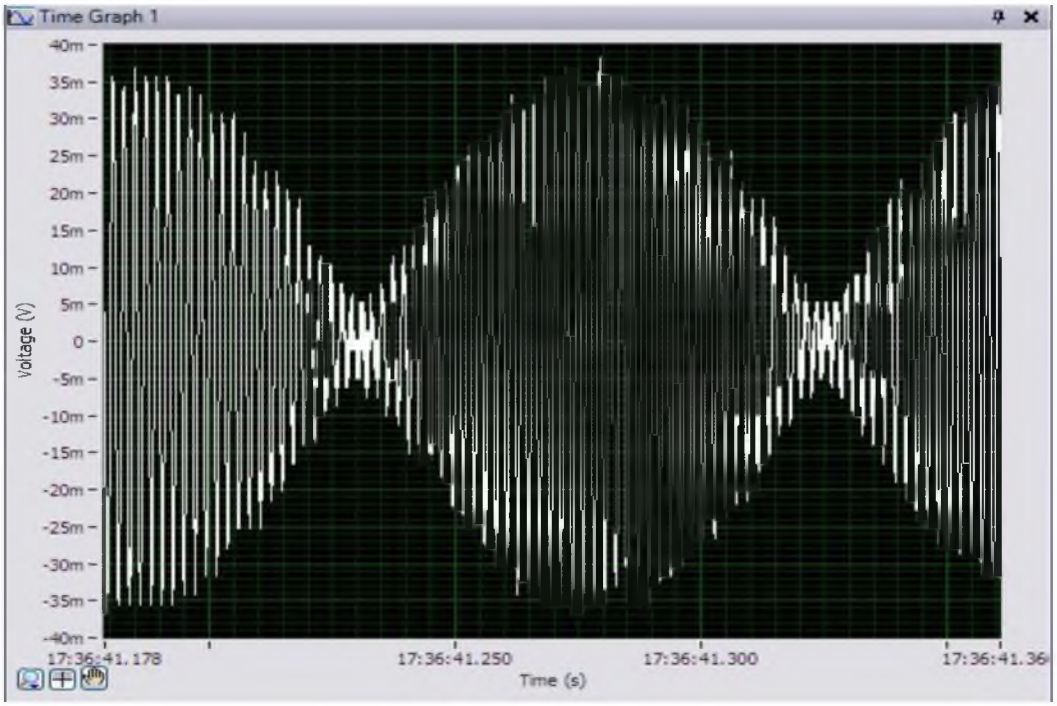

(c)

Figure 4.29: Continued

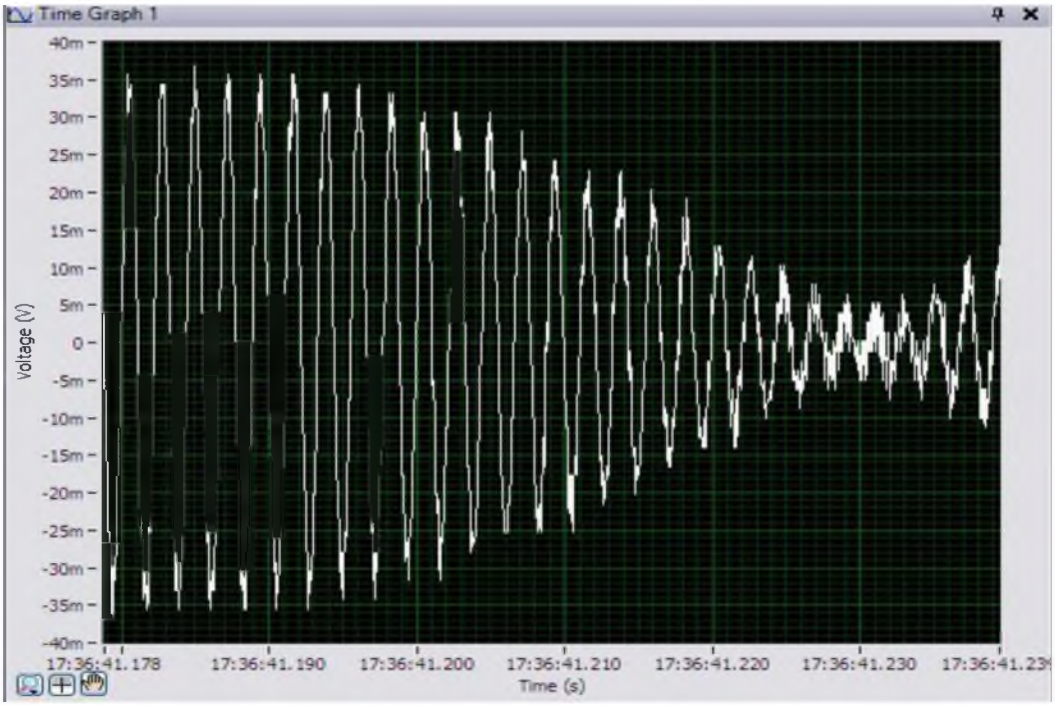

(d)

Figure 4.29: Continued

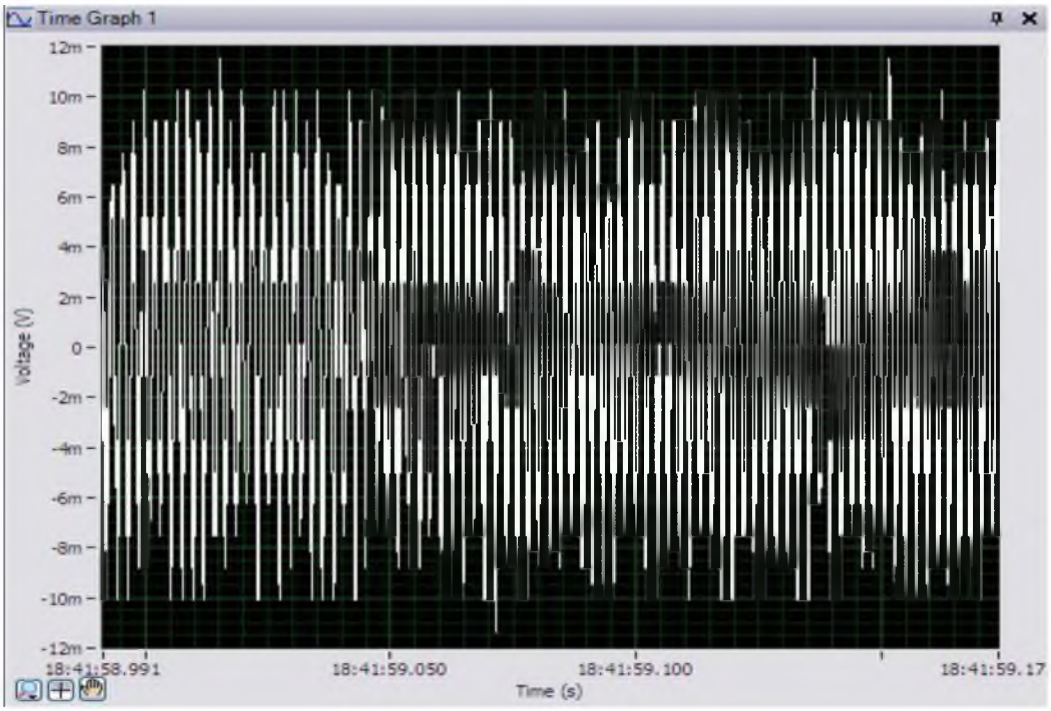

(a)

Figure 4.30: A comparison of signals for 90° crossing lasers with that of a single laser (6 cm spatial distance), where (a) represents the signal from a single laser in a time interval of 0.18 seconds, (b) represents the signal from a single laser in a time interval of 0.06 seconds, (c) represents the "beat" signal from 90° crossing lasers in a time interval of 0.18 seconds, and (d) represents the "beat" signal from 90° crossing lasers in a time interval of 0.06 seconds.

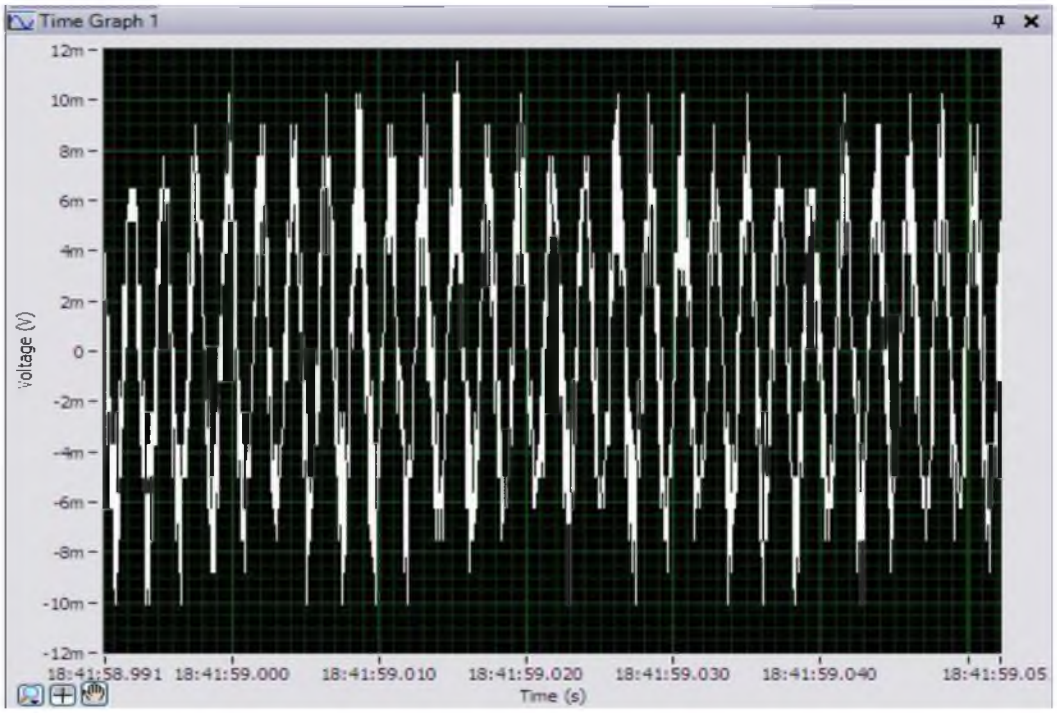

(b)

Figure 4.30: Continued

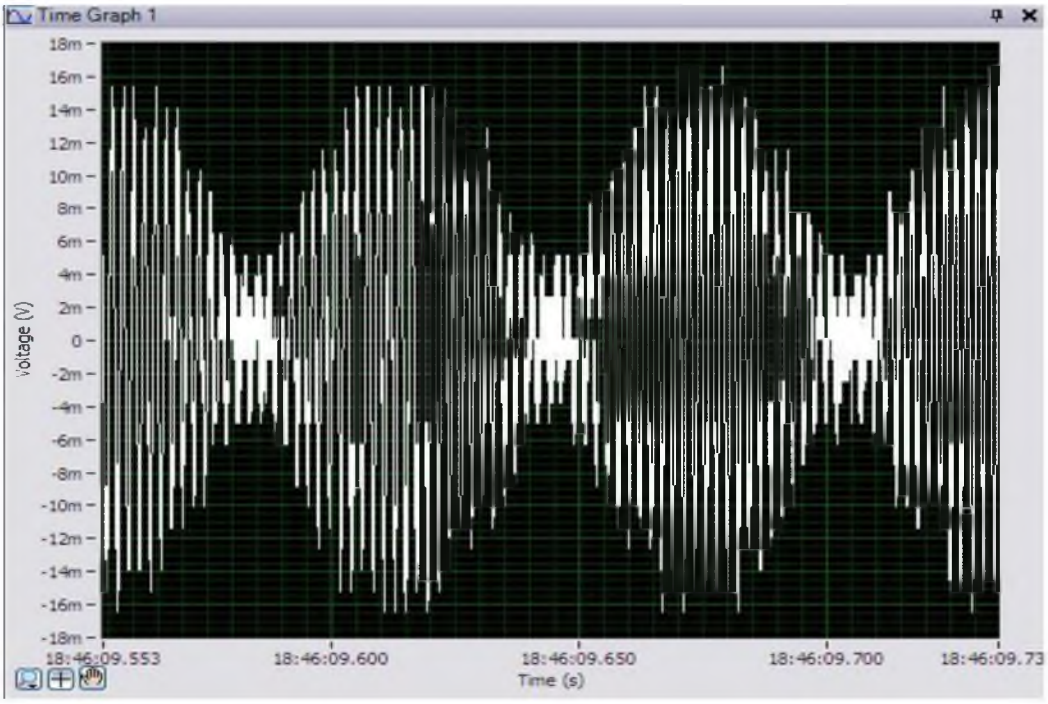

(c)

Figure 4.30: Continued

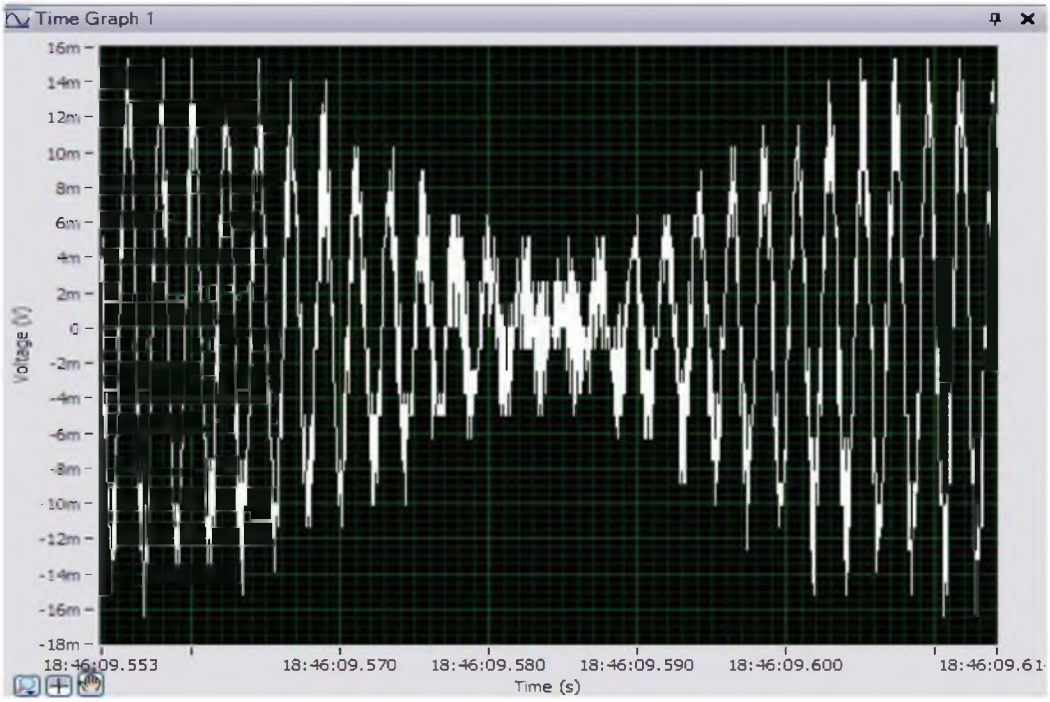

(d)

Figure 4.30: Continued

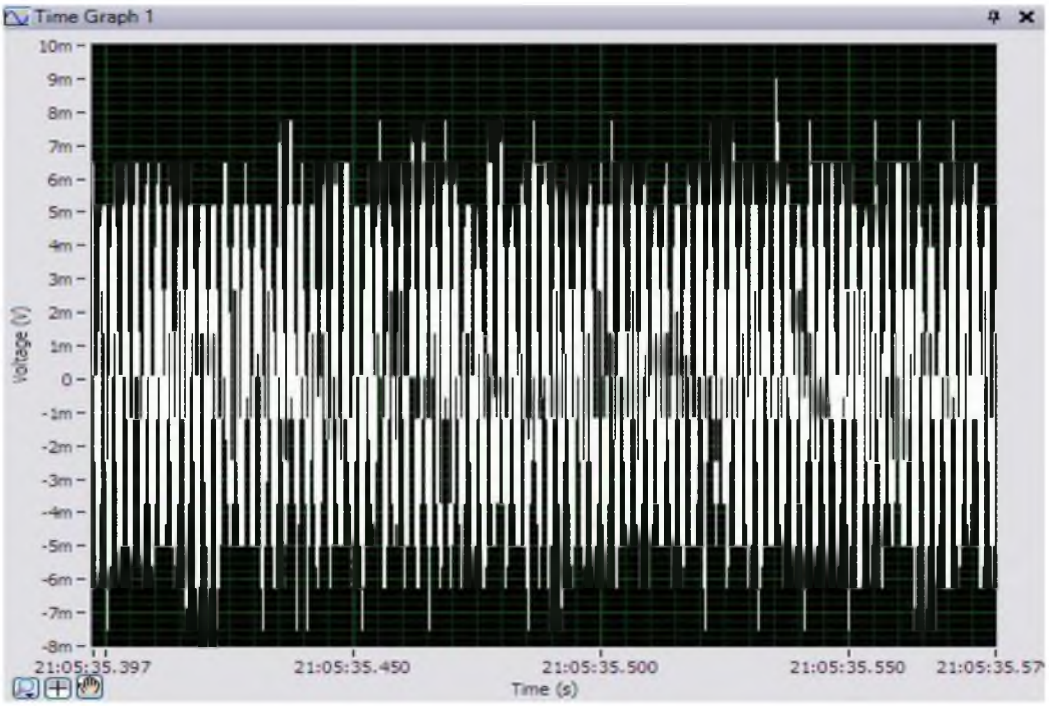

(a)

Figure 4.31: A comparison of signals for 90° crossing lasers with that of a single laser (12 centimeters spatial distance), where (a) represents the signal from a single laser in a time interval of 0.18 seconds, (b) represents the signal from a single laser in a time interval of 0.06 seconds, (c) represents the "beat" signal from 90° crossing lasers in a time interval of 0.18 seconds, and (d) represents the "beat" signal from 90° crossing lasers in a time interval of 0.06 seconds.

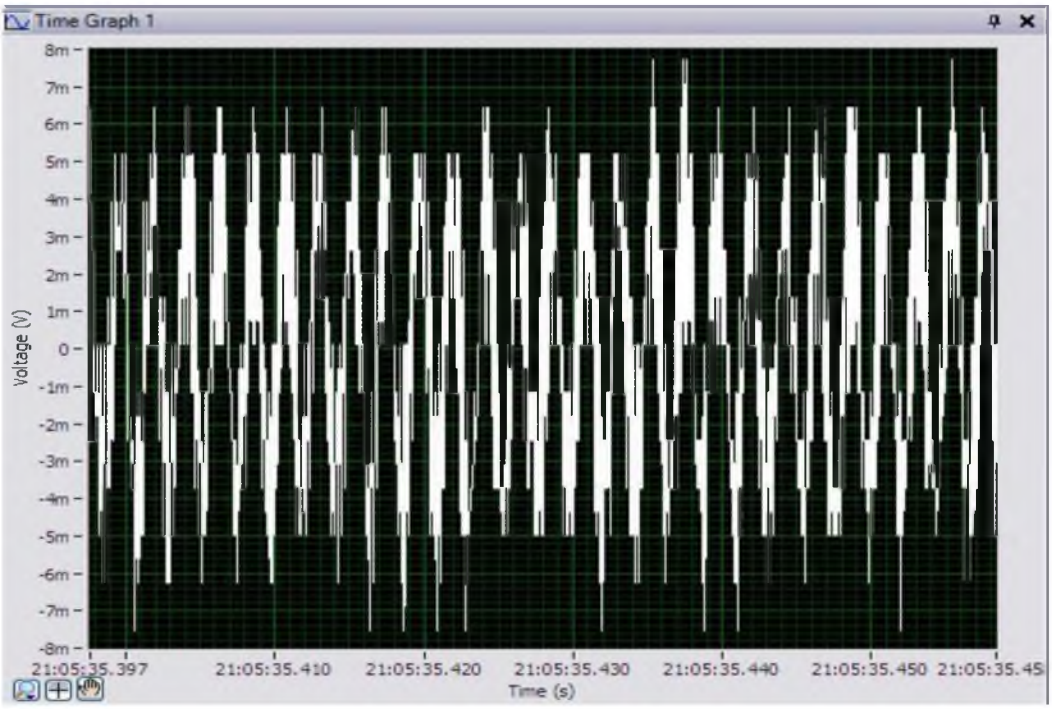

(b)

Figure 4.31: Continued

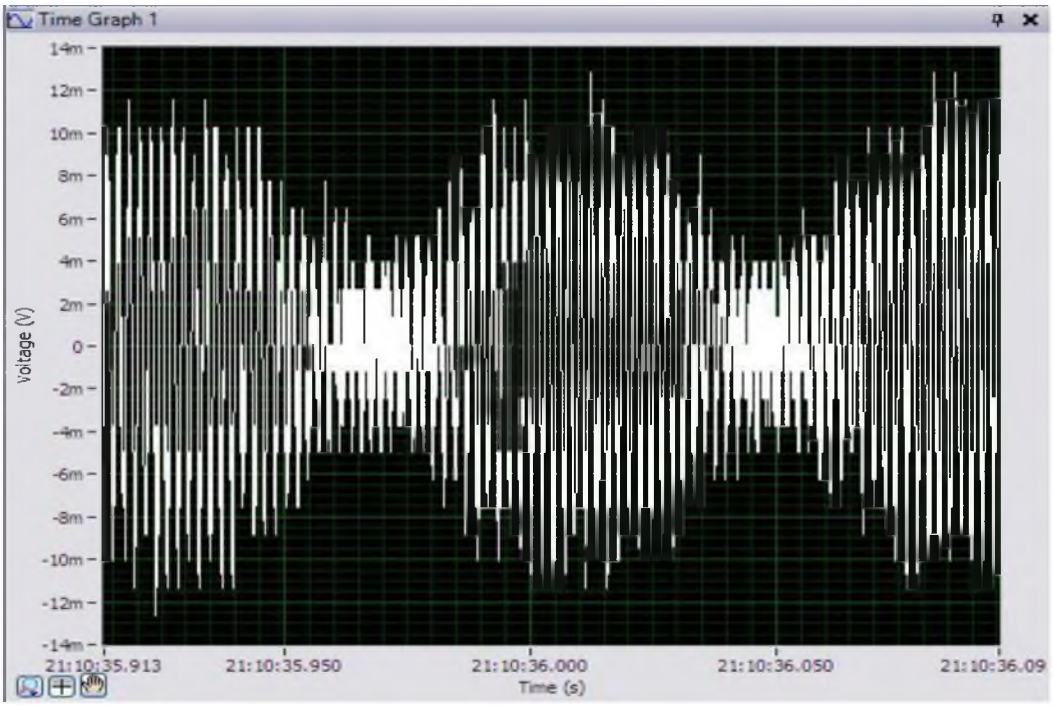

(c)

Figure 4.31: Continued

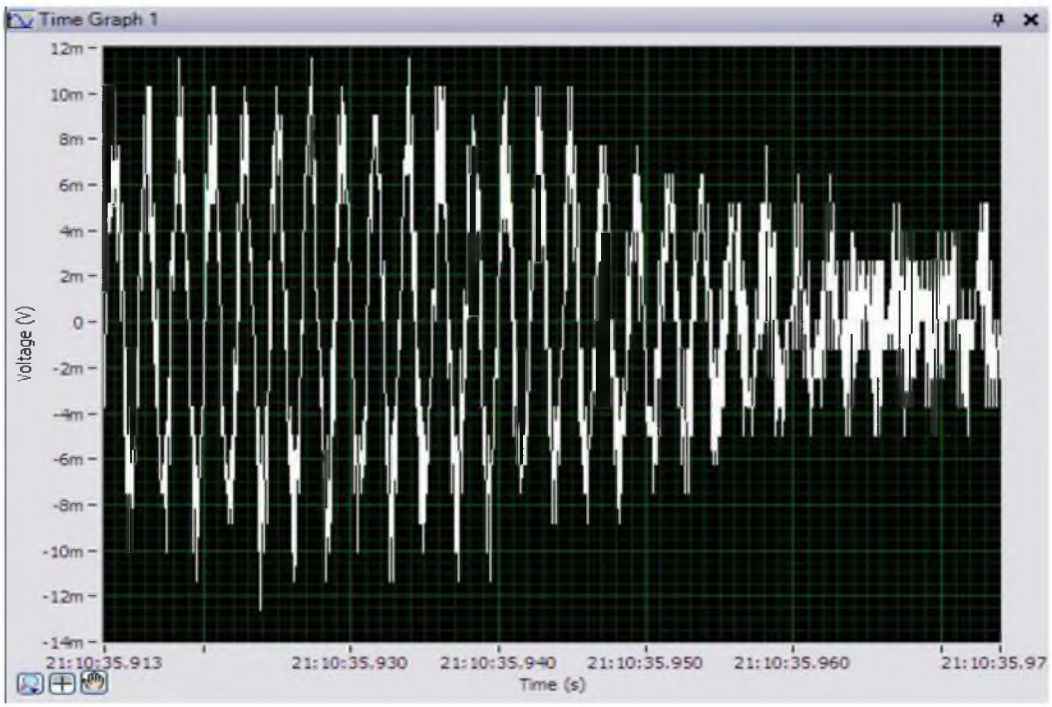

(d)

Figure 4.31: Continued

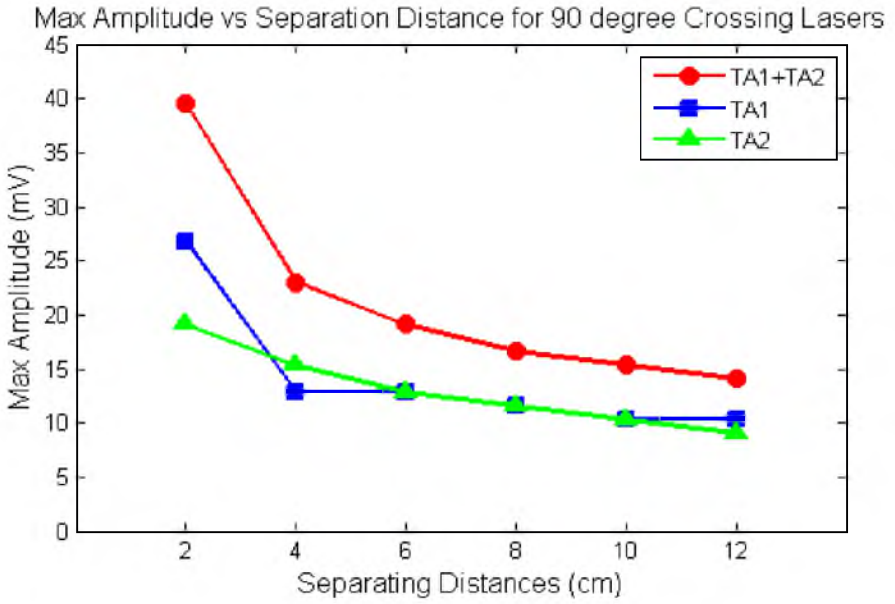

(a)

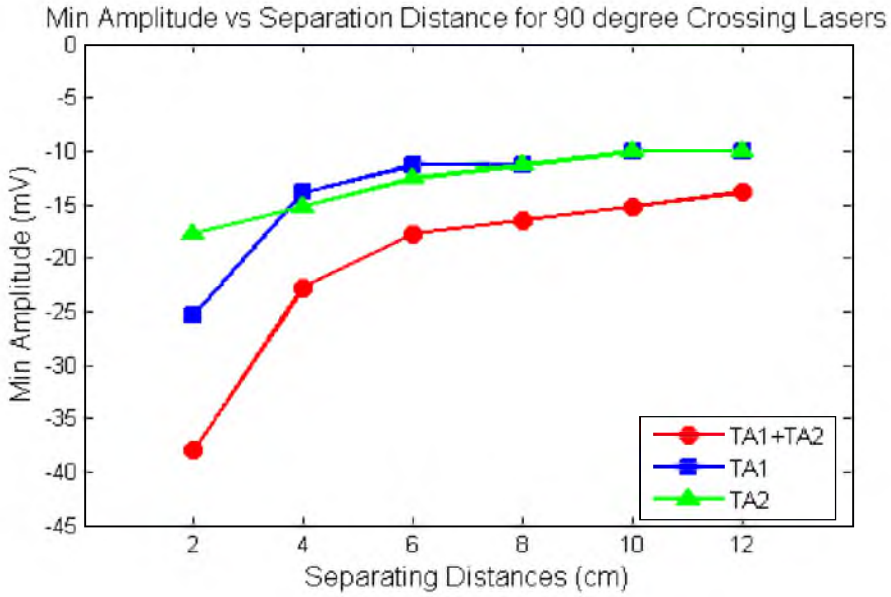

(b)

Figure 4.32: Amplitude recorded for the beating signal when both 90^{o} crossing lasers TA1 and TA2 were in-phase in comparison to that of a single laser (TA1 or TA2) at various separating distances, where (a) represents the Maximum Amplitude, and (b) represents the Minimum Amplitude.

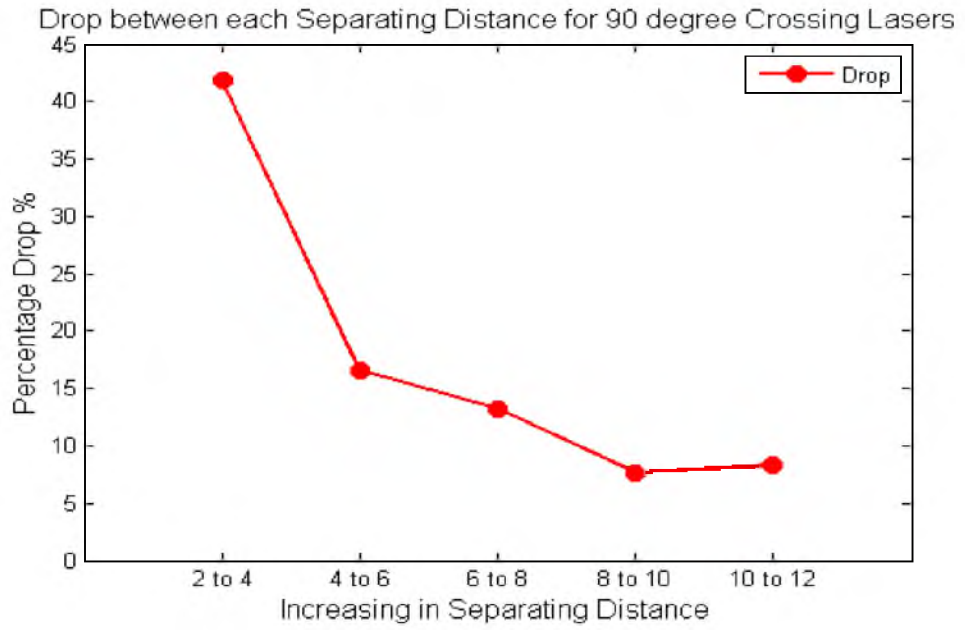

Figure 4.33: Percentage drop in maximum amplitude as the separating distance between the two acoustically coupled 90° crossing lasers is increased from 0 to 12 cm.

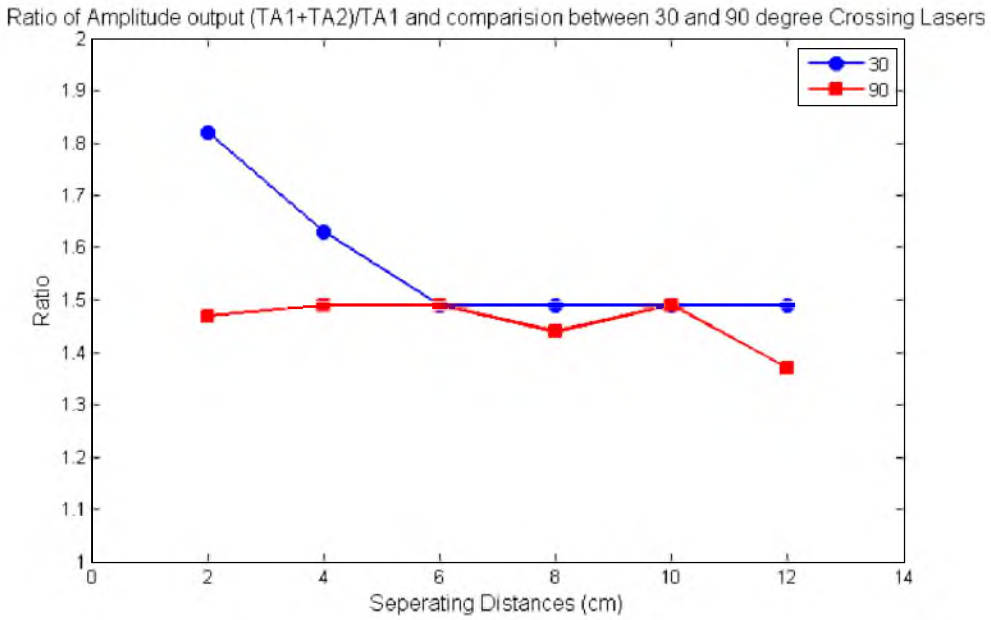

Figure 4.34: The amplitude ratios for the 30 and 90° crossing lasers at various separating distances.

Table 4.1: Fundamental frequencies recorded using Lab-View Signal Express (30^o crossing angle).

Fundamental frequencies recorded when lasers TA1 and TA2 are operating individually.		
Time in seconds	*Frequency of laser TA1* (ω_1) *measured in Hz*	*Frequency of laser TA2* (ω_2) *measured in Hz*
0	440.68	443.03
15	447.81	450.86
30	452.26	456.28
45	455.73	459.82
60	458.16	461.95

Table 4.2: Fundamental frequencies recorded using Lab-View Signal Express (90^o crossing angle).

Fundamental frequencies recorded when lasers TA1 and TA2 are operating individually.		
Time in seconds	*Frequency of laser TA1* (ω_1) *measured in Hz*	*Frequency of laser TA1* (ω_1) *measured in Hz*
0	439.22	437.11
15	446.59	446.42
30	452.00	452.35
45	455.51	455.99
60	458.15	458.56

CHAPTER 5

SUMMARY OF TEST RESULTS AND DISCOVERIES

5.1 Summary of Test Results

The objective of this thesis was to study the interaction between the sound waves generated by two identical thermoacoustic lasers and the acoustic coupling effect of the laser pair. Different coupling configurations were tested to vary the effects of coupling between the two lasers. Particularly, the crossing angles and the distances between the openings of the two lasers were varied and the respective coupled acoustic waves were measured using different measuring techniques. Three crossing angles 0, 30, and 90^{o}, and 5 different separating distances between the openings of the two lasers, varying from 2 to 12 cm in increments of 2 cm, were the different configurations we studied. Two quarter wavelength thermoacoustic lasers with nearly equal power ratings were used in the different coupling experiments. The stack was always placed in the middle of the resonator tube in our experiments for maximum acoustic energy output. The fundamental frequency of each laser was in the neighborhood of 440-460 Hz when powered. The amplitude output for each laser varied depending upon the input electric power.

Sound pressure levels were measured in three different orientations (0, 45, and 90^{o}) from the open end of the tube, in order to study the nature of the spherical sound waves exiting the laser tube. For all the orientations, there was a slight variance in

pressure levels in the close vicinity of the open end of the laser tube, whereas at distances greater than 10 cm away from the open end, the pressure levels were approximately equal.

Coupling between the two lasers was very critical and influential. First coupling was done at 0^{o} crossing angle, where the lasers were parallel to each other and separated by a distance of 1 m. In this particular case, the signals beat with the difference in the natural frequency. The frequency of each laser was different at onset and it was not possible to synchronize the two lasers with their mismatching frequencies. An increase in distance between the two parallel lasers increases the volume of air acting in between them. This atmospheric air acts as resistance and does not allow the two lasers to alter their frequencies. Therefore, this has resulted in large detuning and weak coupling between the two parallel lasers. One interesting factor observed in this particular case of coupling is that there was an increase in output amplitude, when the two lasers were in-phase with each other, and the resulting amplitude was greater than that of a single laser. In this case, synchronization and phase locking between the two lasers was not observed.

Synchronization (mode-locking) was observed when the crossing angle was changed to 30 and 90^{o}. In this case, the sound waves were focused with the opening ends of the laser tubes in close proximity. The output acoustic amplitude for the synchronized signal was always less compared to that of a single laser. We observed only out-of-phase synchronization for the two phase locked lasers. The oscillating pressure was out-of-phase at the openings of the two laser tubes, which resulted in the gas being reverted back into the lasers. These antiphase pressure oscillations resulted in decreased amplitude output for the synchronized signal. In some cases during the experiments, there was a

delay in achieving synchronization. One cause was due to the initial mistuning of the frequencies when the lasers started running. If the frequencies of the lasers were in proximity (but not equal), synchronization was still achieved; however, it was delayed by a certain amount of time. Another important factor to be considered was the ratio of the output amplitudes of the two lasers. This ratio should be close to 1 ± 0.038, in order to achieve synchronization. The last important factor was considered to be human error, which was the variation in time delay associated with turning on the second laser with respect to turning on the first. This delay was crucial, because the time taken for the lasers to alter each other's frequencies and achieve synchronization totally depended upon it.

Synchronization was not achieved when the openings of the two lasers were moved far apart from one another in their own respective crossing angles (30 or 90^{o}). The reason behind this was simple: the coupling was weak due to large detuning between the two lasers. There was an increase in volume of atmospheric air acting in between the two lasers, when they were moved far apart. This air acted as a resistance between the two sound waves and did not allow them to synchronize (mode-lock) in a particular frequency or phase. An interesting observation was that the uncoupled signals beat with a difference in the natural frequency, and this beating signal has a maximum amplitude output when the signals from the two lasers were particularly in-phase. This maximum recorded amplitude was more than that of the acoustic amplitude output recorded for a single laser.

5.2 Discoveries

Important discoveries found in this thesis:

(1) Synchronization of a thermoacoustic laser pair was achieved by acoustic coupling when the open ends of the two lasers were in proximity and the angle between their longitudinal axes was not very large.

(2) Synchronization was easier to achieve when the acoustic amplitude ratios of both lasers were close to unity and the difference in their natural frequencies at the time of coupling was approximately equal to 0.

(3) The amplitude of the synchronized (mode-locked) acoustic waves was always less than that of a single laser, indicating out-of-phase synchronization.

(4) The unsynchronized acoustic waves beat, changing from in-phase to out-of-phase. The amplitude of the unsynchronized waves was greater than that of a single laser when the two lasers were in-phase.

APPENDIX

Table A.1: Specifications of CEN-TECH 98025 multimeter

Power Requirements	9V Battery
Frequency	45 to 450 Hz
DC Amps	Range: 200mA/2000mA/20mA/ 10A
Accuracy	(@0mA-200mA) 1.2%±2D; (@10A) 3%±2D
DC Voltage	Ranges: 200mV/2000mV 20/200/1000V
Accuracy	(@200mV) 0.5%±1D (@2000mV-200V) 1%±2D (@1000V) 1%±2D
Resistance	Ranges: 200/2000/20K/200K/2000K Ohm

Table A.2: Specifications of Tenma 72-942 sound level meter

Standard applied	IEC651 type 2, ANSI S1.4 type 2
Frequency range	31.5Hz to 8kHz
Measuring level range	30 to 130dB
Frequency weighting	A/C
Microphone	½ inch electret condenser microphone
Display	LCD
Resolution	0.1 dB
Display Up data	0.5 sec
Time weighting	FAST(125mS), SLOW(1 sec.)
Level ranges	Lo: 30-100dB Hi: 60-130dB
Accuracy	± 1.5dB (under reference conditions)
Maximum hold	Hold readings the Maximum Value, with decay < 1dB/3minutes
Operation temperature	0 to 40°C (32 to 104°F)
Operation humidity	10 to 90%RH
Dimensions	201(L) x 55(W) x 32(H) mm
Weight	230g (including battery)

Table A.3: Specifications of NI USB 6009

Feature	**NI USB-6009**
AI Resolution	14 bits differential, 13 bits single ended
Maximum AI Sample Rate, Single Channel*	48kS/s
Maximum AI Sample Rate, Multiple Channels (Aggregate)*	48kS/s
DIO Configuration	Open Collector or Active Drive
* System Dependant	

Table A.4: Analog terminal assignments for NI USB 6009

Terminal Signal	Single-Ended Mode Signal	Differential Mode
1	GND	GND
2	AI 0	AI 0+
3	AI 4	AI 0-
4	GND	GND
5	AI 1	AI 1+
6	AI 5	AI 1-
7	GND	GND
8	AI 2	AI 2+
9	AI 6	AI 2-
10	GND	GND
11	AI 3	AI 3+
12	AI 7	AI 3-
13	GND	GND
14	AO 0	AO 0
15	AO 1	AO 1
16	GND	GND

REFERENCES

1. Swift, G.W. Thermoacoustic Engines. *Acoust. Soc. Am.* **1988,** *84*(4), 1145.

2. Rayleigh, L. *The Theory of Sound*; Vol. 2nd edition. Dover Publications: New York, 1945.

3. Rott, N. *Thermally driven acoustic oscillations.*"(I-IV), Math. Phys.

4. Yazaki, T.; Tominaga, A.; Narahara, Y. Experiments on thermally driven acoustic oscillations of gaseous helium. *Low Temp. Phys.* **1980,** *41*(1), 45.

5. Feldman, K.T. and R.L. Carter, A study of heat driven thermal pressure oscillations in a gas. *Heat Trans.* **1970**, *92*, 536.

6. Feldman, K.T. A study of heat driven thermal pressure oscillations in a gas. Ph.D. Thesis, University of Missouri, 1966.

7. Wheatley, J.; Hofler, T.; Swift G.; Migliori, A. Intrinsically irreversible thermoacoustic engine. *Phys. Rev. Lett*, **1983**, *50*(7), 499.

8. Hofler, T. Acoustic cooling engine. U.S. Patent 201, 1988.

9. Ceperley, P.H. A pistonless Sturling engine- The travelling wave heat engine. *Acoust. Soc. Am.* **1979**, *66*(5), 1508.

10. Backhaus, S.; Swift, G.W. A thermoacoutic-Stirling heat engine: Detailed study. *Acoust. Soc. Am.* **2000**, *107*(6), 3186.

11. McDonald, B.G.; Symko, O.G. Coupling of mid audio frequency thermoacoustic prime movers. *Acoust. Soc. Am.* **2009**, *125*(4), 2563.

12. Gillman, B.J., A Study of Thermoacoustic Engines. Ph.D. Thesis, University of Utah, 2009.

13. Spoor, P.S.; Swift, G.W. Mode-locking of acoustic resonators and its applications to vibration cancellation in acoustic heat engines. *Acoust. Soc. Am.* **1999,** *106*(3), 1353.

14. Spoor, P.S.; Swift, G.W. The Huygens entrainment phenomena and thermoacoustic engines. *Acoust. Soc. Am*. **2000**, *108*(2), 588.

15. Coltman, J.W. Sounding mechanism of the flute and organ pipe. *Acoust. Soc. Am*. **1968**, *44*(4), 983.

16. Karpov, S.; Prosperetti, A. A nonlinear model of thermoacoustic devices. *Acoust. Soc. Am*, **2002**, *112*(4) 1431.

17. Pol, B.V.d. The nonlinear theory of electric oscillations. *Proc. Inst. Rad. Eng.* **1934**, *22*, 1051.

18. Bennett, M.; Schatz, M; Rockwood, H; Wiesenfeld, K. Hugyens clocks. *Proceedings: Mathematical, Physical and Engineering Sciences. Royal Soc. Lond. A*. **2002**, *458*, 563.

19. Pikovsky, A.; Rosenblum, M. Synchronization: from pendulum clocks to chaotic oscillators and chemical oscillations. *Contemporary Physics*. **2003**, *44*(5), 401.

20. Bouasse, H.; Fouche, M. *Instruments a Vent*. Librairie Delagrave: Paris, 1929.

21. Abel, M.; Bergweiler, S.; Gerhard-Multhaupt, R. Synchronization of organ pipes: experimental observations and modeling. *Acoust. Soc. Am*. **2006**, *119*(4), 2467.

22. Marrison, W.A. U.S. Patent 2,836,033, 1958.

23. Symko, O.G.; Abdel-Rahman, E.; Kwon, Y.S.; Emmi, M.; Behunin, R. Design and development of high-frequency thermoacoustic engines for thermal management in microelectronics. *Microelectronics*, **2004**, *35*, 185-191.

24. Garrett, S.L. Acoustic laser kit instructions, Penn State University, 2005.

25. Chen, K. Acoustic energy output and coupling effect of a pair of thermoacoustic lasers. *Int. J. Energy Research*, **2011**.

26. Bass, H.E. A study of element interaction in thermoacoustic engines, 1995.

27. Dowling, A.P.; Williams, F. Sound and Source of Sound. *Ellis Horwood Limited*: West Sussex, England, 1983.

28. Kline, S.J.; McClintock, F.A. Describing uncertainties in single sample experiments. *ASME*. **1953**, *75*, 3-8.

29. Tontechnik-Rechner-sengpieaudio. *Sound Pressure p and the inverse distance law 1/r*. 2010; Available from: http://www.sengpieaudio.com/calculator-distancelaw.htm.July 2010.

30. Chen, R.L.; Garrett, S.L. The solar/heat driven thermoacoustic engine. *Acoust. Soc. Am*. **1998**, *103*(5), 2841-2842.

31. Arnott, W.P.;Raspet, P.; Bass, H.E. Thermoacoutic Engines. *Proceeding of IEEE Ultrasonics Society*, **1991**, 995-1003.